Supplementary Information (SI) for Chemical Science.
This journal is © The Royal Society of Chemistry 2024

Supplementary Information

Construction of intermolecular σ-hole interactions in rare earth metallocene complexes using a 2,3,4,5-tetraiodopyrrolyl anion

Francis Delano IV,[a] Florian Benner,[a] Seoyun Jang,[a] Samuel M. Greer,[b] and Selvan Demir[a]*

[a]Department of Chemistry, Michigan State University, 578 South Shaw Lane, East Lansing, Michigan 48824, USA
[b]Los Alamos National Laboratory (LANL), Los Alamos, New Mexico 87545, United States

*Correspondence to: sdemir@chemistry.msu.edu (S.D.)

Table of Contents

X-Ray Crystallography **S7**

Table S1. Crystal data and structure refinement of $Cp^*_2RE(TIP)$ S7

Table S2. Crystal data and structure refinement of $Cp^*_2RE(TIP)$ from 110 to 130 K S8

Table S3. Crystal data and structure refinement of $Cp^*_2RE(TIP)$ from 140 to 160 K S9

Table S4. Crystal data and structure refinement of $Cp^*_2RE(TIP)$ from 170 to 190 K S10

Table S5. Crystal data and structure refinement of $Cp^*_2RE(TIP)$ from 200 to 220 K S11

Table S6. Crystal data and structure refinement of $Cp^*_2RE(TIP)$ from 230 to 250 K S12

Table S7. Crystal data and structure refinement of $Cp^*_2RE(TIP)$ from 260 to 280 K S13

Table S8. Crystal data and structure refinement of $Cp^*_2RE(TIP)$ at 290 and 300 K S14

Table S9. Crystal data and structure refinement of $Cp^*_2RE(DMP)$ S15

Figure S1. Structure of $Cp^*_2Y(TIP)$, **1–Y** S16

Figure S2. Structure of $Cp^*_2Y(TIP)$, **1–Y**, with thermal ellipsoids drawn at 50% S16

Figure S3. Structure of $Cp^*_2Gd(TIP)$, **1–Gd** S17

Figure S4. Structure of $Cp^*_2Gd(TIP)$, **1–Gd**, with thermal ellipsoids drawn at 50% S17

Figure S5. Structure of $Cp^*_2Dy(TIP)$, **1–Dy**, with thermal ellipsoids drawn at 50% from 100 to 260 K S18

Figure S6. Structure of $Cp^*_2Dy(TIP)$, **1–Dy**, with thermal ellipsoids drawn at 50% from 270 to 300 K S19

Figure S7. Labeled structure of $Cp^*_2Y(TIP)$, **1–Y** S19

Figure S8. Unit Cell of $Cp^*_2Dy(TIP)$, **1–Dy** S20

Figure S9. Temperature dependence of the Dy–N distance S20

Figure S10. Temperature dependence of pyrrolyl interatomic distances S21

Figure S11. Temperature dependence of intermolecular I^1–I^3 interatomic distances S21

Figure S12. Temperature dependence of intermolecular I^1–I^4 interatomic distances S22

Figure S13. Temperature dependence of intermolecular I^3–I^3 interatomic distances S22

Figure S14. Structure of $Cp^*_2Y(DMP)$, **2–Y** S23

Figure S15. Structure of $Cp^*_2Y(DMP)$, **2–Y**, with thermal ellipsoids drawn at 50% S23

Figure S16. Structure of $Cp^*_2Dy(DMP)$, **2–Dy** S24

Figure S17. Structure of $Cp^*_2Dy(DMP)$, **2–Dy**, with thermal ellipsoids drawn at 50% S24

Figure S18. Unit Cell of $Cp^*_2Y(DMP)$, **2–Y** S25

NMR Spectroscopy **S26**
Figure S19. ^{1}H NMR spectrum of TIPH S26
Figure S20. ^{13}C NMR spectrum of TIPH S26
Figure S21. ^{1}H NMR spectrum of Cp*$_2$Y(TIP), **1–Y** S27
Figure S22. ^{13}C NMR spectrum of Cp*$_2$Y(TIP), **1–Y** S27
Figure S23. ^{1}H–^{1}H gCOSY spectrum of Cp*$_2$Y(TIP), **1–Y** S27
Figure S24. ^{1}H NMR spectrum of Cp*$_2$Y(DMP), **2–Y** S28
Figure S25. ^{13}C{^{1}H} NMR spectrum of Cp*$_2$Y(DMP), **2–Y** S29
Figure S26. ^{1}H–^{1}H gCOSY spectrum of Cp*$_2$Y(DMP), **2–Y** S29
Figure S27. ^{1}H–^{13}C gHSQC spectrum of Cp*$_2$Y(DMP), **2–Y** S30

IR Spectroscopy **S31**
Figure S28. FTIR spectrum of TIP S31
Figure S29. FTIR spectrum of Cp*$_2$Y(TIP), **1–Y** S31
Figure S30. FTIR spectrum of Cp*$_2$Gd(TIP), **1–Gd** S32
Figure S31. FTIR spectrum of Cp*$_2$Dy(TIP), **1–Dy** S32
Figure S32. FTIR spectrum of Cp*$_2$Y(DMP), **2–Y** S33
Figure S33. FTIR spectrum of Cp*$_2$Dy(TIP), **2–Dy** S33

UV-vis Spectroscopy **S34**
Figure S34. UV-vis absorption spectrum of Cp*$_2$Y(TIP), **1–Y**, with calculated transitions S34
Figure S35. UV-vis absorption spectra of Cp*$_2$RE(DMP) S34

Magnetic Data **S35**
Figure S36. Variable-temperature dc magnetic susceptibility data ($\chi_M T$ *vs*. *T*) of Cp*$_2$Gd(TIP), **1–Gd** S35
Figure S37. Variable-temperature dc magnetic susceptibility data ($\chi_M T$ *vs*. *T*) of Cp*$_2$Dy(TIP), **1–Dy** S35
Figure S38. Variable-temperature dc magnetic susceptibility data ($\chi_M T$ *vs*. *T*) of Cp*$_2$Dy(DMP), **2–Dy** S36
Figure S39. In-phase (χ_M') components of the ac magnetic Susceptibility for Cp*$_2$Dy(TIP), **1–Dy**, under zero applied dc field S36
Figure S40. Out-of-phase (χ_M'') components of the ac magnetic susceptibility for Cp*$_2$Dy(TIP), **1–Dy**, under zero applied dc field S37
Figure S41. Cole−Cole plots for ac magnetic susceptibility of Cp*$_2$Dy(TIP), **1–Dy**, collected under zero applied dc field S37
Figure S42. Out-of-phase components of the ac magnetic susceptibility (χ_M'') for Cp*$_2$Dy(TIP), **1–Dy**, ranging from 0 to 1500 Oe applied dc fields S38
Figure S43. In-phase (χ_M') components of the ac magnetic susceptibility for Cp*$_2$Dy(TIP), **1–Dy**, under a 1250 Oe applied dc field S38
Figure S44. Out-of-phase (χ_M'') components of the ac magnetic susceptibility for Cp*$_2$Dy(TIP), **1–Dy**, under a 1250 Oe applied dc field S39

Figure S45. Cole−Cole plots for ac magnetic susceptibility of Cp*$_2$Dy(TIP), **1–Dy**, collected under a 1250 Oe applied dc field S39
Figure S46. Plot of the natural log of the relaxation time, τ, *vs*. inverse temperature, 1/*T*, for Cp*$_2$Dy(TIP), **1–Dy** S40
Figure S47. Field-dependent magnetization data for Cp*$_2$Gd(TIP), **1–Gd** S40
Figure S48. Field-dependent reduced magnetization data for Cp*$_2$Gd(TIP), **1–Gd** S41
Figure S49. Field-dependent magnetization data for Cp*$_2$Dy(TIP), **1–Dy** S41
Figure S50. Field-dependent reduced magnetization data for Cp*$_2$Dy(TIP), **1–Dy** S42
Figure S51. Variable-field magnetization (*M)* data for Cp*$_2$Dy(TIP), **1–Dy** S42
Figure S52. Magnified variable-field magnetization (*M)* data for Cp*$_2$Dy(TIP), **1–Dy** S43
Figure S53. Out-of-phase (χ_M'') components of the ac magnetic susceptibility for Cp*$_2$Dy(DMP), **2–Dy**, under zero applied dc field S43
Figure S54. Out-of-phase components of the ac magnetic susceptibility (χ_M'') for Cp*$_2$Dy(DMP), **2–Dy**, ranging from 0 to 1550 Oe applied dc fields S44
Figure S55. In-phase (χ_M') components of the ac magnetic susceptibility for Cp*$_2$Dy(DMP), **2–Dy**, under a 1450 Oe applied dc field S44
Figure S56. Out-of-phase (χ_M'') components of the ac magnetic susceptibility for Cp*$_2$Dy(DMP), **2–Dy**, under a 1450 Oe applied dc field S45
Figure S57. Cole−Cole plots for ac magnetic susceptibility of Cp*$_2$Dy(DMP), **2–Dy**, collected under a 1450 Oe applied dc field S45
Figure S58. Plot of the natural log of the relaxation time, τ, *vs*. inverse temperature, 1/*T*, for Cp*$_2$Dy(DMP), **2–Dy** S46
Figure S59. Field-dependent magnetization data for Cp*$_2$Dy(DMP), **2–Dy** S46
Figure S60. Field-dependent reduced magnetization data for Cp*$_2$Dy(DMP), **2–Dy** S47
Figure S61. Variable-field magnetization (*M)* data for Cp*$_2$Dy(DMP), **2–Dy** S47

EPR Spectroscopy S48
Table S10. Spin Hamiltonian parameters for Cp*$_2$Gd(TIP) S48

***Ab Initio* Calculations S49**
Method for CASSCF calculations S49

Table S11. Calculated Kramers doublet (KD) energies, associated magnetic moments, *g*-tensors, and wavefunction composition for Cp*$_2$Dy(TIP), **1–Dy** at 100 K S50
Table S12. Calculated Kramers doublet (KD) energies, associated magnetic moments, *g*-tensors, and wavefunction composition for Cp*$_2$Dy(TIP), **1–Dy** at 200 K S50
Table S13. Calculated Kramers doublet (KD) energies, associated magnetic moments, *g*-tensors, and wavefunction composition for Cp*$_2$Dy(TIP), **1–Dy** at 300 K S51
Table S14. Calculated Kramers doublet (KD) energies, associated magnetic moments, *g*-tensors, and wavefunction composition for Cp*$_2$Dy(DMP), **2–Dy** at 100 K S51
Table S15. Calculated crystal field parameters for Cp*$_2$Dy(TIP), **1–Dy** at 100 K S52
Table S16. Calculated crystal field parameters for Cp*$_2$Dy(TIP), **1–Dy** at 200 K S52
Table S17. Calculated crystal field parameters for Cp*$_2$Dy(TIP), **1–Dy** at 300 K S53
Table S18. Calculated crystal field parameters for Cp*$_2$Dy(DMP), **2–Dy** at 100 K S53
Table S19. Calculated average transition dipole moments for Cp*$_2$Dy(TIP), **1–Dy** at 100 K S54
Table S20. Calculated average transition dipole moments for Cp*$_2$Dy(TIP), **1–Dy** at 200 K S55
Table S21. Calculated average transition dipole moments for Cp*$_2$Dy(TIP), **1–Dy** at 300 K S56
Table S22. Calculated average transition dipole moments for Cp*$_2$Dy(DMP), **2–Dy** at 100 K S57
Figure S62. Calculated full relaxation barrier for Cp*$_2$Dy(TIP), **1–Dy** S58
Figure S63. Calculated full relaxation barrier for Cp*$_2$Dy(DMP), **2–Dy** S59
Figure S64. Estimated relaxation barrier of Cp*$_2$Dy(TIP), **1–Dy**, with relaxation pathways S60
Figure S65. Estimated relaxation barrier of Cp*$_2$Dy(DMP), **2–Dy**, with relaxation pathways S61
Figure S66. Plot of *g*-tensor components of Cp*$_2$Dy(TIP), **1–Dy** S62
Figure S67. Plot of *g*-tensor components of Cp*$_2$Dy(DMP), **2–Dy** S62
Table S23. Spin-orbit coupling constants and Slater Condon parameters of **1–Dy** and **2–Dy** S63
Figure S68. Variable-temperature dc magnetic susceptibility data ($\chi_M T$ *vs*. *T*) of Cp*$_2$Dy(TIP), **1–Dy**, with *ab initio* calculated values S64
Figure S69. Variable-temperature dc magnetic susceptibility data ($\chi_M T$ *vs*. *T*) of Cp*$_2$Dy(DMP), **2–Dy**, with *ab initio* calculated values S64
Figure S70. Field-dependent magnetization data of Cp*$_2$Dy(TIP), **1–Dy**, with the *ab initio* calculated values S65

Figure S71. Field-dependent magnetization data of Cp*$_2$Dy(DMP), **2–Dy**, with the *ab initio* calculated values S65

DFT Calculations **S66**
Method for Estimating pK_a values S66
Table S24. Computed Gibbs free energies and pK_a values S67
Table S25. Computed energies of solvation S67
Table S26. Computed and average experimental bond metrics of Cp*$_2$Y(TIP), **1–Y** S68
Table S27. Computed and average experimental bond metrics of Cp*$_2$Y(TIP), **1–Y**, highlighting the Y–TIP interaction S69
Figure S72. Comparison of experimental FTIR spectrum and calculated stretching frequencies of Cp*$_2$Y(TIP), **1–Y** S70
Table S28. Major contributions of the TDDFT calculated transitions of **1–Y** S71
Table S29. Second order perturbation analysis of the NLMOs of **1–Y** S74
Table S30. Computed and average experimental bond metrics of Cp*$_2$Y(DMP), **2–Y** S78
Table S31. Computed and average experimental bond metrics of Cp*$_2$Y(DMP), **2–Y**, highlighting the Y–DMP interaction S79
Figure S73. Comparison of experimental FTIR spectrum and calculated stretching frequencies Cp*$_2$Y(DMP), **2–Y** S80
Figure S74. Frontier orbitals of Cp*$_2$Y(DMP), **2–Y** S81
Table S32. Second order perturbation analysis of the NLMOs of **2–Y** S82
Table S33. Optimized coordinates of Cp*$_2$Y(TIP), **1–Y** S85
Table S34. Optimized coordinates of Cp*$_2$Y(DMP), **2–Y** S87
Table S35. Optimized coordinates of Cp*$_2$Dy(TIP), **1–Dy** at 100 K S89
Table S36. Optimized coordinates of Cp*$_2$Dy(TIP), **1–Dy** at 200 K S91
Table S37. Optimized coordinates of Cp*$_2$Dy(TIP), **1–Dy** at 300 K S93
Table S38. Optimized coordinates of Cp*$_2$Dy(DMP), **2–Dy** at 100 K S95

References S97

X-Ray Crystallography

Table S1. Crystal data and structural refinement of Cp*$_2$RE(TIP), (RE = Y (**1–Y**), Gd (**1–Gd**), Dy (**1–Dy**)). **1–RE** crystallized with one dichloromethane solvent molecule in the lattice as: Cp*$_2$RE(TIP)·CH_2Cl_2.

Compound	**1–Y**	**1–Gd**	**1–Dy**
Empirical formula	$C_{25}H_{32}Cl_2I_4NY$	$C_{25}H_{32}Cl_2I_4NGd$	$C_{25}H_{32}Cl_2I_4NDy$
CCDC Number	2350214	2350213	2350192
Formula weight (g mol^{-1})	1013.92	1082.26	1087.51
Temperature (K)	100.0(2)	99.8(6)	100.01(10)
Crystal system	Monoclinic	Monoclinic	Monoclinic
Space group	$P2_1/c$	$P2_1/c$	$P2_1/c$
Unit Cell Dimensions			
a (Å)	10.30610(10)	10.3396(2)	10.3100(2)
b (Å)	14.2414(2)	14.3064(3)	14.2475(2)
c (Å)	21.2495(4)	21.2014(4)	21.2431(4)
α (°)	90	90	90
β (°)	101.465(2)	101.314(2)	101.444(2)
γ (°)	90	90	90
Volume (Å^3)	3056.63(8)	3075.22(11)	3058.40(10)
Z	4	4	4
ρ_{calc} (g cm^{-3})	2.203	2.338	2.362
μ (mm^{-1})	36.121	6.361	6.671
F(000)	1896.0	1996.0	2004.0
Crystal size (mm^3)	0.2 × 0.14 × 0.06	0.38 × 0.22 × 0.08	0.353 × 0.275 × 0.111
Radiation	Cu Kα (λ = 1.54184)	Mo Kα (λ = 0.71073)	Mo Kα (λ = 0.71073)
2Θ range for data collection (°)	7.52 to 160.552	4.924 to 63.38	4.942 to 63.436
Reflections collected	17339	36647	37524
Independent reflections	5979 R_{int} = 0.0599	8616 R_{int} = 0.0426	8694 R_{int} = 0.0544
Data/restraints/parameters	5979/6/317	8616/0/308	8694/6/317
Goodness-of-fit on F^2	0.999	1.064	1.046
Final R indexes [I>=2σ (I)]	R_1 = 0.0589, wR_2 = 0.1620	R_1 = 0.0301, wR_2 = 0.0686	R_1 = 0.0304, wR_2 = 0.0713
Final R indexes [all data]	R_1 = 0.0646, wR_2 = 0.1699	R_1 = 0.0375, wR_2 = 0.0719	R_1 = 0.0380, wR_2 = 0.0749
Largest diff. peak/hole (e Å^{-3})	2.38/-2.18	2.13/-2.21	1.60/-1.62

Table S2. Crystal data and structural refinement of $Cp^*_2Dy(TIP)$, **1–Dy**, at 110 K (**1–Dy – 110 K**), 120 K (**1–Dy – 120 K**), and 130 K (**1–Dy – 130 K**). **1–Dy** crystallized with one dichloromethane solvent molecule in the lattice as: $Cp^*_2Dy(TIP)\cdot CH_2Cl_2$.

Compound	**1–Dy – 110 K**	**1–Dy – 120 K**	**1–Dy – 130 K**
Empirical formula	$C_{25}H_{32}Cl_2I_4NDy$	$C_{25}H_{32}Cl_2I_4NDy$	$C_{25}H_{32}Cl_2I_4NDy$
CCDC Number	2350209	2350204	2350212
Formula weight (g mol^{-1})	1087.51	1087.51	1087.51
Temperature (K)	110.01(10)	120.01(10)	130.15(10)
Crystal system	Monoclinic	Monoclinic	Monoclinic
Space group	$P2_1/c$	$P2_1/c$	$P2_1/c$
Unit Cell Dimensions			
a (Å)	10.31657(18)	10.32380(19)	10.33049(19)
b (Å)	14.2556(2)	14.2662(2)	14.2778(2)
c (Å)	21.2459(4)	21.2517(4)	21.2557(4)
α (°)	90	90	90
β (°)	101.4755(17)	101.5232(18)	101.5531(18)
γ (°)	90	90	90
Volume ($Å^3$)	3062.15(9)	3066.90(10)	3071.64(10)
Z	4	4	4
ρ_{calc} (g cm^{-3})	2.359	2.355	2.352
μ (mm^{-1})	6.662	6.652	6.642
F(000)	2004.0	2004.0	2004.0
Crystal size (mm^3)	0.353 × 0.275 × 0.111	0.353 × 0.275 × 0.111	0.353 × 0.275 × 0.111
Radiation	Mo Kα (λ = 0.71073)	Mo Kα (λ = 0.71073)	Mo Kα (λ = 0.71073)
2Θ range for data collection (°)	4.94 to 63.47	4.936 to 63.418	4.934 to 63.384
Reflections collected	37662	37712	37863
Independent reflections	8713 R_{int} = 0.0526	8716 R_{int} = 0.0505	8742 R_{int} = 0.0506
Data/restraints/parameters	8713/6/317	8716/6/317	8742/6/317
Goodness-of-fit on F^2	1.041	1.040	1.032
Final R indexes [I>=2σ (I)]	R_1 = 0.0308, wR_2 = 0.0733	R_1 = 0.0289, wR_2 = 0.0660	R_1 = 0.0297, wR_2 = 0.0661
Final R indexes [all data]	R_1 = 0.0389, wR_2 = 0.0770	R_1 = 0.0376, wR_2 = 0.0697	R_1 = 0.0394, wR_2 = 0.0704
Largest diff. peak/hole (e $Å^{-3}$)	1.51/-1.75	1.21/-1.44	1.16/-1.26

Table S3. Crystal data and structural refinement of $Cp^*_2Dy(TIP)$, **1–Dy**, at 140 K (**1–Dy – 140 K**), 150 K (**1–Dy – 150 K**), and 160 K (**1–Dy – 160 K**). **1–Dy** crystallized with one dichloromethane solvent molecule in the lattice as: $Cp^*_2Dy(TIP)\cdot CH_2Cl_2$.

Compound	**1–Dy – 140 K**	**1–Dy – 150 K**	**1–Dy – 160 K**
Empirical formula	$C_{25}H_{32}Cl_2I_4NDy$	$C_{25}H_{32}Cl_2I_4NDy$	$C_{25}H_{32}Cl_2I_4NDy$
CCDC Number	2350203	2350207	2350202
Formula weight (g mol^{-1})	1087.51	1087.51	1087.51
Temperature (K)	140.15(10)	150.0(1)	160.0(1)
Crystal system	Monoclinic	Monoclinic	Monoclinic
Space group	$P2_1/c$	$P2_1/c$	$P2_1/c$
Unit Cell Dimensions			
a (Å)	10.33800(19)	10.3440(2)	10.3478(2)
b (Å)	14.2897(3)	14.3003(3)	14.3119(3)
c (Å)	21.2600(4)	21.2652(4)	21.2778(4)
α (°)	90	90	90
β (°)	101.5874(18)	101.6271(19)	101.6536(19)
γ (°)	90	90	90
Volume ($Å^3$)	3076.66(10)	3081.07(11)	3086.22(11)
Z	4	4	4
ρ_{calc} (g cm^{-3})	2.348	2.344	2.341
μ (mm^{-1})	6.631	6.621	6.610
F(000)	2004.0	2004.0	2004.0
Crystal size (mm^3)	0.353 × 0.275 × 0.111	0.353 × 0.275 × 0.111	0.353 × 0.275 × 0.111
Radiation	Mo Kα (λ = 0.71073)	Mo Kα (λ = 0.71073)	Mo Kα (λ = 0.71073)
2Θ range for data collection (°)	4.93 to 63.36	4.928 to 63.52	4.926 to 63.37
Reflections collected	37940	38238	38312
Independent reflections	8758 R_{int} = 0.0511	8771 R_{int} = 0.0517	8785 R_{int} = 0.0524
Data/restraints/parameters	8758/6/317	8771/6/317	8785/6/317
Goodness-of-fit on F^2	1.028	1.050	1.059
Final R indexes [I>=2σ (I)]	R_1 = 0.0297, wR_2 = 0.0664	R_1 = 0.0293, wR_2 = 0.0648	R_1 = 0.0297, wR_2 = 0.0654
Final R indexes [all data]	R_1 = 0.0396, wR_2 = 0.0708	R_1 = 0.0384, wR_2 = 0.0682	R_1 = 0.0396, wR_2 = 0.0692
Largest diff. peak/hole (e $Å^{-3}$)	1.16/-1.28	1.02/-1.12	1.23/-1.39

Table S4. Crystal data and structural refinement of $Cp^*_2Dy(TIP)$, **1–Dy**, at 170 K (**1–Dy – 170 K**), 180 K (**1–Dy – 180 K**), and 190 K (**1–Dy – 190 K**). **1–Dy** crystallized with one dichloromethane solvent molecule in the lattice as: $Cp^*_2Dy(TIP)\cdot CH_2Cl_2$.

Compound	**1–Dy – 170 K**	**1–Dy – 180 K**	**1–Dy – 190 K**
Empirical formula	$C_{25}H_{32}Cl_2I_4NDy$	$C_{25}H_{32}Cl_2I_4NDy$	$C_{25}H_{32}Cl_2I_4NDy$
CCDC Number	2350198	2350200	2350199
Formula weight (g mol^{-1})	1087.51	1087.51	1087.51
Temperature (K)	170.0(1)	180.0(1)	190.0(1)
Crystal system	Monoclinic	Monoclinic	Monoclinic
Space group	$P2_1/c$	$P2_1/c$	$P2_1/c$
Unit Cell Dimensions			
a (Å)	10.3485(2)	10.3538(2)	10.3596(2)
b (Å)	14.3166(3)	14.3266(3)	14.3374(3)
c (Å)	21.2970(5)	21.3096(5)	21.3250(5)
α (°)	90	90	90
β (°)	101.719(2)	101.766(2)	101.800(2)
γ (°)	90	90	90
Volume ($Å^3$)	3089.48(12)	3094.51(13)	3100.47(13)
Z	4	4	4
ρ_{calc} (g cm^{-3})	2.338	2.334	2.330
μ (mm^{-1})	6.603	6.593	6.580
F(000)	2004.0	2004.0	2004.0
Crystal size (mm^3)	0.353 × 0.275 × 0.111	0.353 × 0.275 × 0.111	0.353 × 0.275 × 0.111
Radiation	Mo Kα (λ = 0.71073)	Mo Kα (λ = 0.71073)	Mo Kα (λ = 0.71073)
2Θ range for data collection (°)	4.926 to 63.358	4.922 to 63.56	4.92 to 63.514
Reflections collected	38295	38434	38506
Independent reflections	8797 R_{int} = 0.0516	8816 R_{int} = 0.0541	8841 R_{int} = 0.0547
Data/restraints/parameters	8797/6/317	8816/6/317	8841/6/317
Goodness-of-fit on F^2	1.050	1.057	1.039
Final R indexes [I>=2σ (I)]	R_1 = 0.0306, wR_2 = 0.0677	R_1 = 0.0316, wR_2 = 0.0706	R_1 = 0.0321, wR_2 = 0.0721
Final R indexes [all data]	R_1 = 0.0421, wR_2 = 0.0723	R_1 = 0.0438, wR_2 = 0.0756	R_1 = 0.0442, wR_2 = 0.0767
Largest diff. peak/hole (e $Å^{-3}$)	1.10/-1.12	1.12/-1.44	1.09/-1.51

Table S5. Crystal data and structural refinement of $Cp^*_2Dy(TIP)$, **1–Dy**, at 200 K (**1–Dy – 200 K**), 210 K (**1–Dy – 210 K**), and 220 K (**1–Dy – 220 K**). **1–Dy** crystallized with one dichloromethane solvent molecule in the lattice as: $Cp^*_2Dy(TIP)\cdot CH_2Cl_2$.

Compound	**1–Dy – 200 K**	**1–Dy – 210 K**	**1–Dy – 220 K**
Empirical formula	$C_{25}H_{32}Cl_2I_4NDy$	$C_{25}H_{32}Cl_2I_4NDy$	$C_{25}H_{32}Cl_2I_4NDy$
CCDC Number	2350196	2350211	2350206
Formula weight (g mol^{-1})	1087.51	1087.51	1087.51
Temperature (K)	200.0(1)	210.0(1)	220.0(1)
Crystal system	Monoclinic	Monoclinic	Monoclinic
Space group	$P2_1/c$	$P2_1/c$	$P2_1/c$
Unit Cell Dimensions			
a (Å)	10.3635(2)	10.3697(2)	10.3772(2)
b (Å)	14.3461(3)	14.3573(3)	14.3687(3)
c (Å)	21.3369(5)	21.3576(5)	21.3762(5)
α (°)	90	90	90
β (°)	101.833(2)	101.856(2)	101.907(2)
γ (°)	90	90	90
Volume ($Å^3$)	3104.86(13)	3111.93(12)	3118.76(13)
Z	4	4	4
ρ_{calc} (g cm^{-3})	2.326	2.321	2.316
μ (mm^{-1})	6.571	6.556	6.541
F(000)	2004.0	2004.0	2004.0
Crystal size (mm^3)	0.353 × 0.275 × 0.111	0.353 × 0.275 × 0.111	0.353 × 0.275 × 0.111
Radiation	Mo Kα (λ = 0.71073)	Mo Kα (λ = 0.71073)	Mo Kα (λ = 0.71073)
2Θ range for data collection (°)	4.918 to 63.358	4.916 to 63.306	4.912 to 63.456
Reflections collected	38696	38782	39005
Independent reflections	8865 R_{int} = 0.0542	8878 R_{int} = 0.0558	8903 R_{int} = 0.0563
Data/restraints/parameters	8865/6/317	8878/6/317	8903/6/317
Goodness-of-fit on F^2	1.055	1.051	1.054
Final R indexes [$I>=2\sigma(I)$]	R_1 = 0.0318, wR_2 = 0.0697	R_1 = 0.0331, wR_2 = 0.0727	R_1 = 0.0334, wR_2 = 0.0743
Final R indexes [all data]	R_1 = 0.0438, wR_2 = 0.0740	R_1 = 0.0457, wR_2 = 0.0773	R_1 = 0.0467, wR_2 = 0.0792
Largest diff. peak/hole (e $Å^{-3}$)	1.01/-1.36	1.12/-1.47	1.19/-1.44

Table S6. Crystal data and structural refinement of $Cp^*_2Dy(TIP)$, **1–Dy**, at 230 K (**1–Dy – 230 K**), 240 K (**1–Dy – 240 K**), and 250 K (**1–Dy – 250 K**). **1–Dy** crystallized with one dichloromethane solvent molecule in the lattice as: $Cp^*_2Dy(TIP)\cdot CH_2Cl_2$.

Compound	**1–Dy – 230 K**	**1–Dy – 240 K**	**1–Dy – 250 K**
Empirical formula	$C_{25}H_{32}Cl_2I_4NDy$	$C_{25}H_{32}Cl_2I_4NDy$	$C_{25}H_{32}Cl_2I_4NDy$
CCDC Number	2350210	2350208	2350197
Formula weight (g mol^{-1})	1087.51	1087.51	1087.51
Temperature (K)	230.0(1)	240.0(1)	250.0(1)
Crystal system	Monoclinic	Monoclinic	Monoclinic
Space group	$P2_1/c$	$P2_1/c$	$P2_1/c$
Unit Cell Dimensions			
a (Å)	10.3816(2)	10.3865(2)	10.3931(3)
b (Å)	14.3751(3)	14.3825(3)	14.3920(4)
c (Å)	21.3967(5)	21.4194(5)	21.4414(6)
α (°)	90	90	90
β (°)	101.960(2)	102.000(2)	102.072(3)
γ (°)	90	90	90
Volume ($Å^3$)	3123.84(13)	3129.79(13)	3136.21(14)
Z	4	4	4
ρ_{calc} (g cm^{-3})	2.312	2.308	2.303
μ (mm^{-1})	6.531	6.518	6.505
F(000)	2004.0	2004.0	2004.0
Crystal size (mm^3)	0.353 × 0.275 × 0.111	0.353 × 0.275 × 0.111	0.353 × 0.275 × 0.111
Radiation	Mo Kα (λ = 0.71073)	Mo Kα (λ = 0.71073)	Mo Kα (λ = 0.71073)
2Θ range for data collection (°)	4.91 to 63.234	4.908 to 63.582	4.906 to 63.506
Reflections collected	39034	39147	39250
Independent reflections	8896 R_{int} = 0.0572	8935 R_{int} = 0.0562	8957 R_{int} = 0.0575
Data/restraints/parameters	8896/6/317	8935/6/317	8957/6/317
Goodness-of-fit on F^2	1.055	1.045	1.039
Final R indexes [I>=2σ (I)]	R_1 = 0.0339, wR_2 = 0.0746	R_1 = 0.0341, wR_2 = 0.0741	R_1 = 0.0364, wR_2 = 0.0795
Final R indexes [all data]	R_1 = 0.0486, wR_2 = 0.0802	R_1 = 0.0500, wR_2 = 0.0797	R_1 = 0.0531, wR_2 = 0.0853
Largest diff. peak/hole (e $Å^{-3}$)	1.12/-1.27	0.92/-1.35	0.96/-1.26

Table S7. Crystal data and structural refinement of $Cp^*_2Dy(TIP)$, **1–Dy**, at 260 K (**1–Dy – 260 K**), 270 K (**1–Dy – 270 K**), and 280 K (**1–Dy – 280 K**). **1–Dy** crystallized with one dichloromethane solvent molecule in the lattice as: $Cp^*_2Dy(TIP)\cdot CH_2Cl_2$.

Compound	**1–Dy – 260 K**	**1–Dy – 270 K**	**1–Dy – 280 K**
Empirical formula	$C_{25}H_{32}Cl_2I_4NDy$	$C_{25}H_{32}Cl_2I_4NDy$	$C_{25}H_{32}Cl_2I_4NDy$
CCDC Number	2350205	2350195	2350201
Formula weight (g mol^{-1})	1087.51	1087.51	1087.51
Temperature (K)	260.0(1)	270.0(1)	280.0(1)
Crystal system	Monoclinic	Monoclinic	Monoclinic
Space group	$P2_1/c$	$P2_1/c$	$P2_1/c$
Unit Cell Dimensions			
a (Å)	10.3990(3)	10.4052(3)	10.4058(3)
b (Å)	14.3997(4)	14.4040(4)	14.4072(4)
c (Å)	21.4703(6)	21.4880(7)	21.5108(7)
α (°)	90	90	90
β (°)	102.143(3)	102.191(3)	102.195(3)
γ (°)	90	90	90
Volume ($Å^3$)	3143.08(16)	3147.91(16)	3152.09(17)
Z	4	4	4
ρ_{calc} (g cm^{-3})	2.298	2.295	2.292
μ (mm^{-1})	6.491	6.481	6.472
F(000)	2004.0	2004.0	2004.0
Crystal size (mm^3)	0.353 × 0.275 × 0.111	0.353 × 0.275 × 0.111	0.353 × 0.275 × 0.111
Radiation	Mo Kα (λ = 0.71073)	Mo Kα (λ = 0.71073)	Mo Kα (λ = 0.71073)
2Θ range for data collection (°)	4.904 to 63.582	4.902 to 63.538	4.902 to 63.58
Reflections collected	39342	39345	39364
Independent reflections	8983 R_{int} = 0.0605	8997 R_{int} = 0.0597	8995 R_{int} = 0.0589
Data/restraints/parameters	8983/6/317	8997/6/317	8995/6/317
Goodness-of-fit on F^2	1.044	1.036	1.059
Final R indexes [I>=2σ (I)]	R_1 = 0.0373, wR_2 = 0.0812	R_1 = 0.0372, wR_2 = 0.0802	R_1 = 0.0370, wR_2 = 0.0813
Final R indexes [all data]	R_1 = 0.0558, wR_2 = 0.0880	R_1 = 0.0568, wR_2 = 0.0871	R_1 = 0.0577, wR_2 = 0.0884
Largest diff. peak/hole (e $Å^{-3}$)	1.17/-1.23	0.96/-1.19	1.16/-1.26

Table S8. Crystal data and structural refinement of $Cp^*_2Dy(TIP)$, **1–Dy**, at 260 K (**1–Dy – 290 K**), and 270 K (**1–Dy – 300 K**). **1–Dy** crystallized with one dichloromethane solvent molecule in the lattice as: $Cp^*_2Dy(TIP)\cdot CH_2Cl_2$.

Compound	**1–Dy – 290 K**	**1–Dy – 300 K**
Empirical formula	$C_{25}H_{32}Cl_2I_4NDy$	$C_{25}H_{32}Cl_2I_4NDy$
CCDC Number	2350194	2350193
Formula weight (g mol^{-1})	1087.51	1087.51
Temperature (K)	290.0(1)	300.0(1)
Crystal system	Monoclinic	Monoclinic
Space group	$P2_1/c$	$P2_1/c$
Unit Cell Dimensions		
a (Å)	10.4118(3)	10.4206(3)
b (Å)	14.4128(4)	14.4229(4)
c (Å)	21.5424(7)	21.5777(7)
α (°)	90	90
β (°)	102.244(3)	102.327(3)
γ (°)	90	90
Volume ($Å^3$)	3159.18(16)	3168.25(16)
Z	4	4
ρ_{calc} (g cm^{-3})	2.286	2.280
μ (mm^{-1})	6.458	6.439
F(000)	2004.0	2004.0
Crystal size (mm^3)	0.353 × 0.275 × 0.111	0.353 × 0.275 × 0.111
Radiation	Mo Kα (λ = 0.71073)	Mo Kα (λ = 0.71073)
2Θ range for data collection (°)	4.9 to 63.482	4.898 to 63.432
Reflections collected	39519	39450
Independent reflections	9017 R_{int} = 0.0600	9054 R_{int} = 0.0641
Data/restraints/parameters	9017/6/317	9054/6/317
Goodness-of-fit on F^2	1.040	1.050
Final R indexes [I>=2σ (I)]	R_1 = 0.0373, wR_2 = 0.0817	R_1 = 0.0394, wR_2 = 0.0878
Final R indexes [all data]	R_1 = 0.0595, wR_2 = 0.0888	R_1 = 0.0626, wR_2 = 0.0956
Largest diff. peak/hole (e $Å^{-3}$)	1.02/-1.15	1.16/-1.08

Table S9. Crystal data and structural refinement of $Cp^*_2RE(DMP)$ (RE = Y (**2–Y**) and Dy (**2–Dy**).

Compound	**2–Y**	**2–Dy**
Empirical formula	$C_{26}H_{38}NY$	$C_{26}H_{38}NDy$
CCDC Number	2350215	2350216
Formula weight (g mol^{-1})	454.504	527.07
Temperature (K)	100.0(2)	100.0(2)
Crystal system	Monoclinic	Monoclinic
Space group	$P2_1/c$	$P2_1/c$
Unit Cell Dimensions		
a (Å)	9.34290(6)	9.34360(10)
b (Å)	15.24462(11)	15.2429(2)
c (Å)	16.36886(11)	16.38150(10)
α (°)	90	90
β (°)	98.4832(6)	98.5100(10)
γ (°)	90	90
Volume ($Å^3$)	2305.89(3)	2307.42(4)
Z	4	4
ρ_{calc} (g cm^{-3})	1.309	1.517
μ (mm^{-1})	3.651	17.376
F(000)	961.2	1068.0
Crystal size (mm^3)	0.524 × 0.329 × 0.196	0.283 × 0.174 × 0.138
Radiation	Cu Kα (λ = 1.54184)	Cu Kα (λ = 1.54184)
2Θ range for data collection (°)	7.96 to 160.44	7.964 to 160.548
Reflections collected	19243	25149
Independent reflections	4941 R_{int} = 0.0338	4967 R_{int} = 0.0465
Data/restraints/parameters	4941/0/266	4967/0/265
Goodness-of-fit on F^2	1.025	1.073
Final R indexes [I>=2σ (I)]	R_1 = 0.0257, wR_2 = 0.0673	R_1 = 0.0306, wR_2 = 0.0829
Final R indexes [all data]	R_1 = 0.0276, wR_2 = 0.0686	R_1 = 0.0337, wR_2 = 0.0849
Largest diff. peak/hole (e $Å^{-3}$)	0.48/-0.36	1.89/-1.07

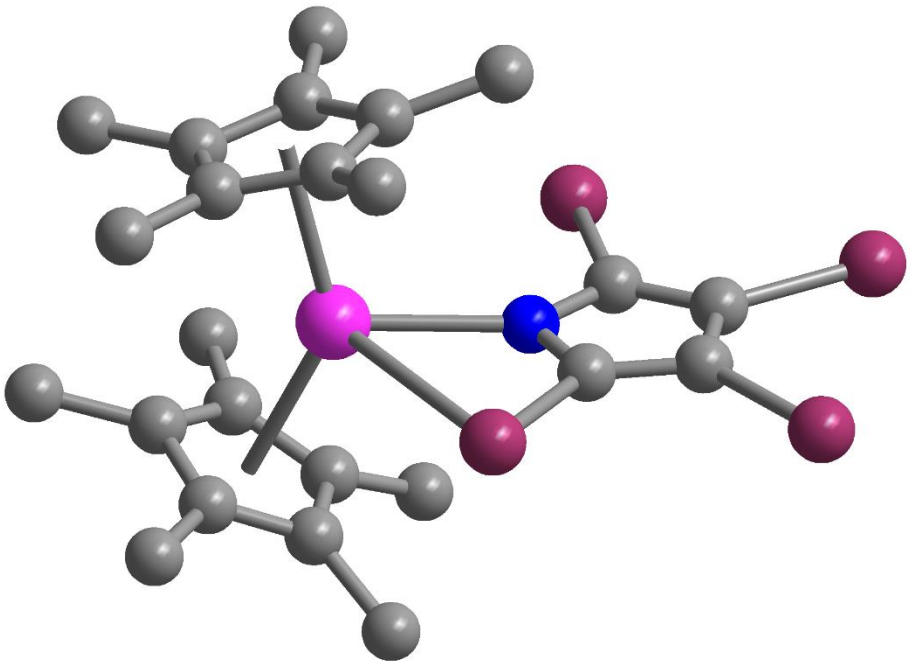

Figure S1. Structure of $Cp^*_2Y(TIP)$, **1–Y**, in a crystal of $Cp^*_2Y(TIP)\cdot CH_2Cl_2$. Pink, purple, blue, and grey spheres represent Y, I, N, and C atoms, respectively. Hydrogen atoms and co-crystallized dichloromethane have been omitted for clarity.

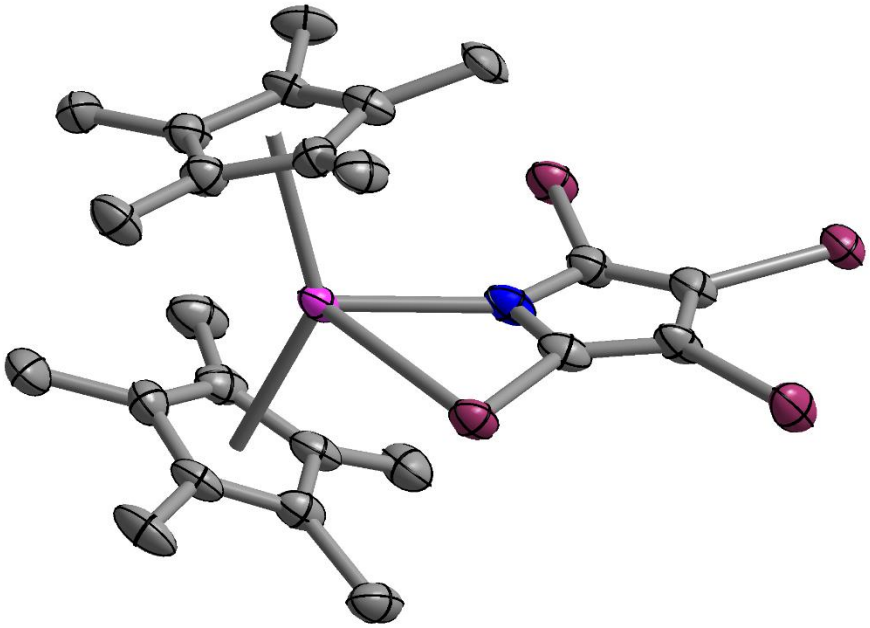

Figure S2. Structure of $Cp^*_2Y(TIP)$, **1–Y**, with thermal ellipsoids drawn at 50%**,** in a crystal of $Cp^*_2Y(TIP)\cdot CH_2Cl_2$. Pink, purple, blue, and grey spheres represent Y, I, N, and C atoms, respectively. Hydrogen atoms and co-crystallized dichloromethane have been omitted for clarity.

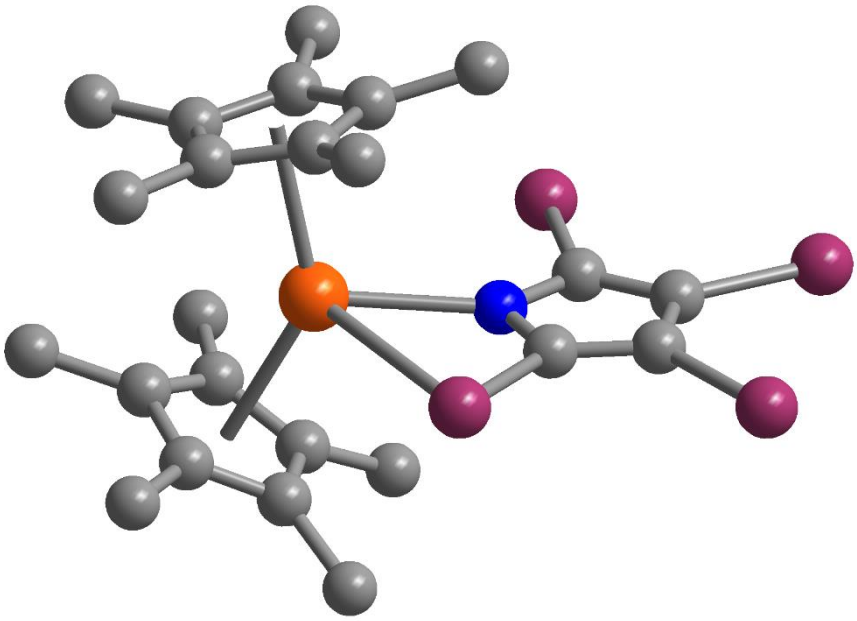

Figure S3. Structure of $Cp^*_2Gd(TIP)$, **1–Gd**, in a crystal of $Cp^*_2Gd(TIP)\cdot CH_2Cl_2$. Orange, purple, blue, and grey spheres represent Gd, I, N, and C atoms, respectively. Hydrogen atoms and co-crystallized dichloromethane have been omitted for clarity.

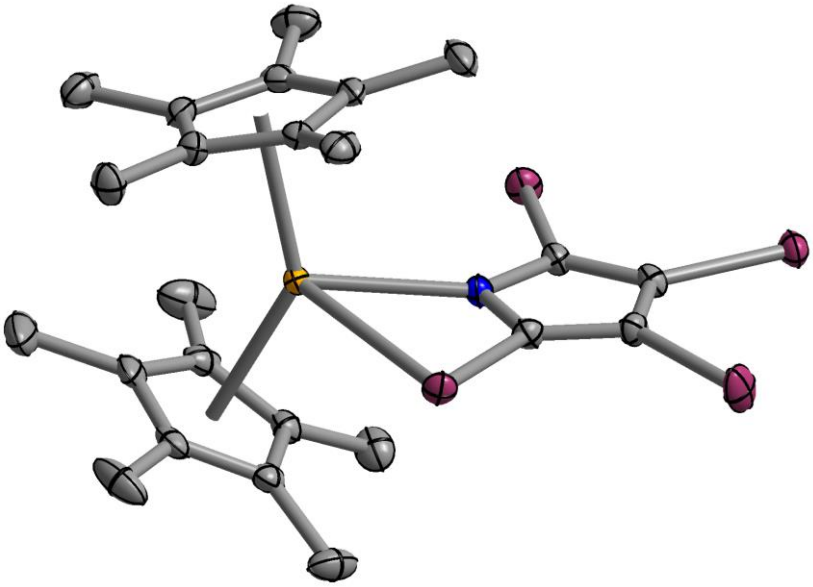

Figure S4. Structure of $Cp^*_2Gd(TIP)$, **1–Gd,** with thermal ellipsoids drawn at 50%**,** in a crystal of $Cp^*_2Gd(TIP)\cdot CH_2Cl_2$. Orange, purple, blue, and grey ellipsoids represent Gd, I, N, and C atoms, respectively. Hydrogen atoms and co-crystallized dichloromethane have been omitted for clarity.

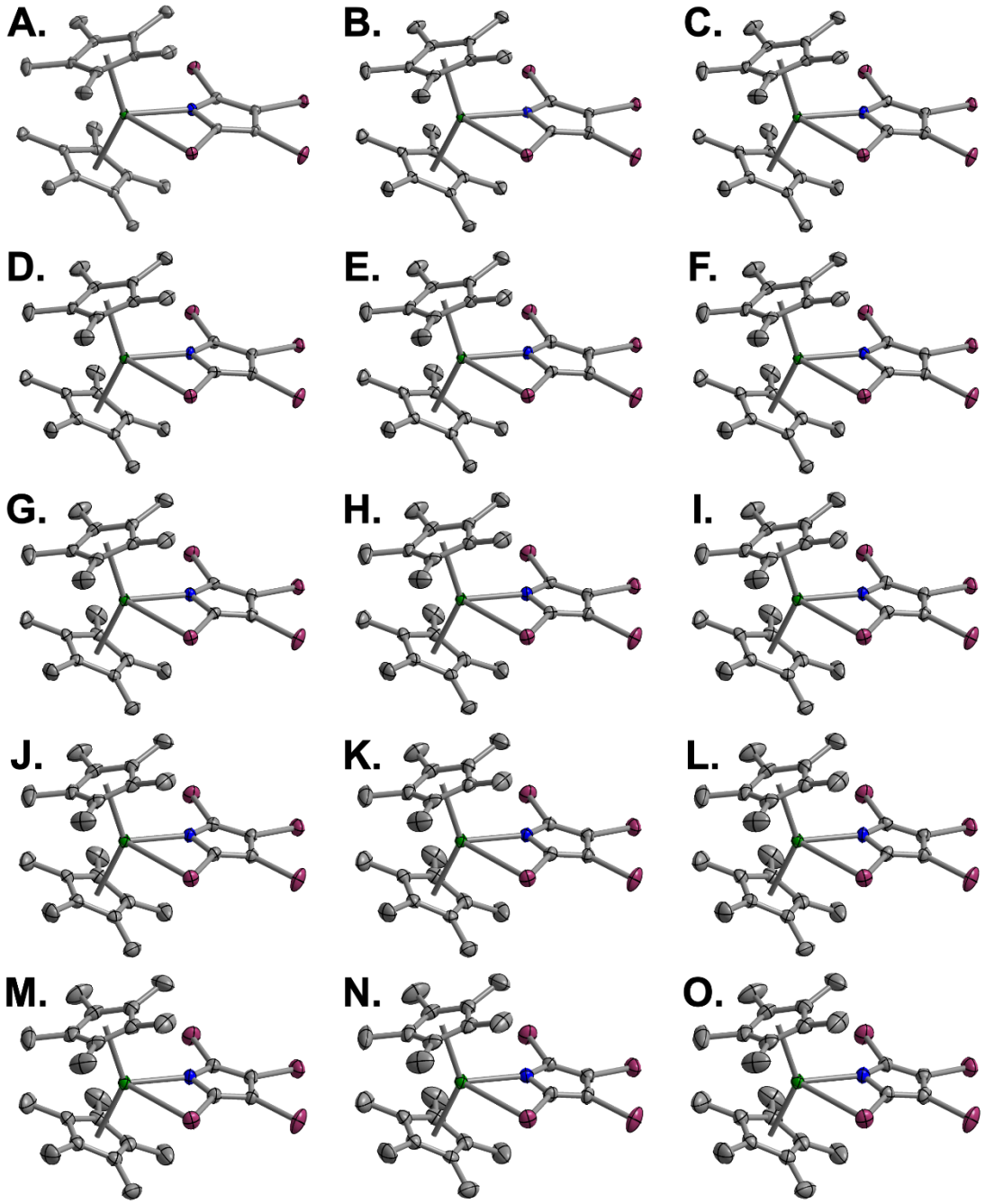

Figure S5. Structure of $Cp^*_2Dy(TIP)$, **1–Dy**, at 100 K (A), 110 K (B), 120 K (C), 130 K (D), 140 K (E), 150 K (F), 160 K (G), 170 K (F), 180 K (G), 190 K (H), 200 K (I), 210 K (J), 220 K (K), 230 K (L), 240 K (M), 250 K (N), and 260 K (O) with thermal ellipsoids drawn at 50%. Green, purple, blue, and grey ellipsoids represent Dy, I, N, and C atoms, respectively. Hydrogen atoms and co-crystallized dichloromethane have been omitted for clarity.

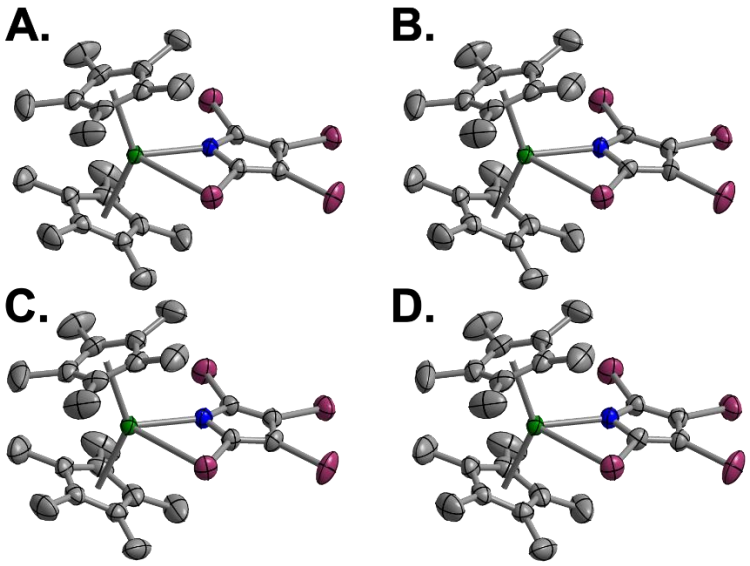

Figure S6. Structure of $Cp^*_2Dy(TIP)$, **1–Dy**, at 270 K (A), 280 K (B), 290 K (C), and 300 K (D) with thermal ellipsoids drawn at 50%. Green, purple, blue, and grey ellipsoids represent Dy, I, N, and C atoms, respectively. Hydrogen atoms and co-crystallized dichloromethane have been omitted for clarity.

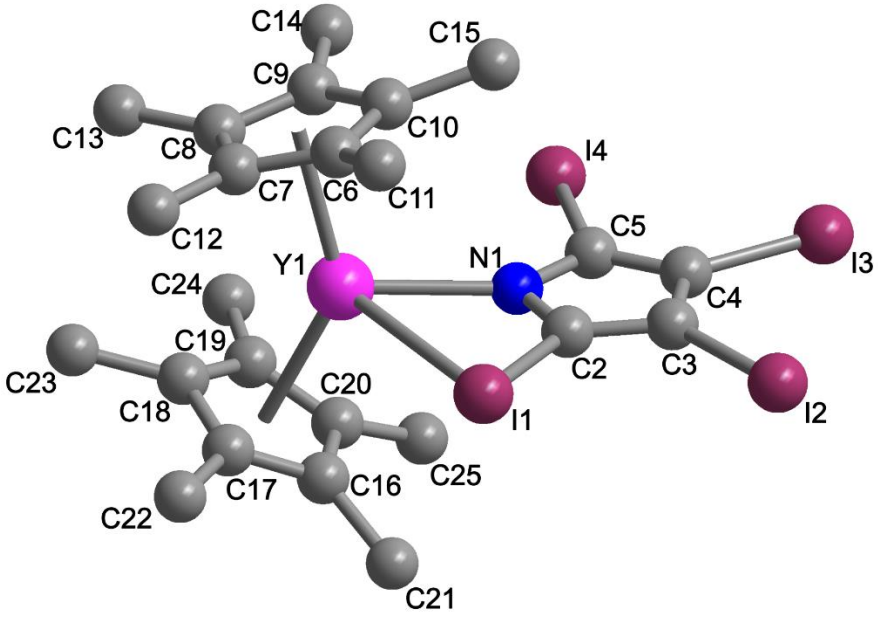

Figure S7. Structure of $Cp^*_2Y(TIP)$, **1–Y**, in a crystal of $Cp^*_2Y(TIP)\cdot CH_2Cl_2$. Pink, purple, blue, and grey spheres represent Y, I, N, and C atoms, respectively. Hydrogen atoms and co-crystallized dichloromethane have been omitted for clarity. Atoms have been labeled for reference (See main text).

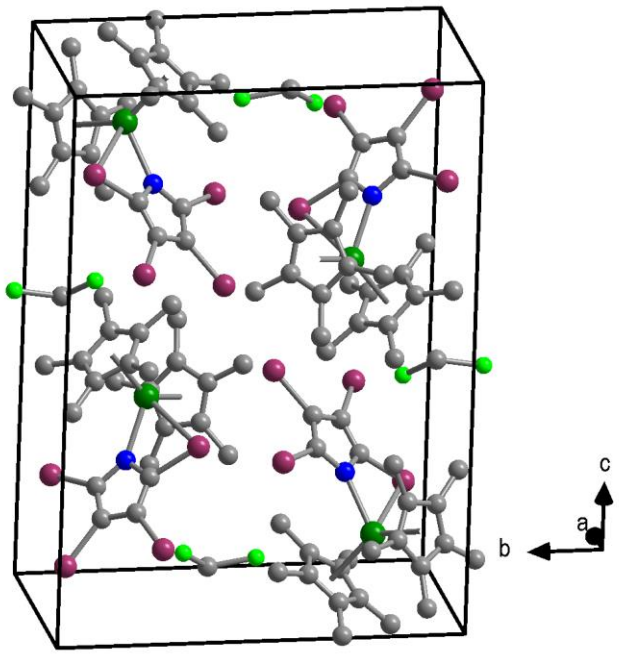

Figure S8. Unit cell of Cp*$_2$Dy(TIP), **1–Dy**. Green, light green, purple, blue, and grey spheres represent Dy, Cl, I, N, and C atoms, respectively. Hydrogen atoms have been omitted for clarity.

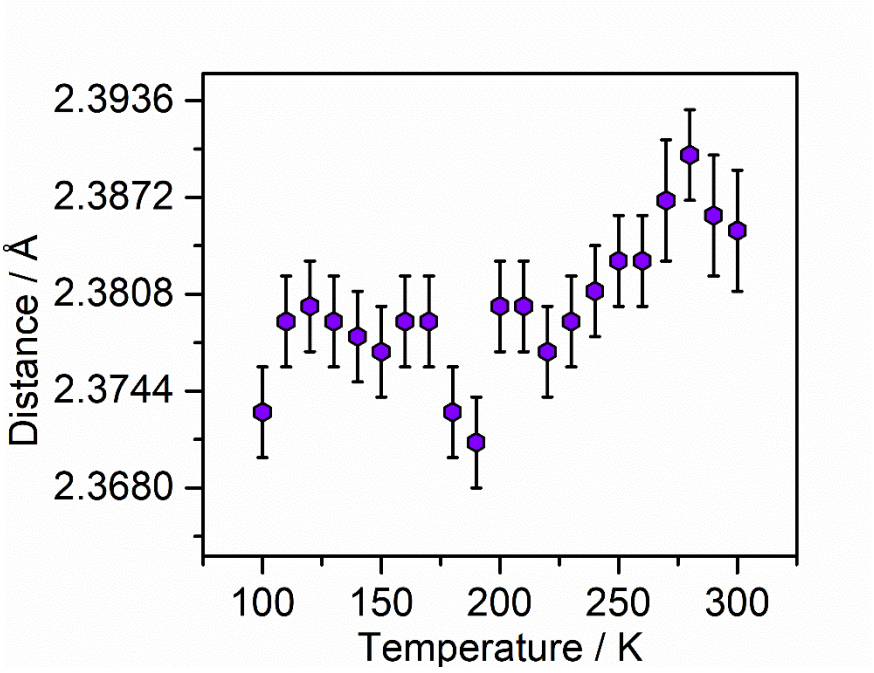

Figure S9. Plot of the temperature dependence of the Dy–N interatomic distance of Cp*$_2$Dy(TIP), **1–Dy**.

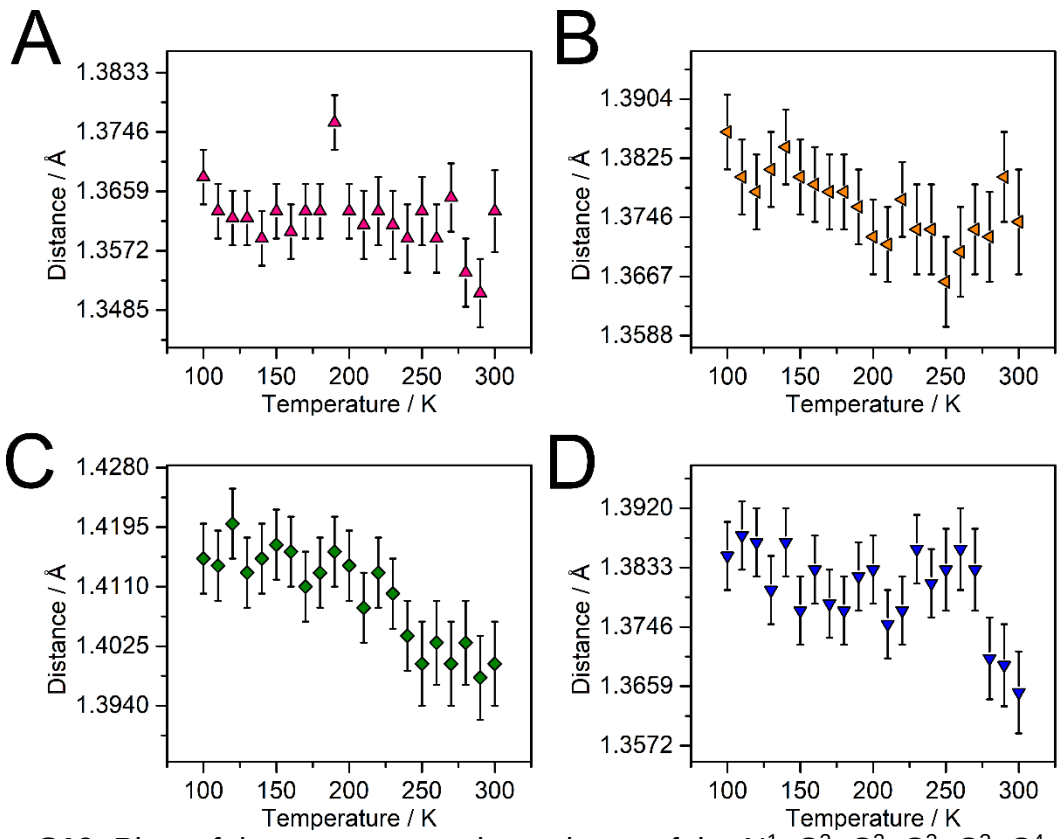

Figure S10. Plots of the temperature dependence of the N^1–C^2, C^2–C^3, C^3–C^4, and C^4–C^5 interatomic distances of Cp*$_2$Dy(TIP), **1–Dy**. See Figure S7 for the relevant atom labels.

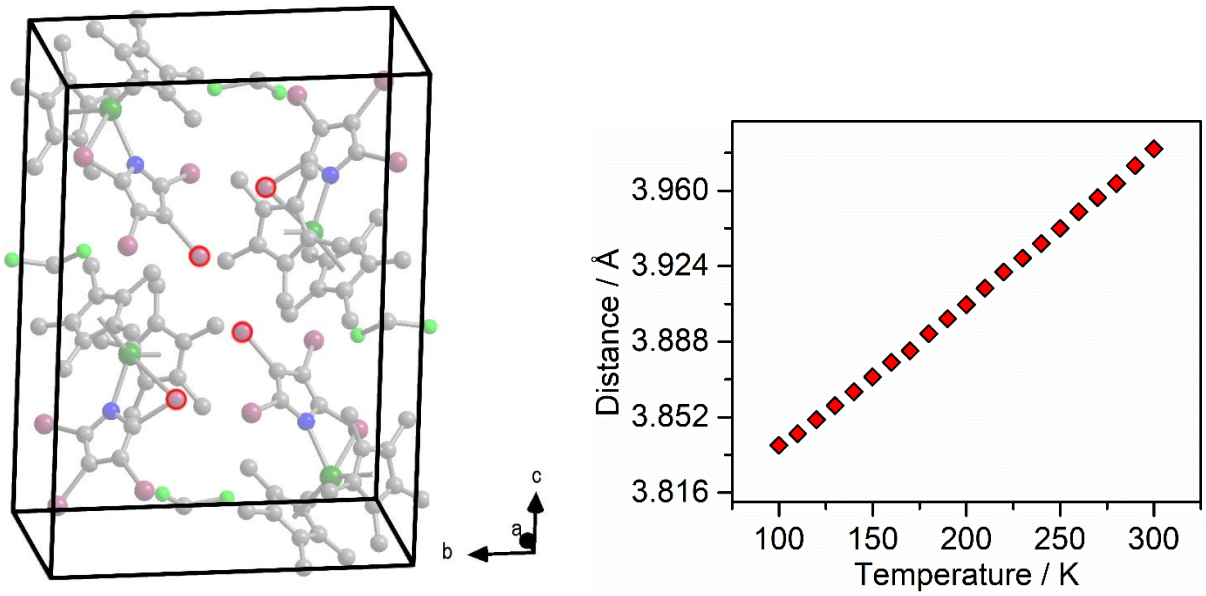

Figure S11. Right, plot of the temperature dependence of the intermolecular I^1–I^3 distances of Cp*$_2$Dy(TIP), **1–Dy**. The relevant atoms are outlined in red in the left unit cell depiction. Error bars are within the radius of the symbols. See Figure S7 for the relevant atom labels.

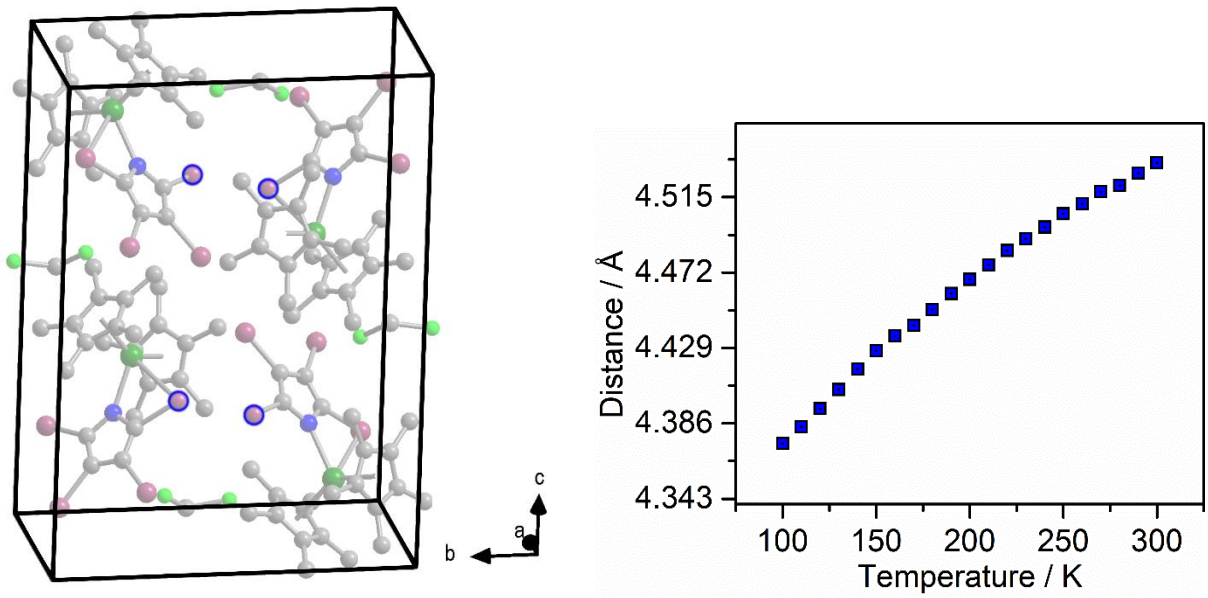

Figure S12. Right, plot of the temperature dependence of the intermolecular I^1–I^4 distances of $Cp^*_2Dy(TIP)$, **1–Dy**. The relevant atoms are outlined in blue in the left unit cell depiction. Error bars are within the radius of the symbols. See Figure S7 for the relevant atom labels.

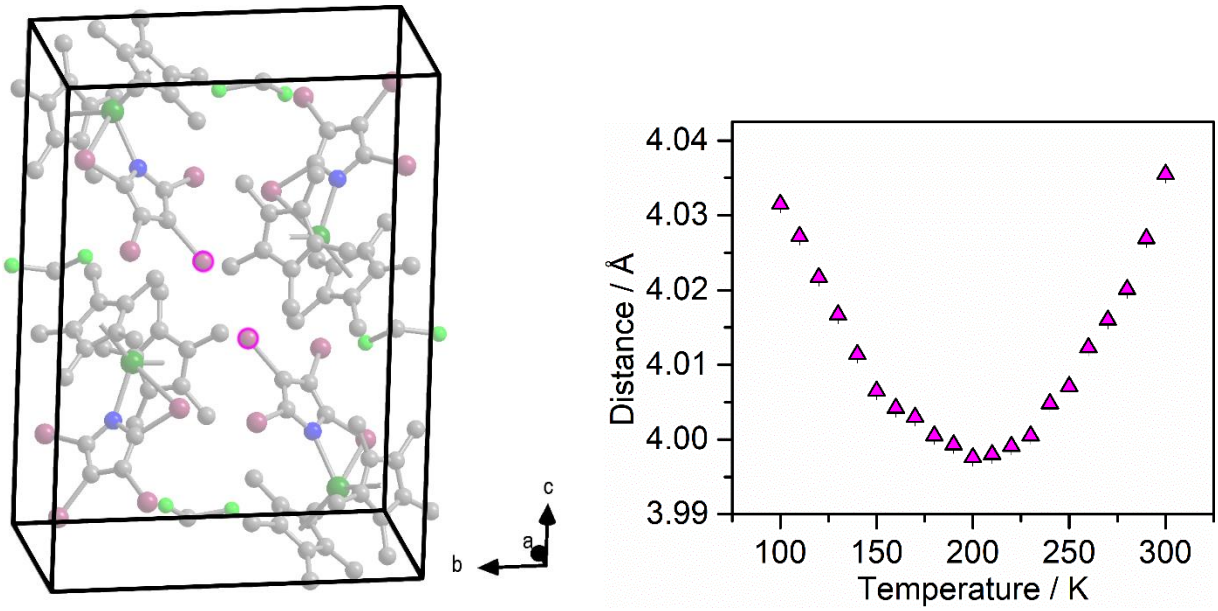

Figure S13. Right, plot of the temperature dependence of the intermolecular I^3–I^3 distances of $Cp^*_2Dy(TIP)$, **1–Dy**. The relevant atoms are outlined in pink in the left unit cell depiction. Error bars are within the radius of the symbols. See Figure S7 for the relevant atom labels.

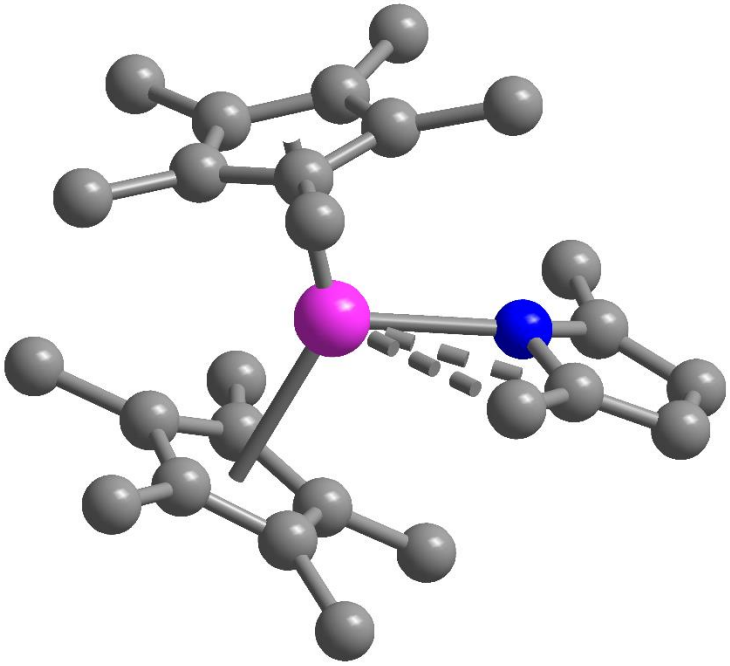

Figure S14. Structure of Cp*$_2$Y(DMP), **2–Y**. Pink, blue, and grey spheres represent Y, N, and C atoms, respectively. Hydrogen atoms have been omitted for clarity.

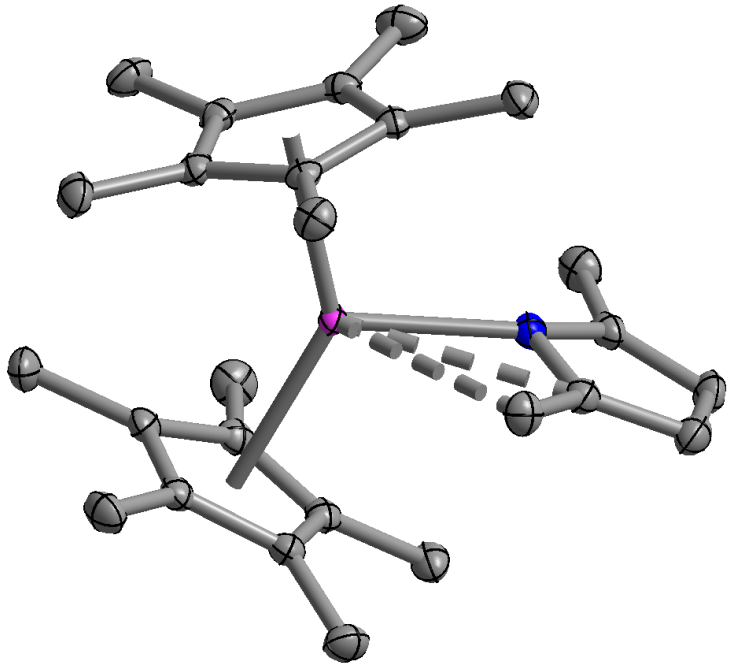

Figure S15. Structure of Cp*$_2$Y(DMP), **2–Y**, with thermal ellipsoids drawn at 50%. Pink, blue, and grey spheres represent Y, N, and C atoms, respectively. Hydrogen atoms have been omitted for clarity.

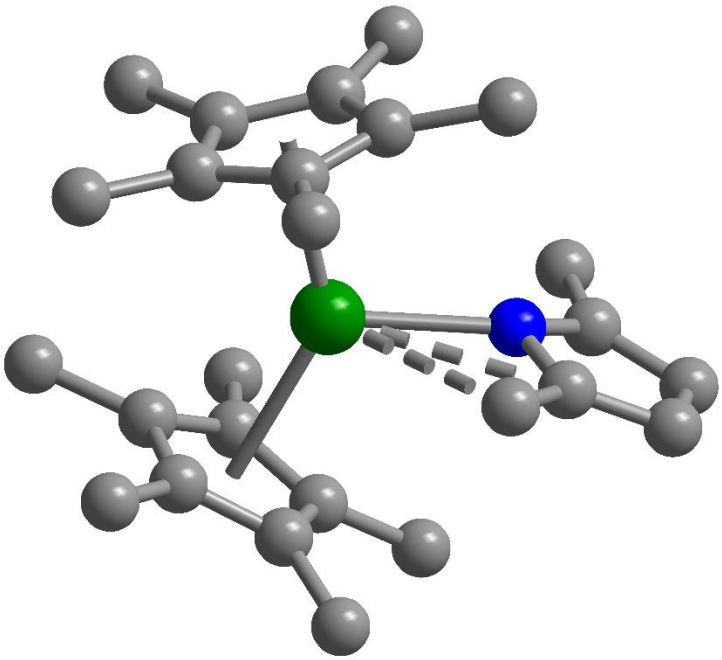

Figure S16. Structure of $Cp^*_2Dy(DMP)$, **2-Dy**. Green, blue, and grey spheres represent Dy, N, and C atoms, respectively. Hydrogen atoms have been omitted for clarity.

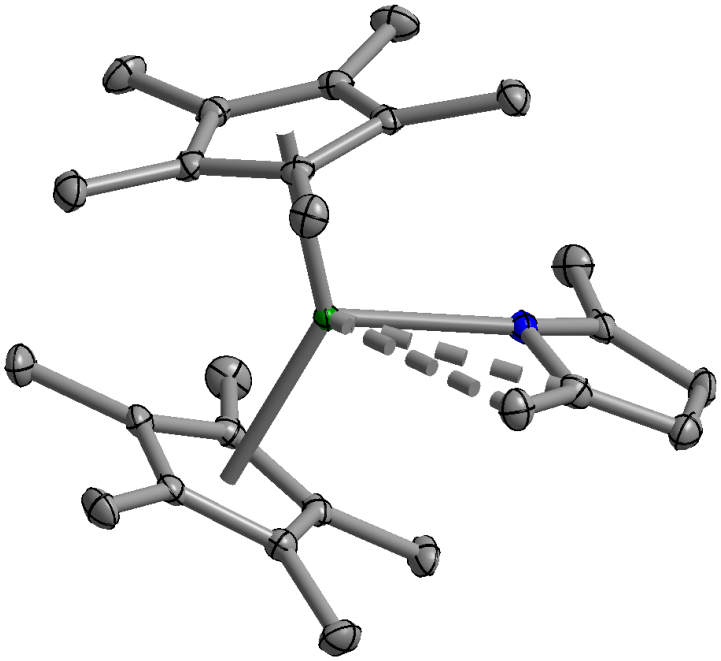

Figure S17. Structure of Cp*2Dy(DMP), **2–Dy**, with thermal ellipsoids drawn at 50%. Green, blue, and grey spheres represent Dy, N, and C atoms, respectively. Hydrogen atoms have been omitted for clarity.

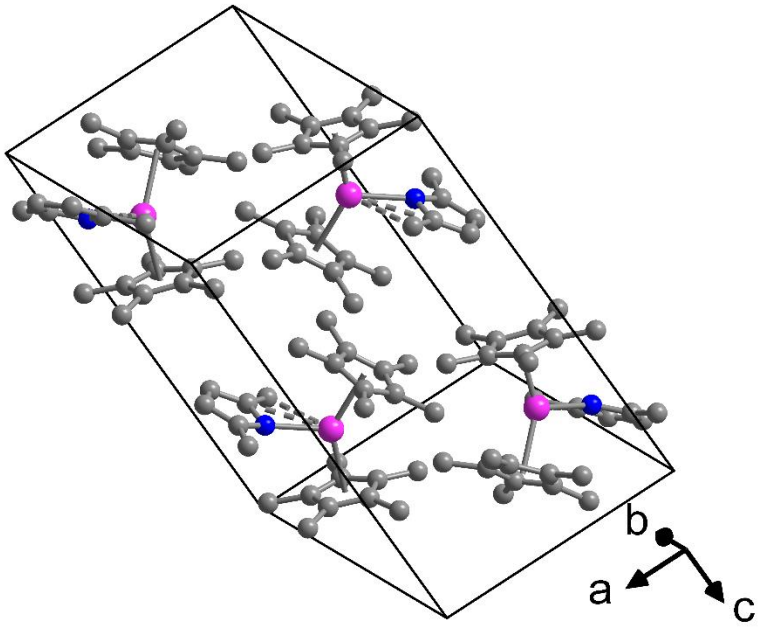

Figure S18. Unit cell of $Cp^*_2Y(DMP)$, **2–Y**. Pink, blue, and grey spheres represent Y, N, and C atoms, respectively. Hydrogen atoms have been omitted for clarity.

NMR Spectroscopy

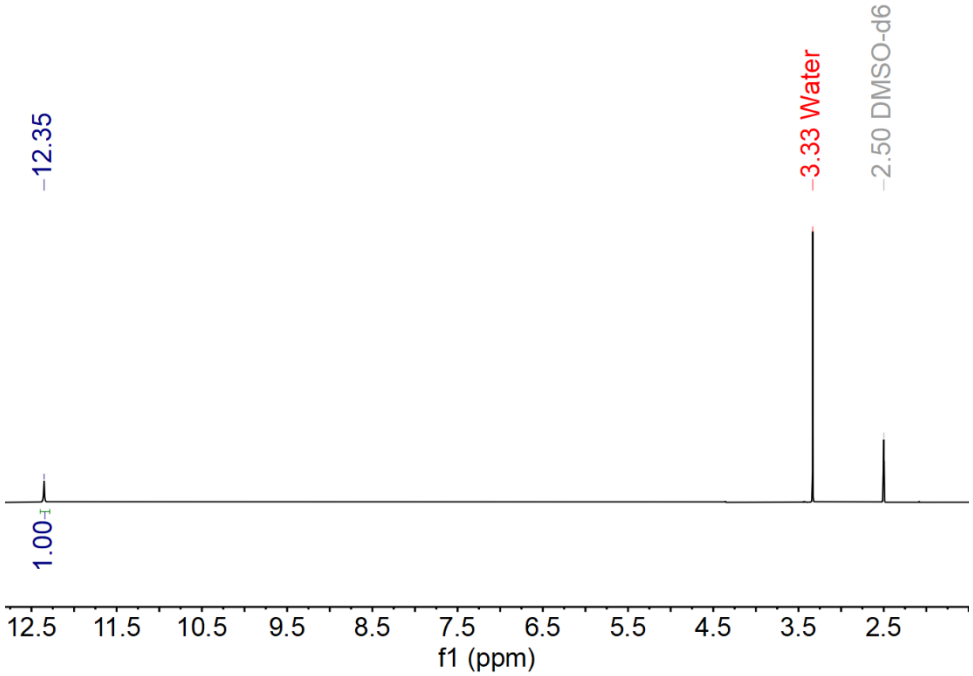

Figure S19. ^{1}H NMR spectrum of TIPH (500 MHz, ppm, DMSO-d_6, 25 °C): δ 12.35 (s, 1 H, *H*NC$_4$I$_4$).

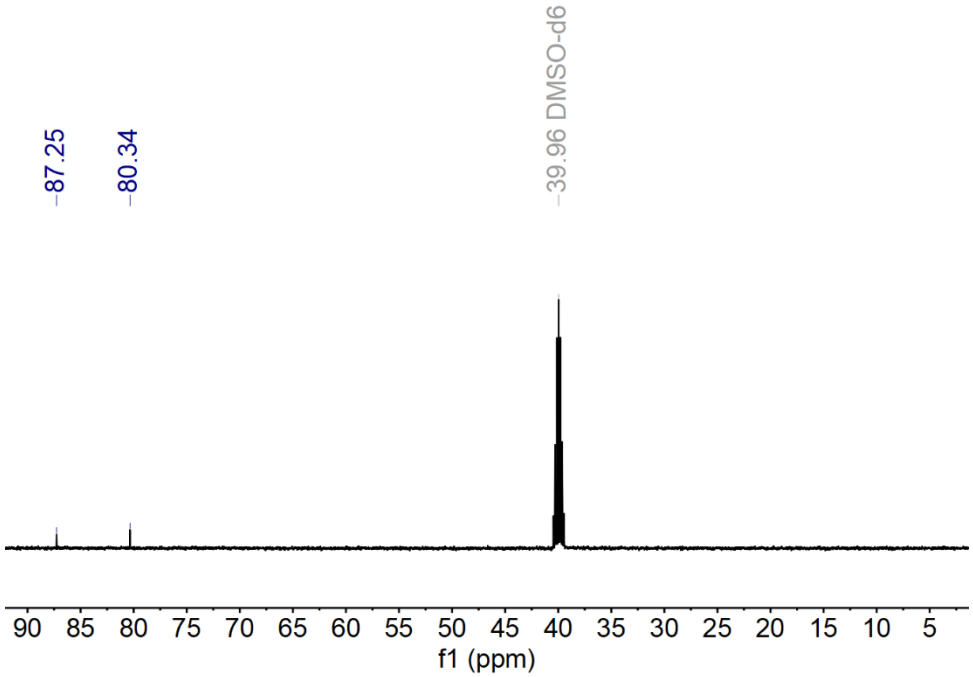

Figure S20. ^{13}C NMR spectrum of TIPH (126 MHz, ppm, DMSO-d_6, 25 °C): δ 87.25 (N*C*$_4$H$_4$), 80.34 (N*C*$_4$H$_4$).

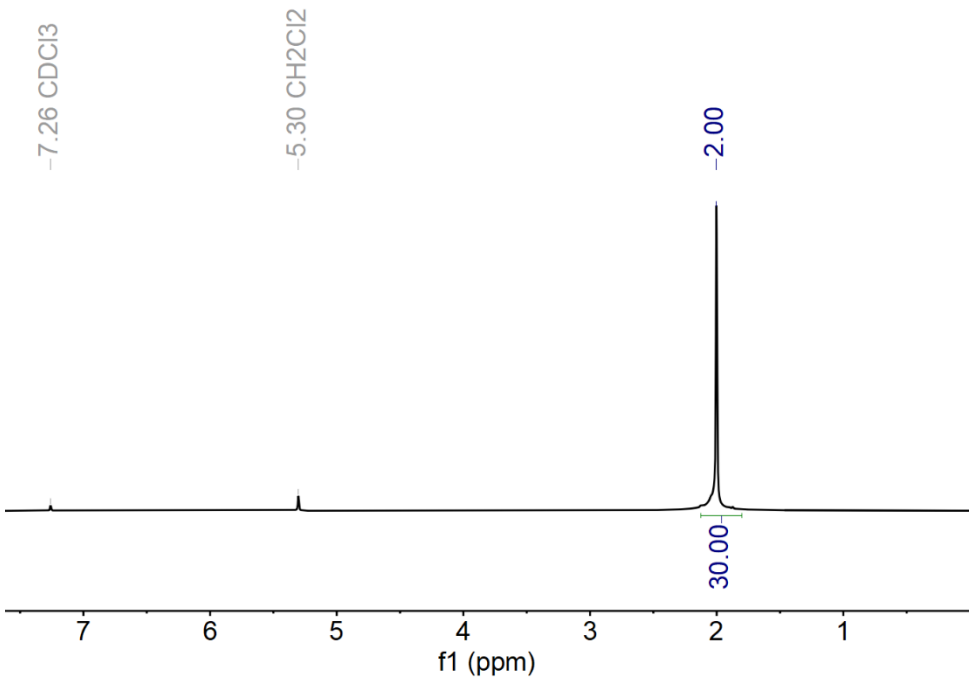

Figure S21. ^{1}H NMR spectrum of Cp*$_2$Y(TIP), **1–Y**, (500 MHz, ppm, chloroform-*d*, 25 °C): *δ* 2.00 (s, 30 H, C$_5$*Me*$_5$).

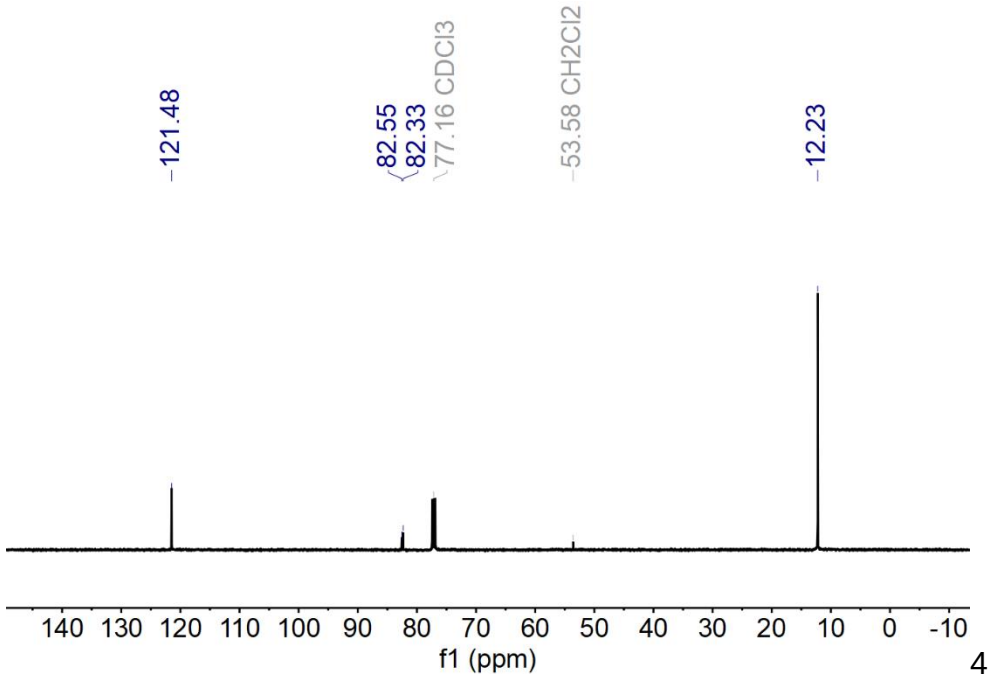

Figure S22. ^{13}C NMR spectrum of Cp*$_2$Y(TIP), **1–Y**, (126 MHz, ppm, chloroform-*d*, 25 °C): *δ* 121.48, (*C*$_5$Me$_5$), 82.55, 82.33 (TIP), 12.23 (C$_5$*Me*$_5$).

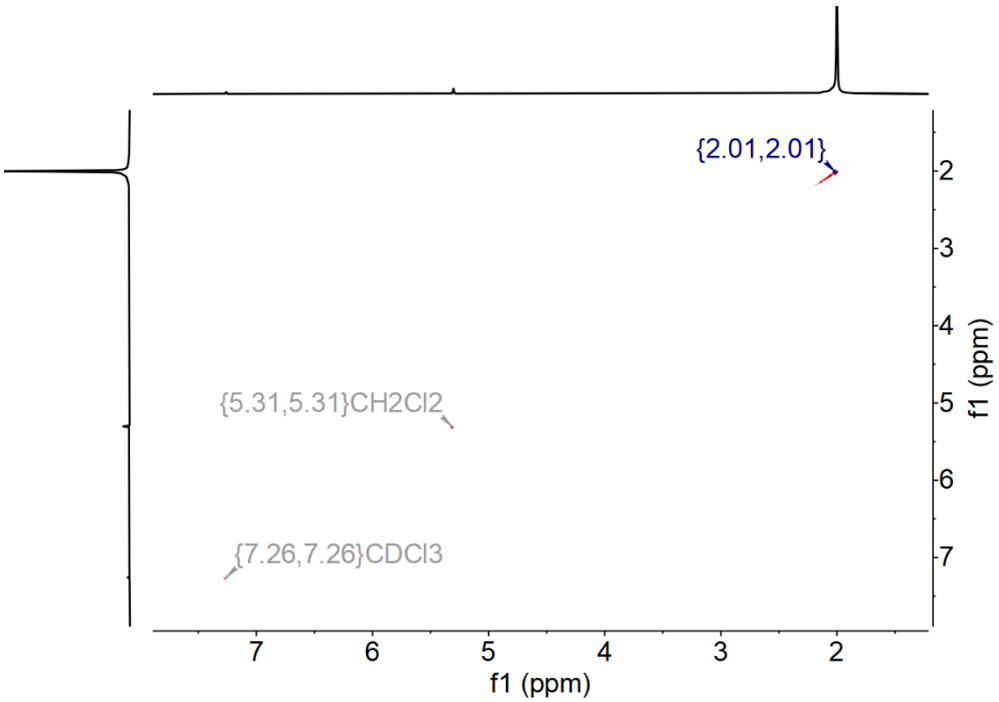

Figure S23. ^{1}H–^{1}H gCOSY spectrum of Cp*$_2$Y(TIP), **1–Y**, (500 MHz, ppm, chloroform-*d*, 25 °C).

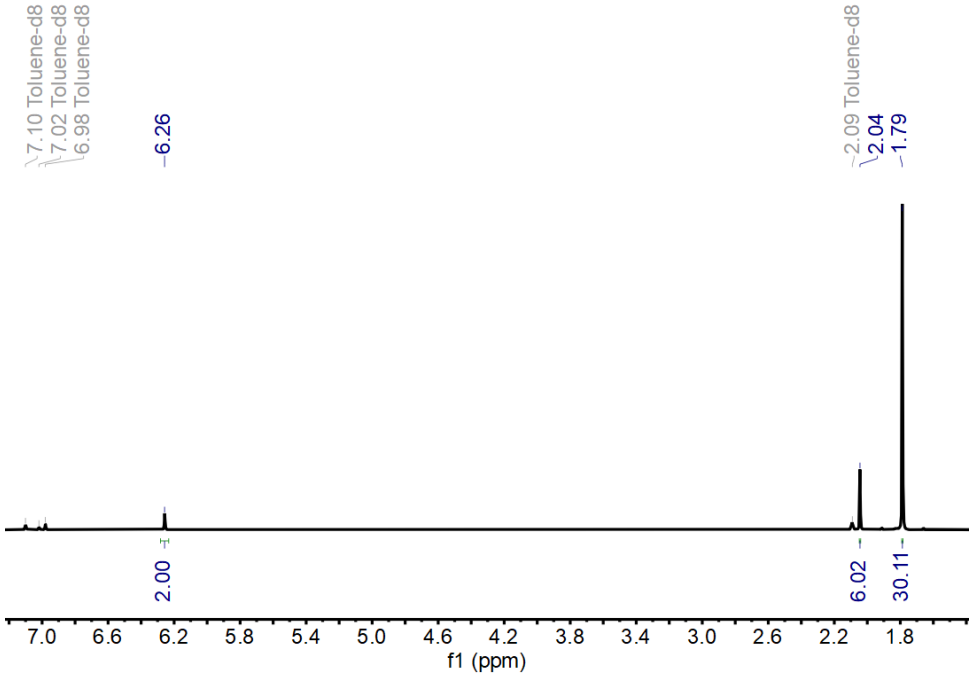

Figure S24. ^{1}H NMR spectrum of Cp*$_2$Y(DMP), **2–Y**, (500 MHz, ppm, toluene–d_8, 25 °C): *δ* 1.79 (s, 30 H, C$_5$*Me*$_5$), 2.04 (s, 6 H, NC$_4$*Me*$_2$H$_2$), 6.26 (s, 2 H, NC$_4$Me$_2$*H*$_2$).

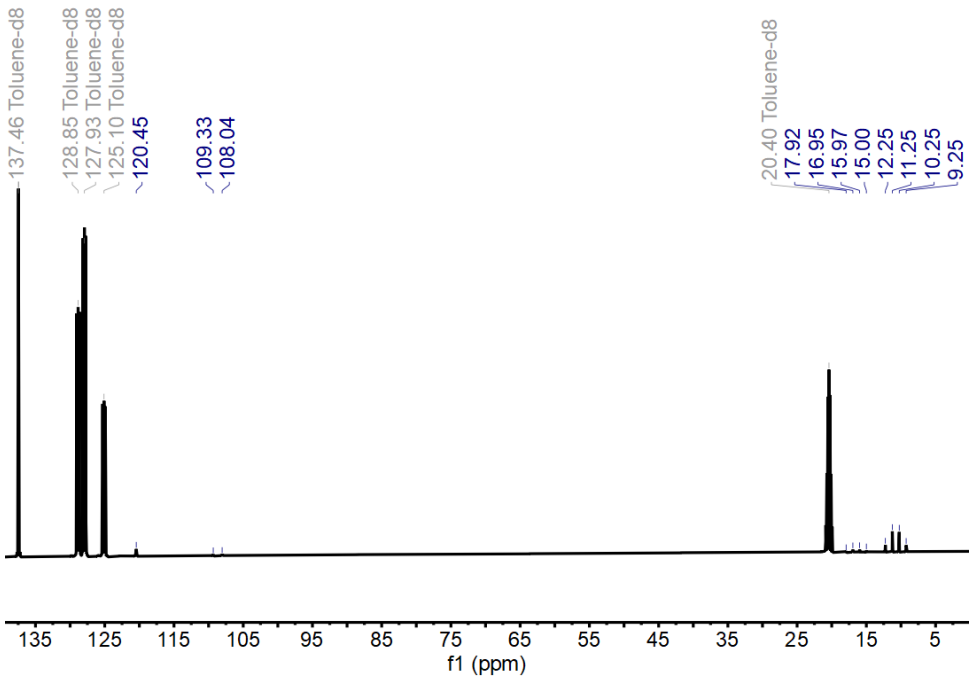

Figure S25. $^{13}C\{^{1}H\}$ NMR spectrum of $Cp^*_2Y(DMP)$, **2–Y**, (126 MHz, ppm, toluene–d_8, 25 °C): δ 120.45, ($\underline{C}_5Me_5$), 109.33 ($N\underline{C}_4Me_2H_2$), 108.04 ($N\underline{C}_4Me_2H_2$), 15.00 – 17.92 (q, $^{1}J_{C–H}$: 121.90 Hz, $NC_4\underline{Me}_2H_2$), 9.25 – 12.24 (q, $^{1}J_{C–H}$: 125.83 Hz, $C_5\underline{Me}_5$).

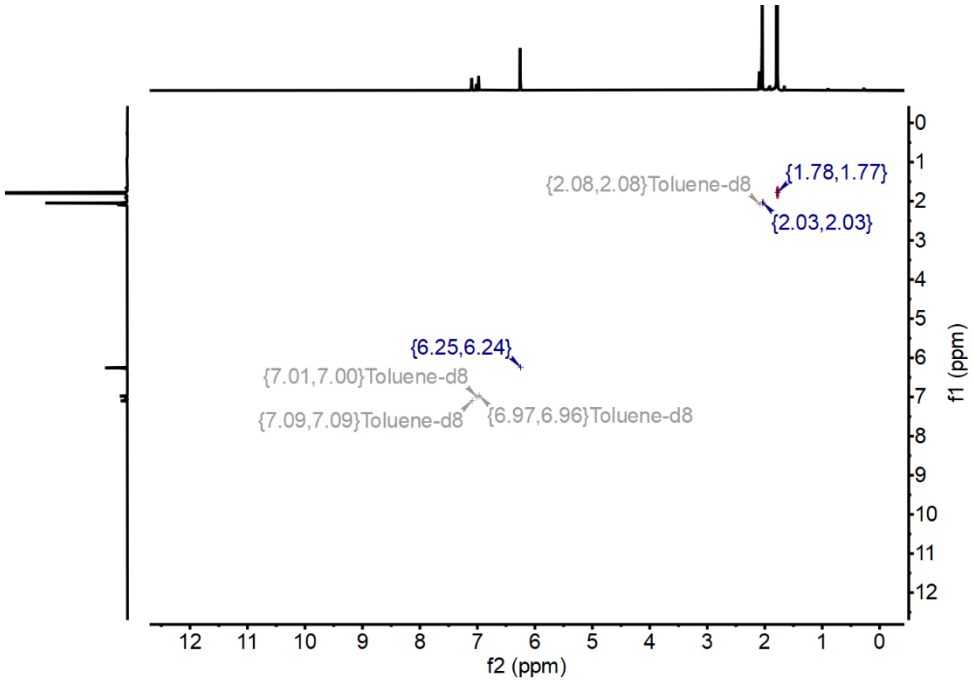

Figure S26. $^{1}H–^{1}H$ gCOSY spectrum of $Cp^*_2Y(DMP)$, **2–Y**. (500 MHz, ppm, toluene–d_8, 25 °C).

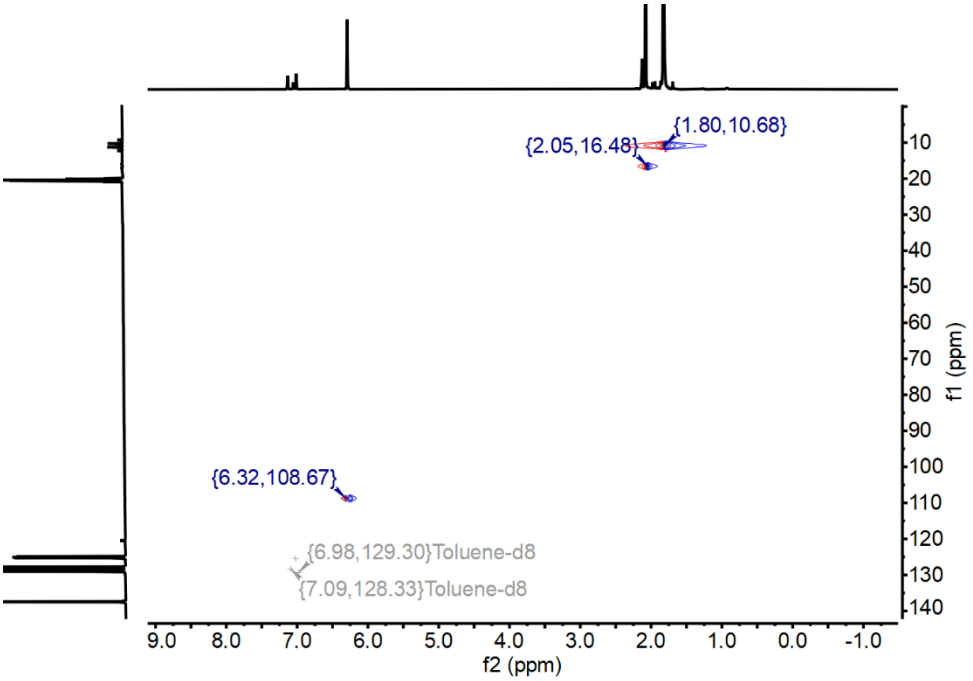

Figure S27. $^{1}H–^{13}C$ gHSQC spectrum of $Cp^{*}_{2}Y(DMP)$, **2–Y**, (500 MHz, ppm, toluene–d_8, 25 °C).

IR Spectroscopy

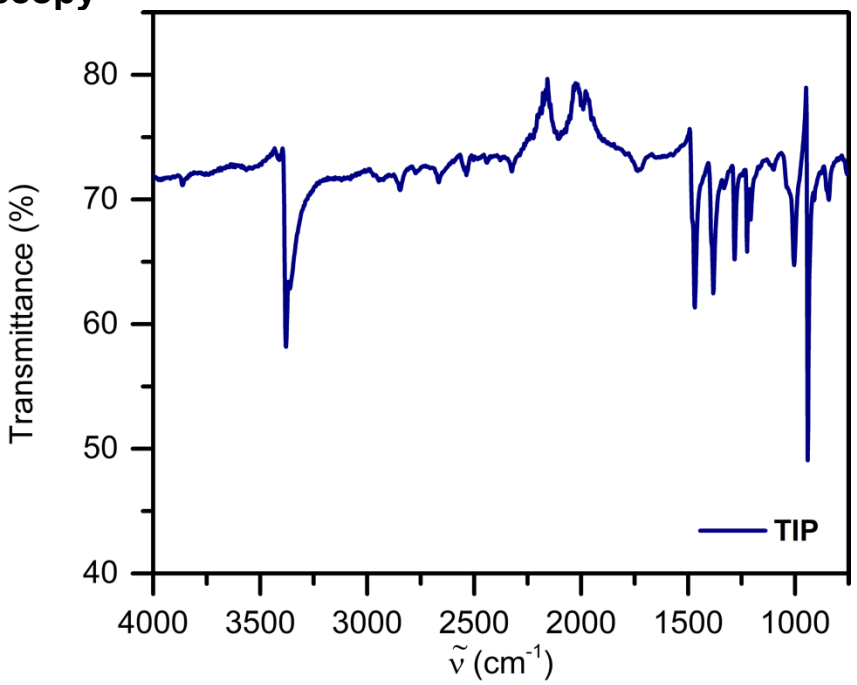

Figure S28. FTIR spectrum of tetraiodopyrrole.

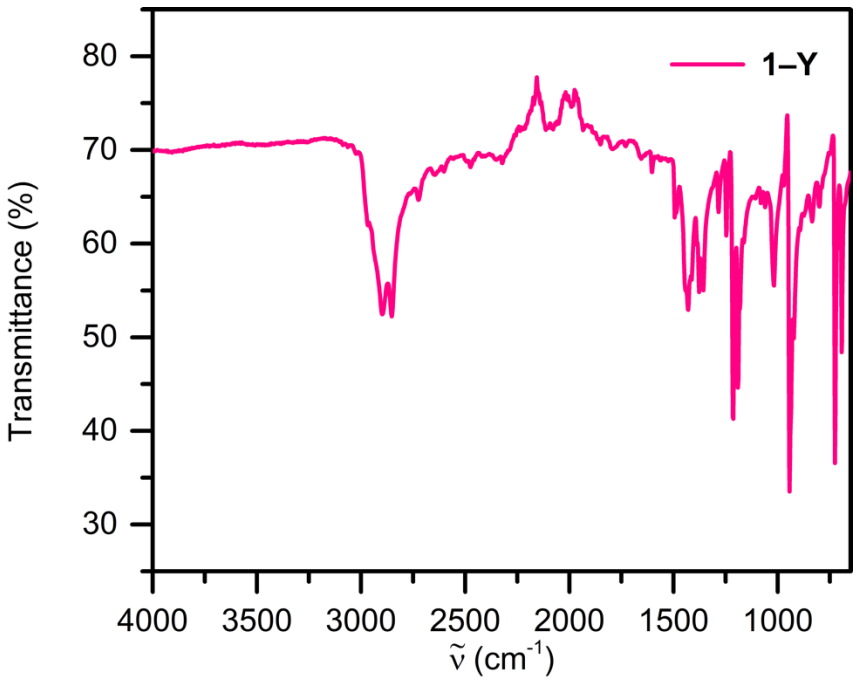

Figure S29. FTIR spectrum of Cp*$_2$Y(TIP), **1–Y**.

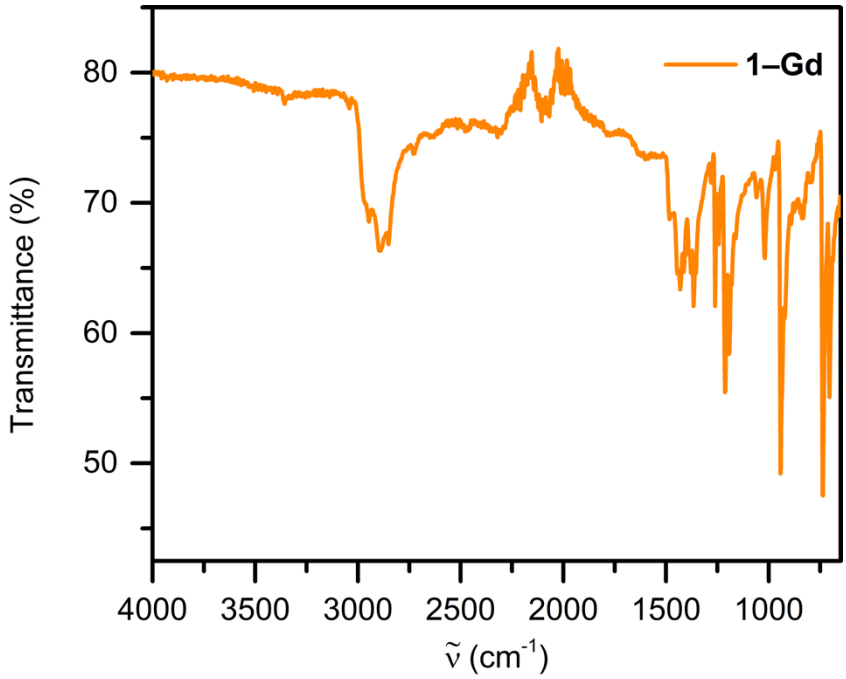

Figure S30. FTIR spectrum of Cp*$_2$Gd(TIP), **1–Gd**.

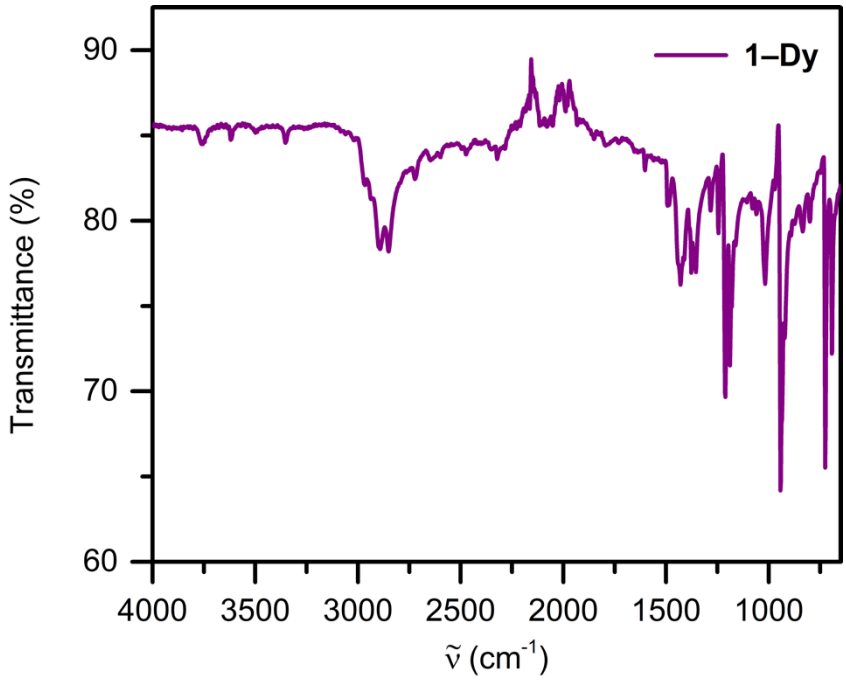

Figure S31. FTIR spectrum of Cp*$_2$Dy(TIP), **1–Dy**.

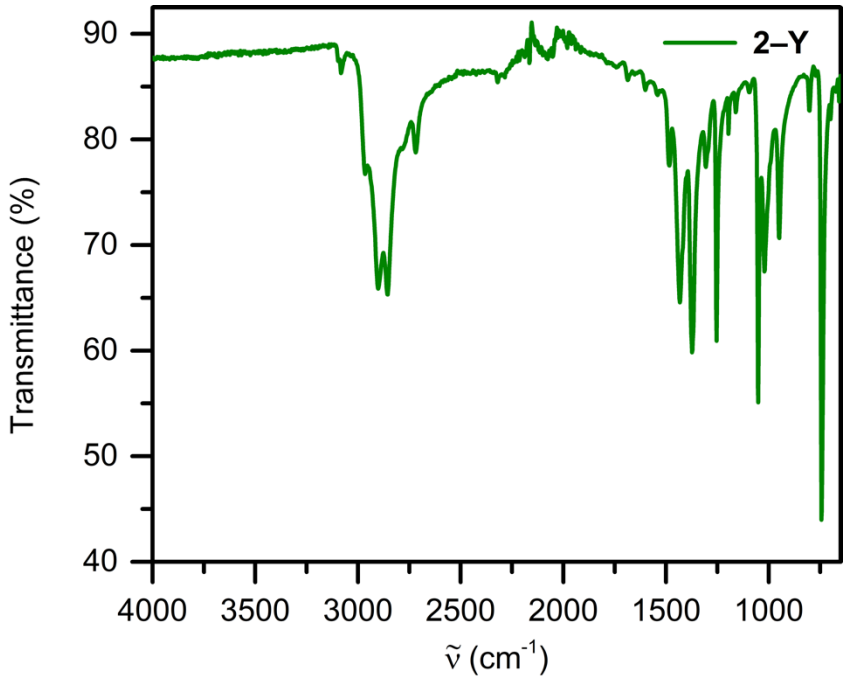

Figure S32. FTIR spectrum of $Cp^*_2Y(DMP)$, **2–Y**.

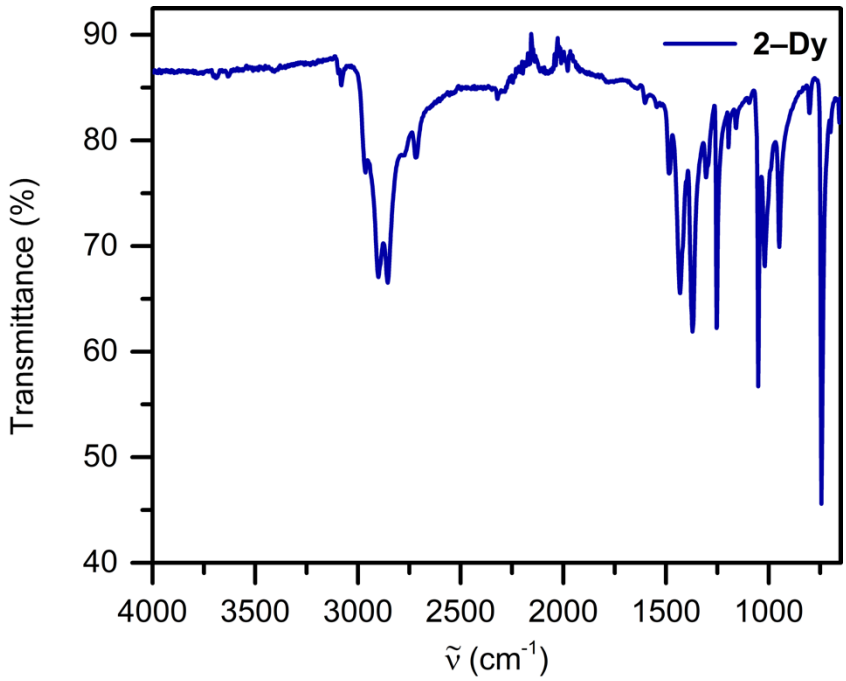

Figure S33. FTIR spectrum of $Cp^*_2Dy(DMP)$, **2–Dy**.

UV-vis Spectroscopy

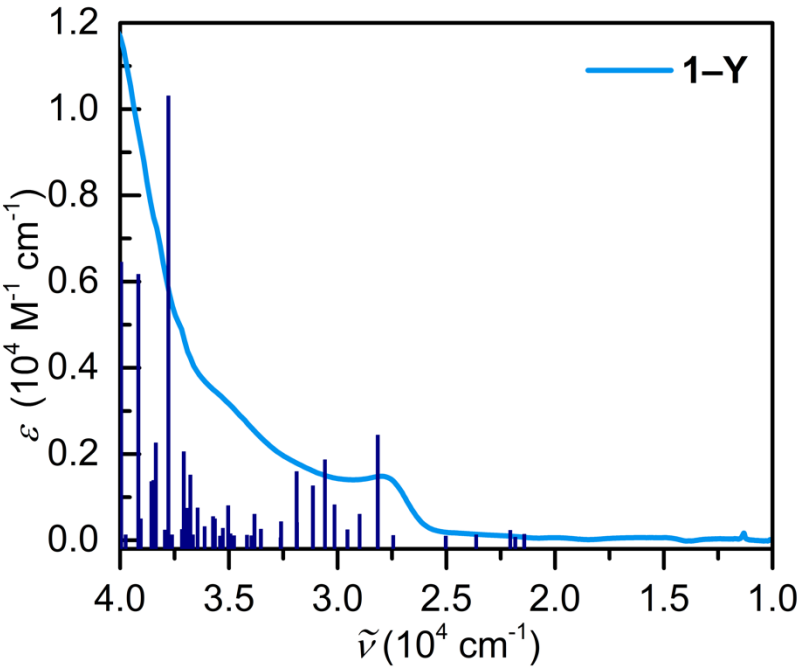

Figure S34. UV-vis absorption spectrum of Cp*$_2$Y(TIP), **1–Y**. The light blue line represents experimental data for **1–Y** whereas the dark blue lines constitute calculated TDDFT transitions.

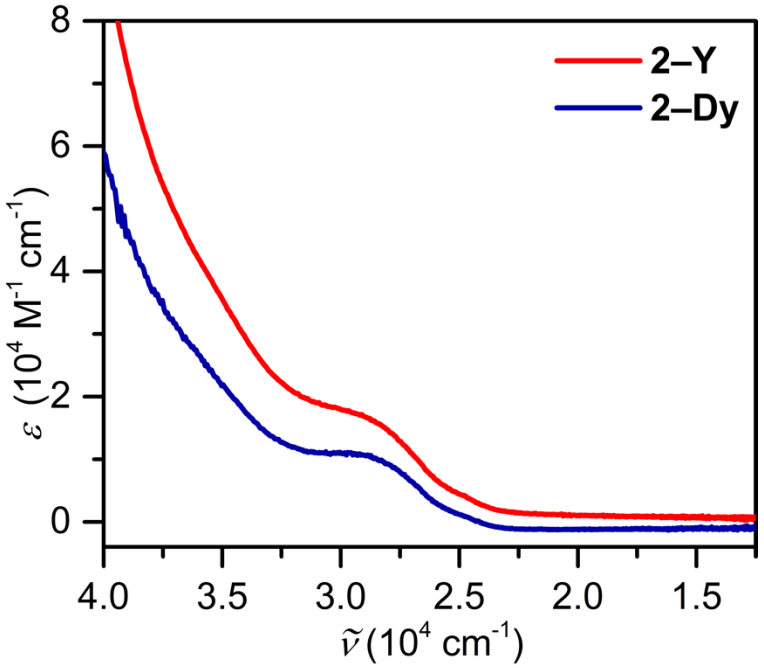

Figure S35. UV-vis absorption spectrum of Cp*$_2$RE(DMP) (RE = Y (**2–Y**), and Dy (**2–Dy**). The red and blue line represent experimental data for **2–Y** and **2–Dy**, respectively.

Magnetic Data

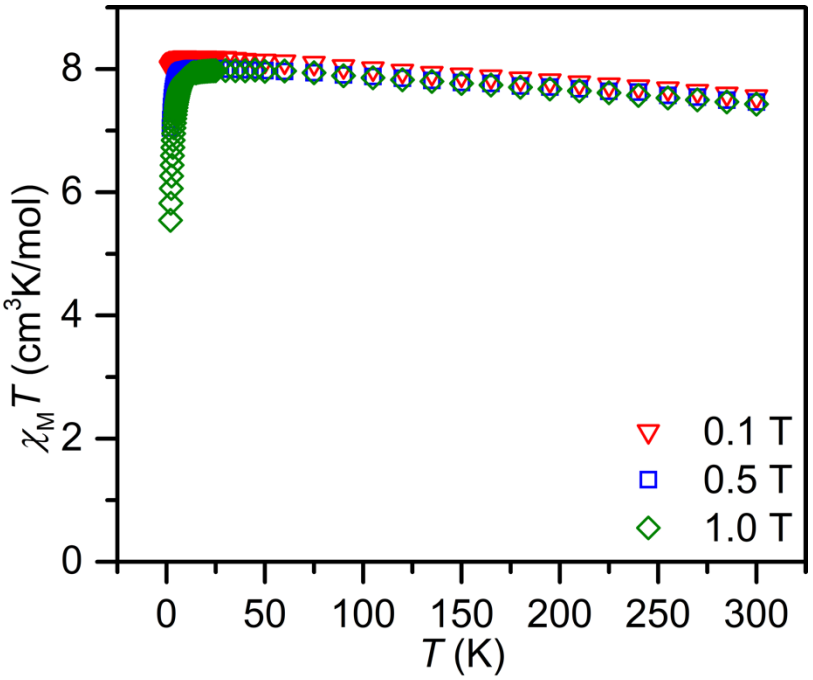

Figure S36. Variable-temperature dc magnetic susceptibility data ($\chi_M T$ *vs.* T) of polycrystalline Cp*$_2$Gd(TIP), **1–Gd**, collected under 0.1, 0.5, and 1 T applied dc fields.

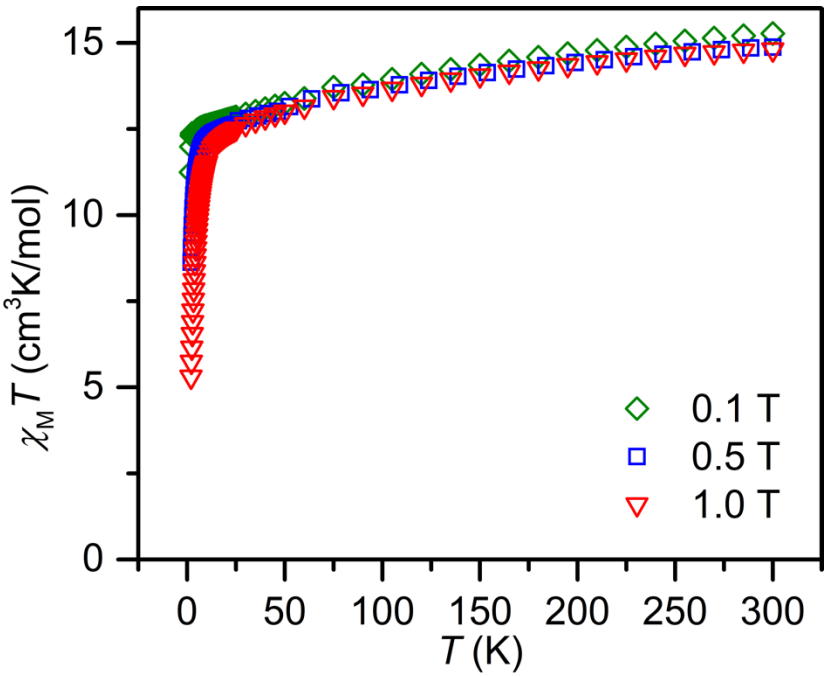

Figure S37. Variable-temperature dc magnetic susceptibility data ($\chi_M T$ *vs.* T) of polycrystalline Cp*$_2$Dy(TIP), **1–Dy**, collected under 0.1, 0.5, and 1 T applied dc fields.

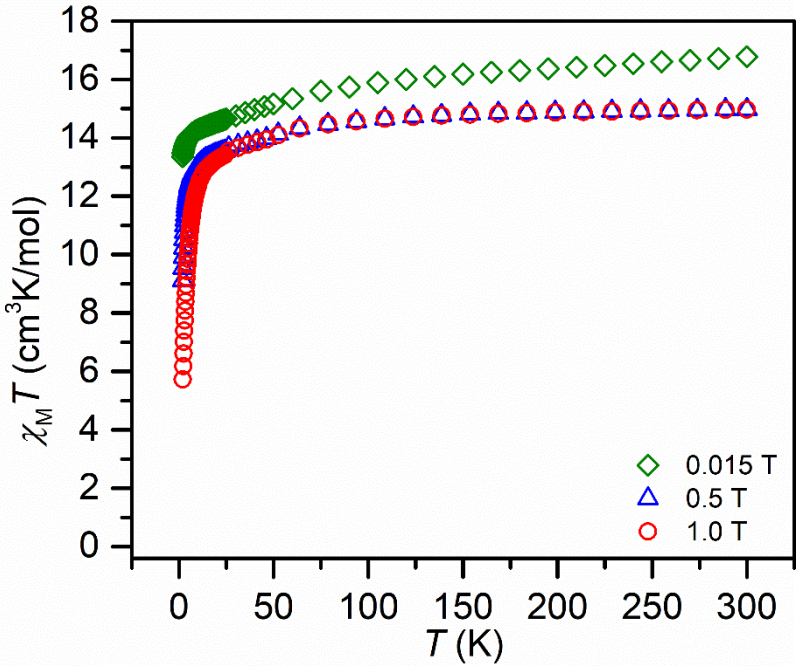

Figure S38. Variable-temperature dc magnetic susceptibility data ($\chi_M T$ *vs.* T) of polycrystalline Cp*$_2$Dy(DMP), **2–Dy**, collected under 0.015, 0.5, and 1 T applied dc fields.

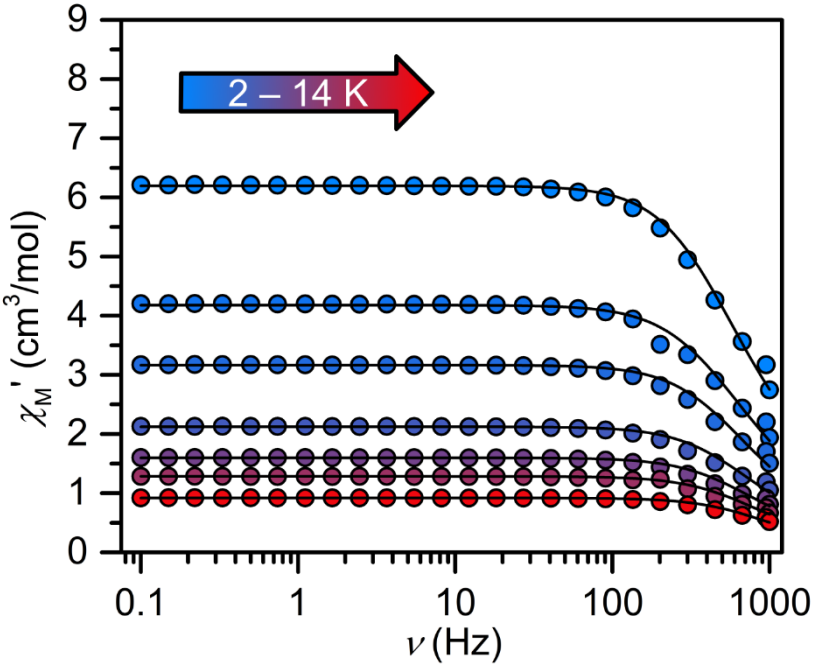

Figure S39. In-phase (χ_M') components of the ac magnetic susceptibility for Cp*$_2$Dy(TIP), **1–Dy**, under zero applied dc field from 2 K (blue circles) to 14 K (red circles). Solid lines represent fits of the data to a Cole-Davidson model.

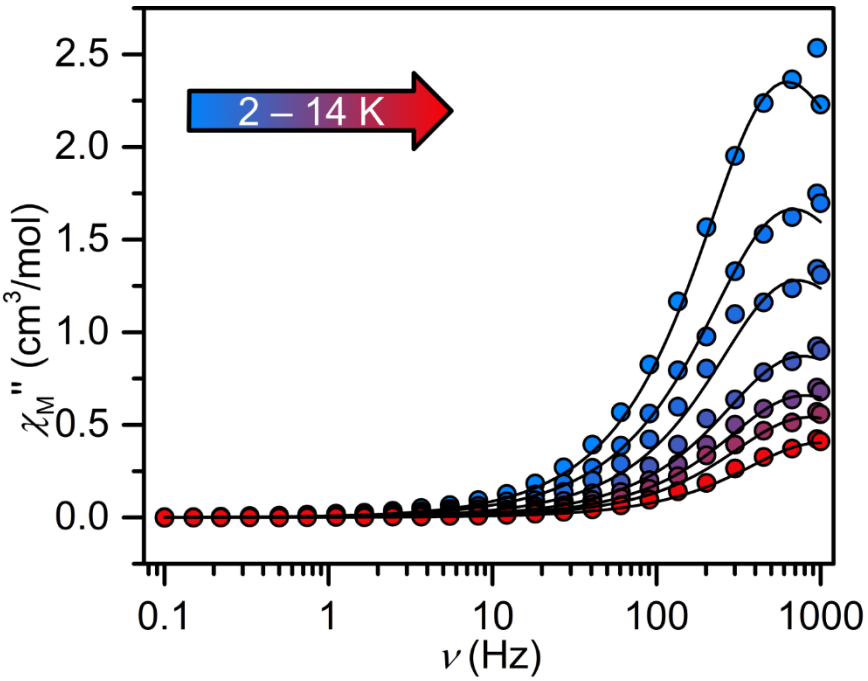

Figure S40. Out-of-phase (χ_M'') components of the ac magnetic susceptibility for Cp*$_2$Dy(TIP), **1–Dy**, under a zero applied dc field from 2 K (blue) to 14 K (red). Solid lines represent fits of the data to a Cole-Davidson model.

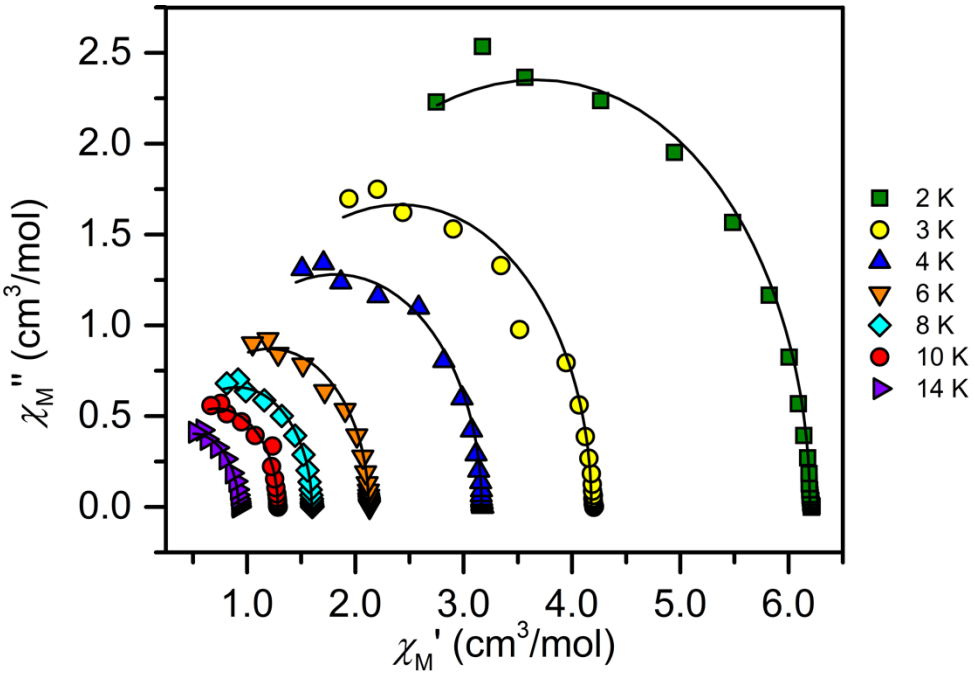

Figure S41. Cole–Cole plots for ac magnetic susceptibility collected from 2 to 14 K under zero applied dc field for Cp*$_2$Dy(TIP), **1–Dy**. Symbols represent experimental data points and the points representing the fits are connected by solid black lines.

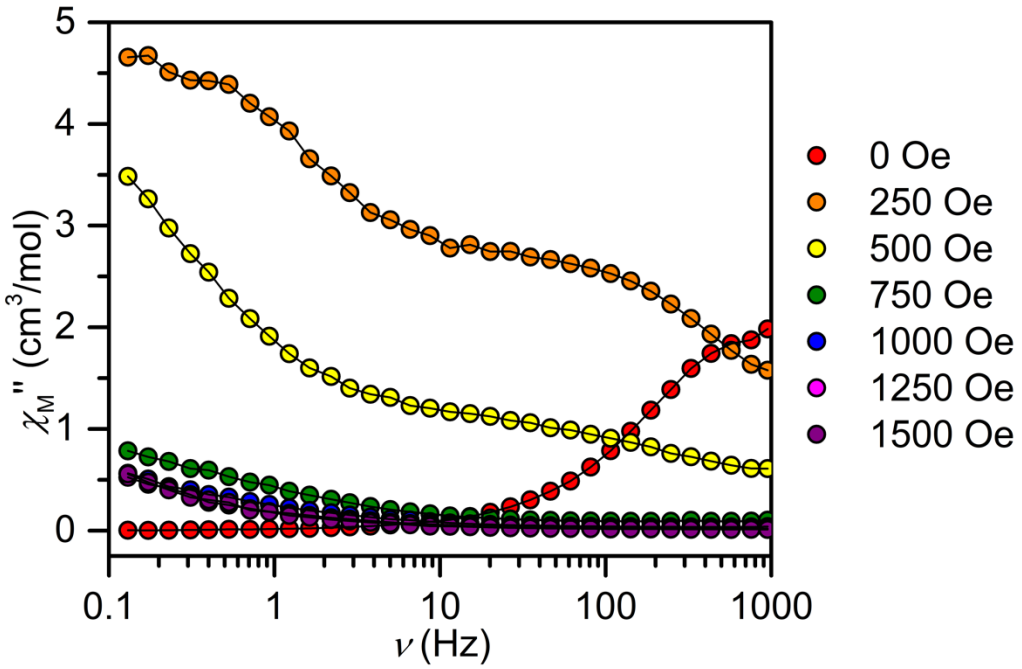

Figure S42. Out-of-phase (χ_M'') components of the ac magnetic susceptibility for Cp*$_2$Dy(TIP), **1–Dy**, at 2 K under dc fields ranging from 0 Oe to 1500 Oe in 250 Oe increments. Solid lines are guides for the eye.

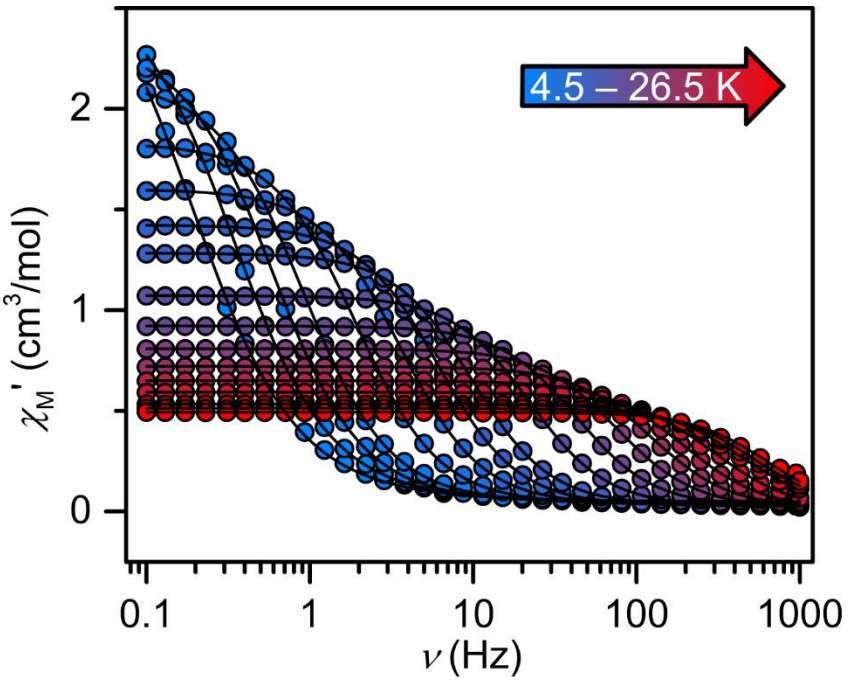

Figure S43. In-phase (χ_M') components of the ac magnetic susceptibility for Cp*$_2$Dy(TIP), **1–Dy**, under a 1250 Oe applied dc field from 4.5 K (blue circles) to 26.5 K (red circles). Solid lines represent fits of the data to a generalized Debye model.

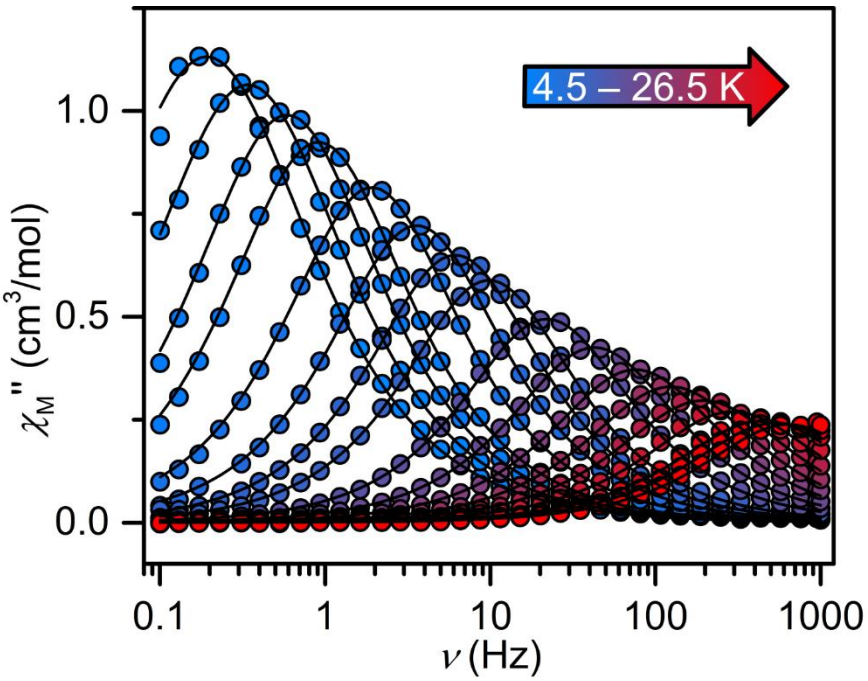

Figure S44. Out-of-phase (χ_M'') components of the ac magnetic susceptibility for Cp*$_2$Dy(TIP), **1–Dy**, under a 1250 Oe applied dc field from 4.5 (blue) to 26.5 K (red). Solid lines represent fits of the data to a generalized Debye model.

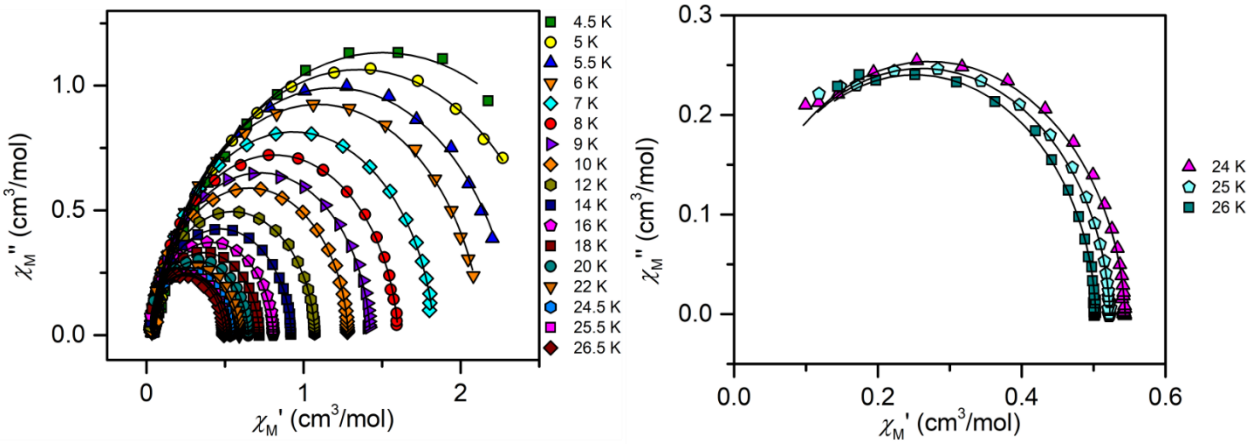

Figure S45. Cole–Cole plots for ac magnetic susceptibility collected from 4.5 to 26.5 K under a 1250 Oe applied dc field for Cp*$_2$Dy(TIP), **1–Dy**. Symbols represent experimental data points and the points representing the fits are connected by solid black lines.

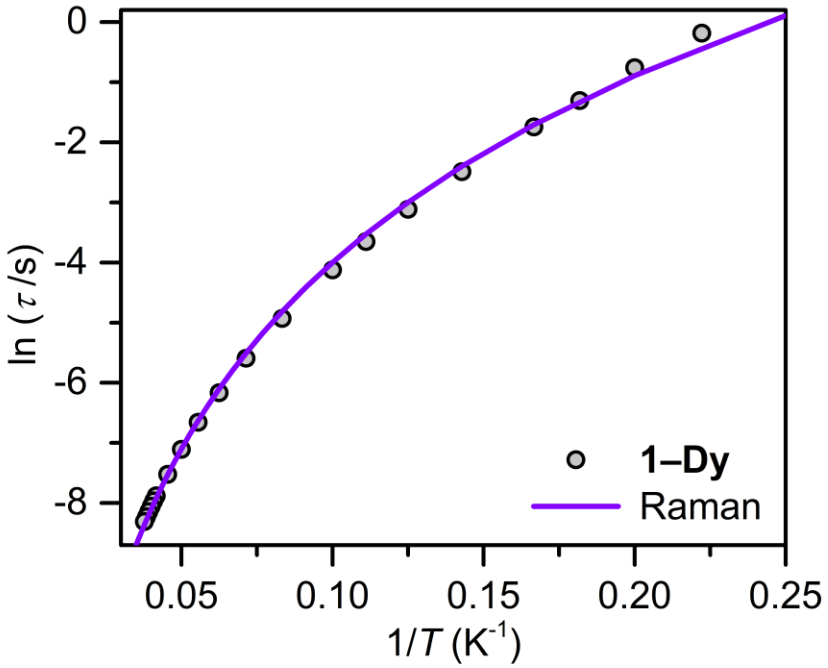

Figure S46. Arrhenius plot of the natural log of the relaxation time, τ, versus the inverse temperature, 1/T, obtained from ac measurements, for 1–Dy (circles). The purple line represents a fit to a Raman process affording C = 0.0018(2) s^{-1} K^{-n}, and n = 4.48(3).

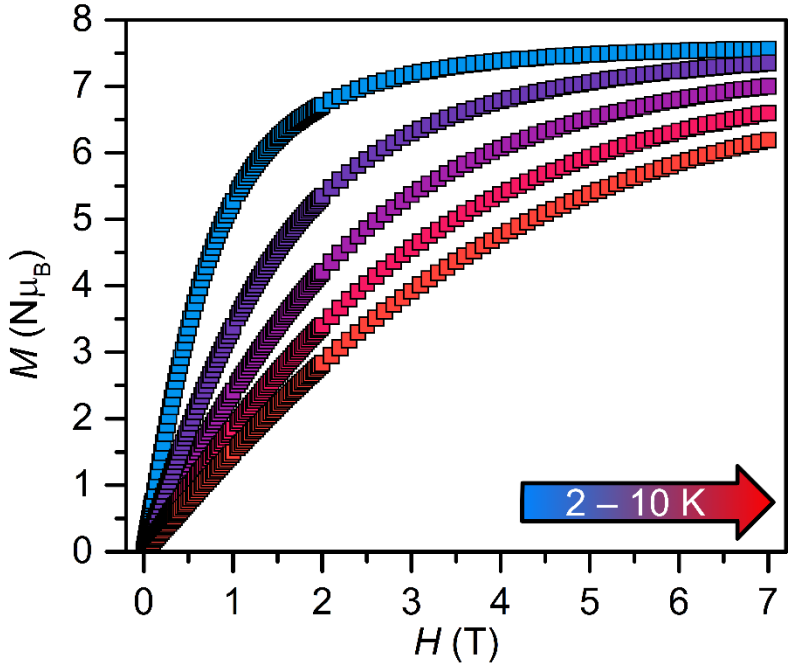

Figure S47. Field-dependent magnetization data for $Cp^*_2Gd(TIP)$, **1–Gd**, between 0 and 7 T from 2 to 10 K.

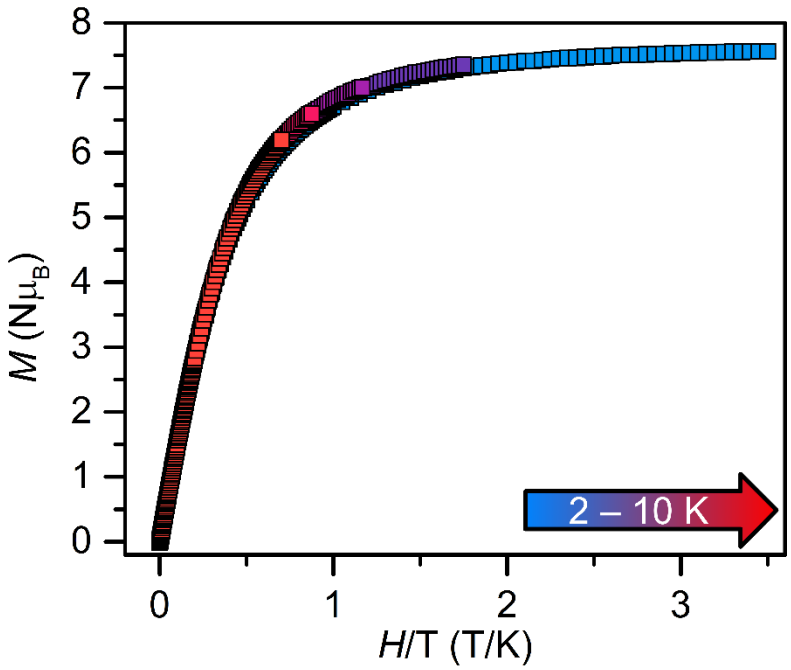

Figure S48. Field-dependent reduced magnetization data for Cp*$_2$Gd(TIP), **1–Gd**, between 0 and 7 T from 2 to 10 K.

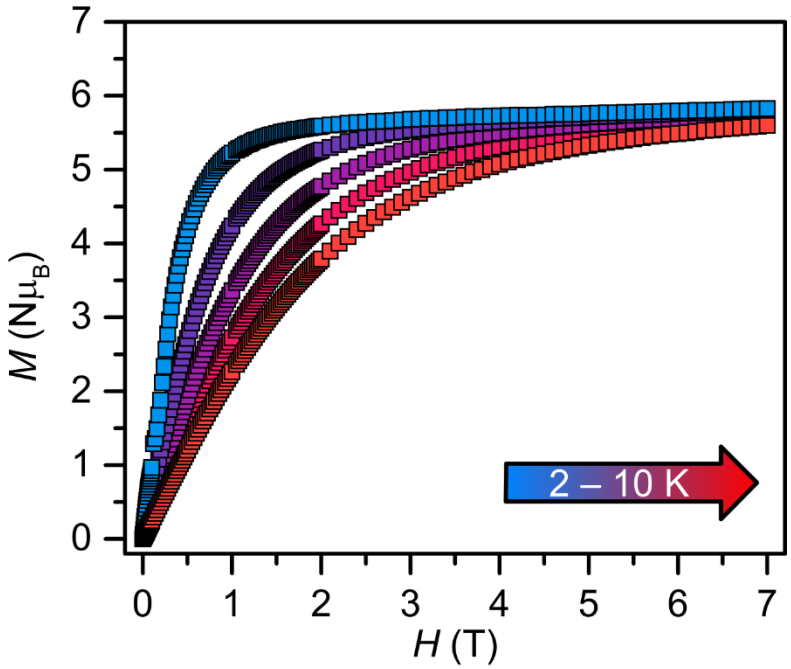

Figure S49. Field-dependent magnetization data for Cp*$_2$Dy(TIP), **1–Dy**, between 0 and 7 T from 2 to 10 K.

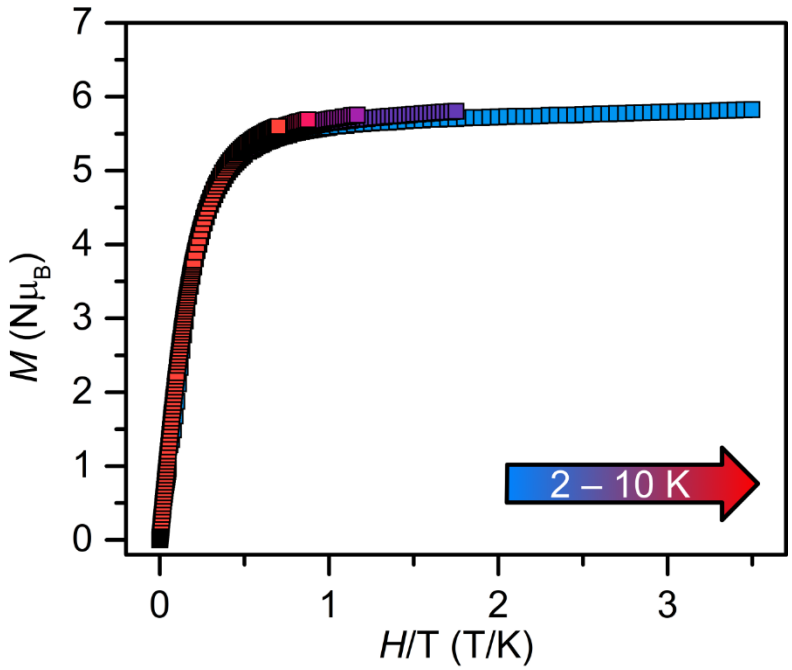

Figure S50. Field-dependent reduced magnetization data for Cp*$_2$Dy(TIP), **1–Dy**, between 0 and 7 T from 2 to 10 K.

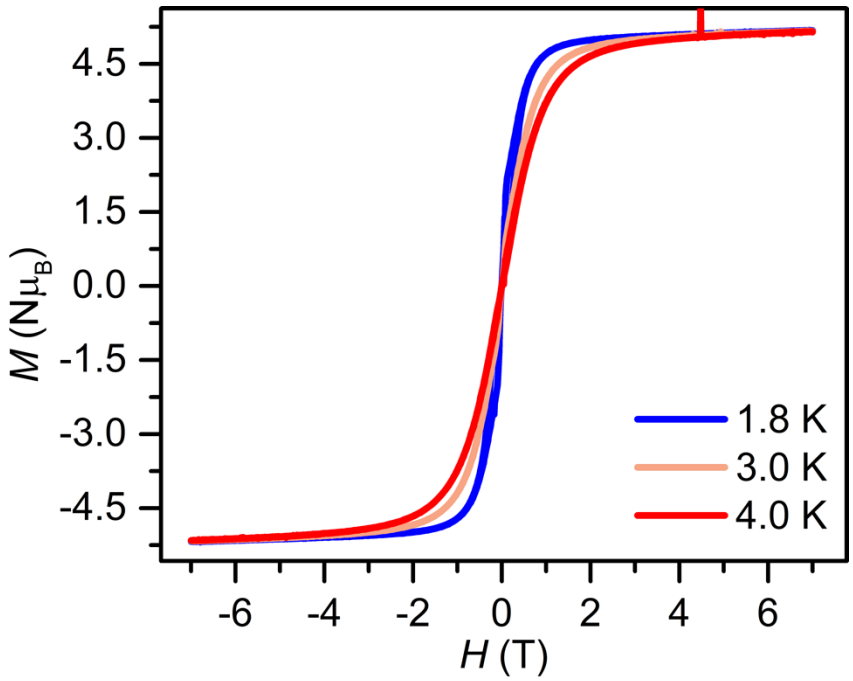

Figure S51. Plot of magnetization (*M*) *vs*. dc magnetic field (*H*) at an average sweep rate of 100 Oe/s for Cp*$_2$Dy(TIP), **1–Dy**, from 1.8 K (blue) to 4 K (red) collected between −7 and +7 T.

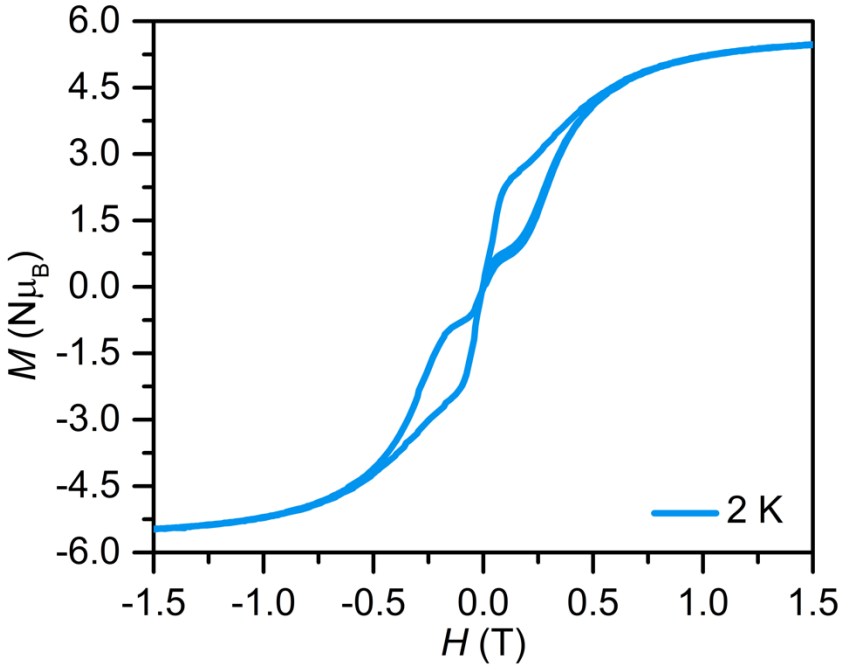

Figure S52. Plot of magnetization (*M*) *vs*. dc magnetic field (*H*) at an average sweep rate of 100 Oe/s for Cp*$_2$Dy(TIP), **1–Dy**, at 2 K from −0.5 and +0.5 T.

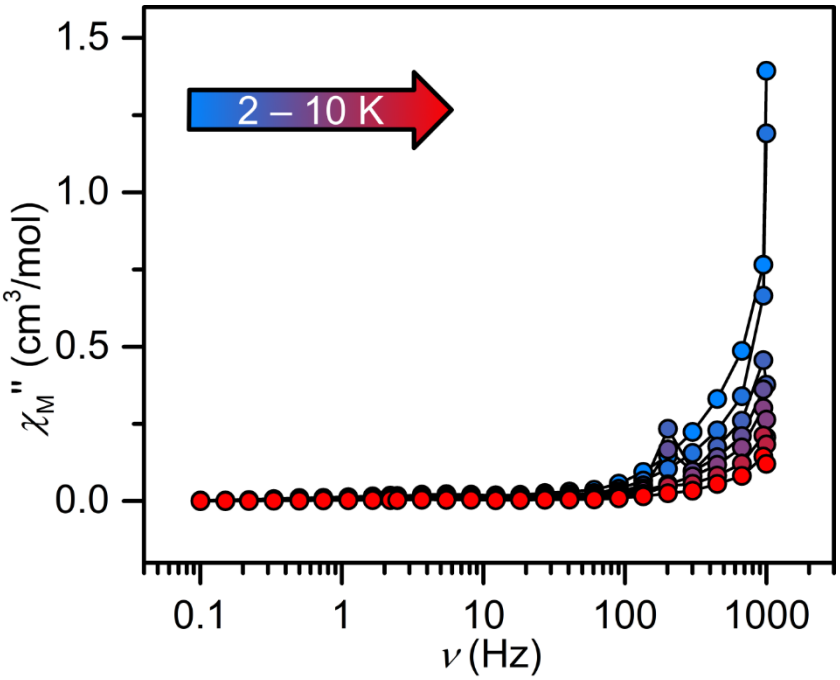

Figure S53. Out-of-phase (χ_M'') components of the ac magnetic susceptibility for Cp*$_2$Dy(DMP), **2–Dy**, under a zero applied dc field from 2 K (blue) to 10 K (red). Solid lines are guides for the eye.

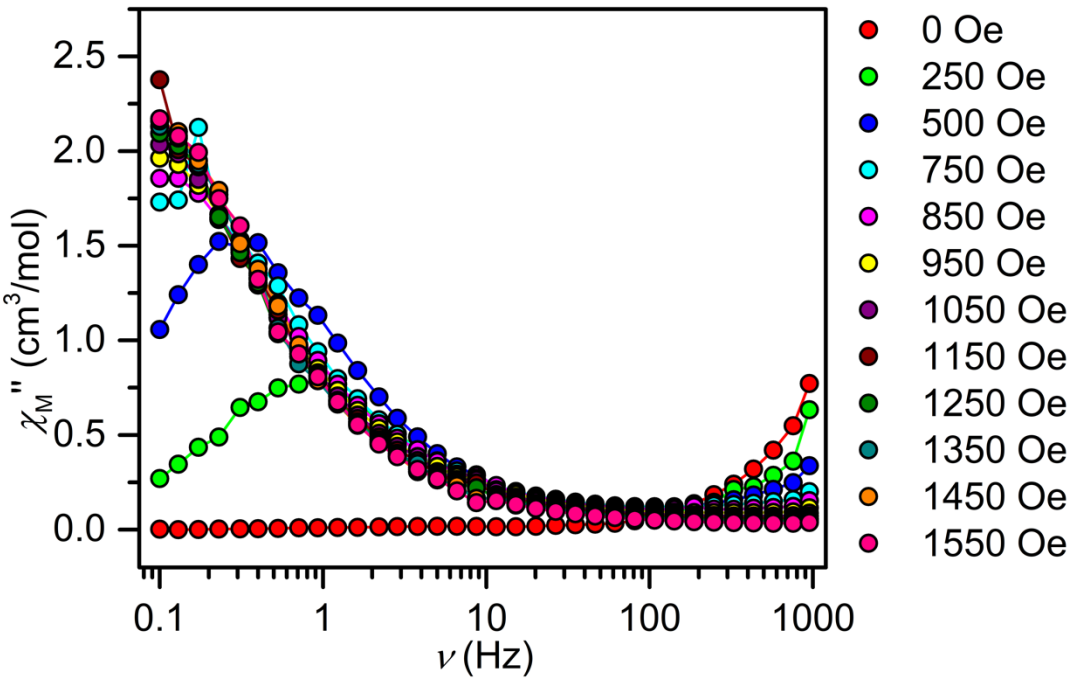

Figure S54. Out-of-phase (χ_M'') components of the ac magnetic susceptibility for Cp*$_2$Dy(DMP), **2–Dy**, at 2 K under dc fields ranging from 0 Oe to 1550 Oe. Solid lines are guides for the eye.

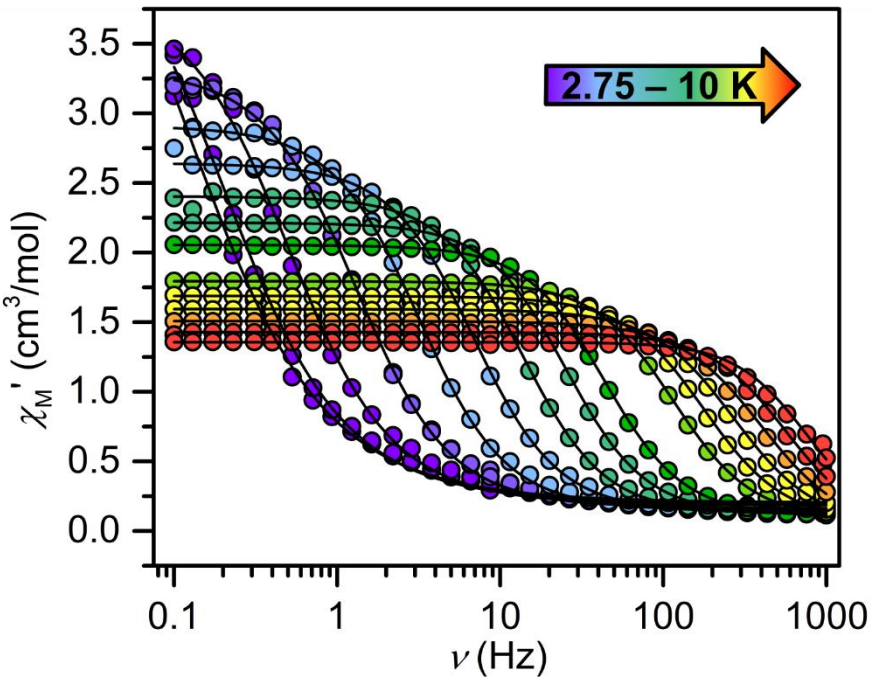

Figure S55. In-phase (χ_M') components of the ac magnetic susceptibility for Cp*$_2$Dy(DMP), **2–Dy**, under a 1450 Oe applied dc field from 2.75 K (purple circles) to 10 K (red circles). Solid lines represent fits of the data to a generalized Debye model.

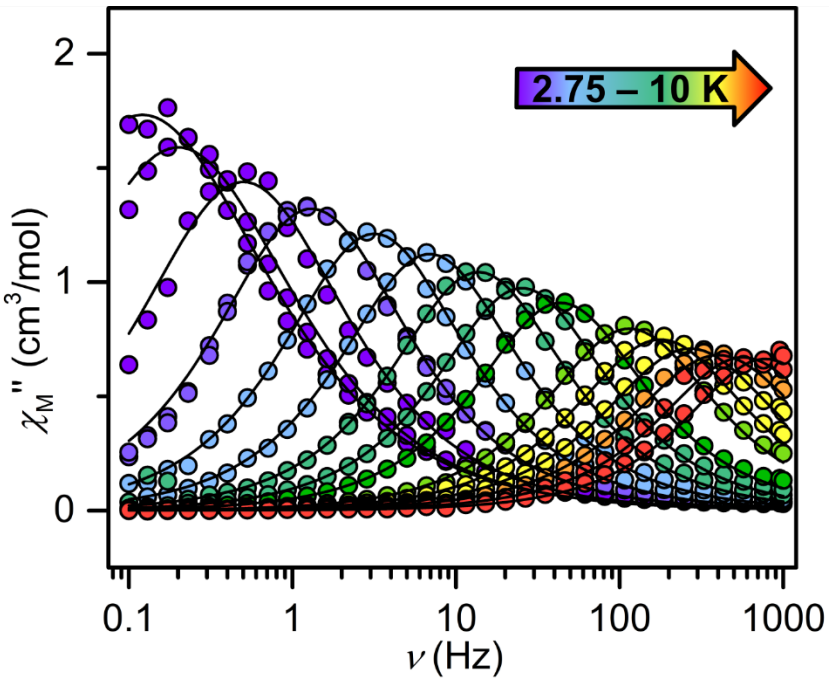

Figure S56. Out-of-phase (χ_M'') components of the ac magnetic susceptibility for Cp*$_2$Dy(DMP), **2–Dy**, under a 1450 Oe applied dc field from 2.75 K (purple) to 10 K (red). Solid lines represent fits of the data to a generalized Debye model.

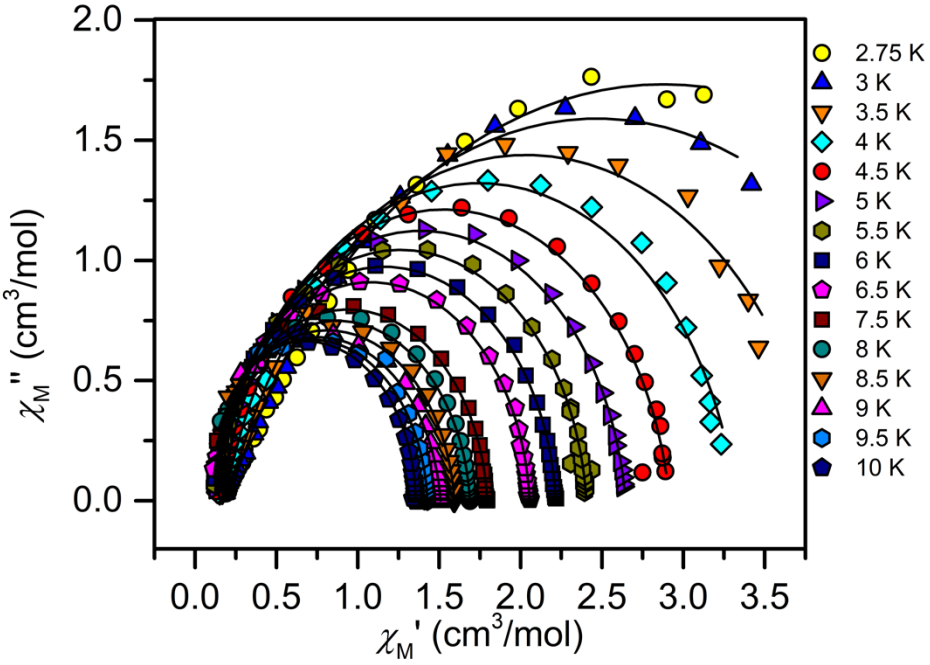

Figure S57. Cole–Cole plots for ac magnetic susceptibility collected from 2.75 to 10 K under a 1450 Oe applied dc field for Cp*$_2$Dy(DMP), **2–Dy**. Symbols represent experimental data points and the points representing the fits are connected by solid black lines.

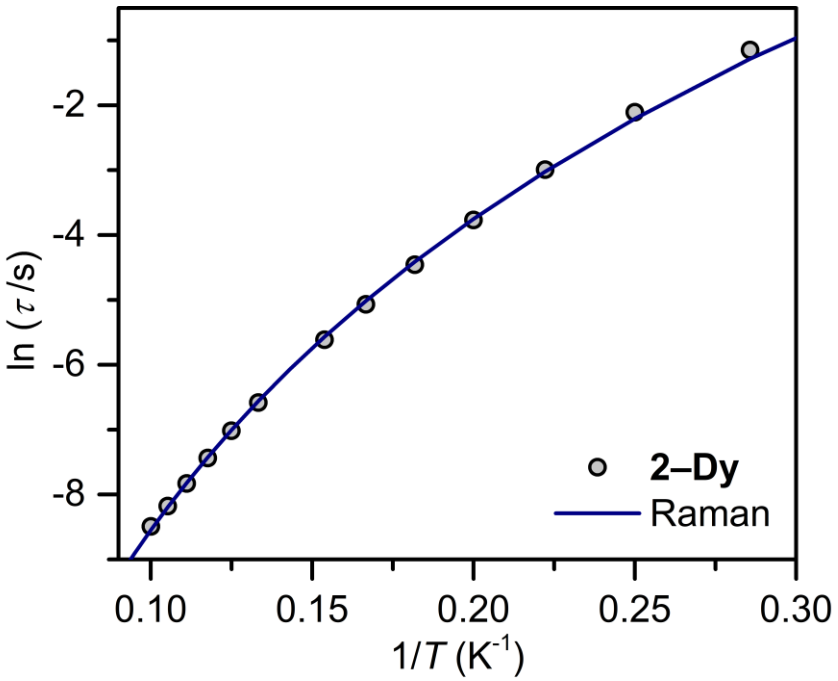

Figure S58. Arrhenius plot of the natural log of the relaxation time, τ, versus the inverse temperature, 1/*T*, obtained from ac measurements, for **2–Dy** (circles). The dark blue line represents a fit to a Raman process affording C = 0.00062(5) s^{-1} K^{-n}, and n = 6.92(4).

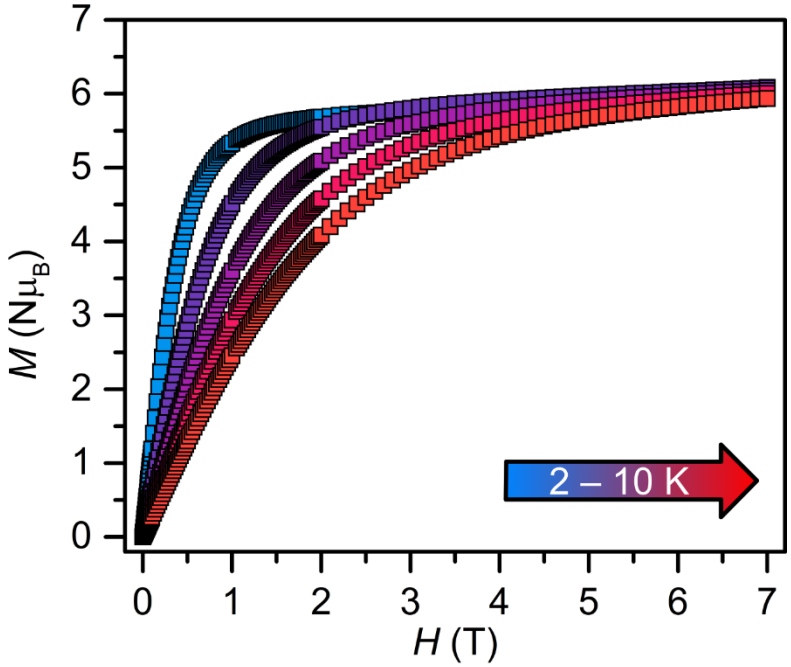

Figure S59. Field-dependent magnetization data for $Cp^*_2Dy(DMP)$, **2–Dy**, between 0 and 7 T from 2 to 10 K.

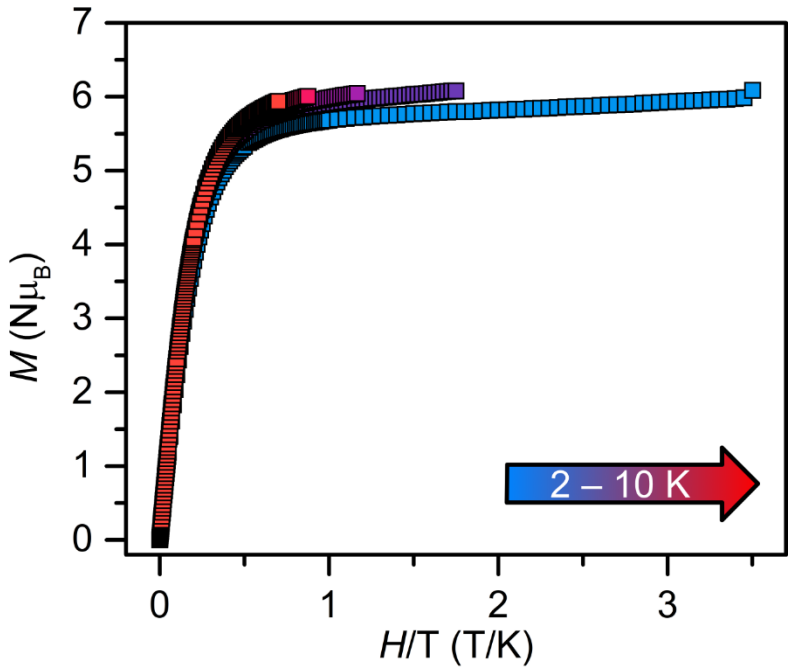

Figure S60. Field-dependent reduced magnetization data for Cp*$_2$Dy(DMP), **2–Dy**, between 0 and 7 T from 2 to 10 K.

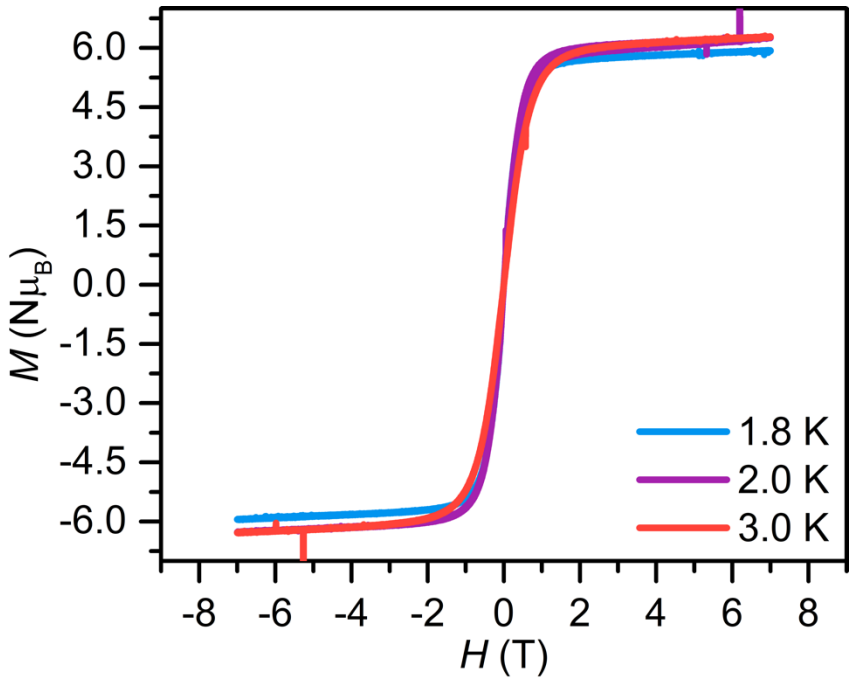

Figure S61. Plot of magnetization (*M*) *vs*. dc magnetic field (*H*) at an average sweep rate of 100 Oe/s for Cp*$_2$Dy(DMP), **2–Dy**, from 1.8 K (blue) to 3 K (red) collected between −7 and +7 T.

EPR Spectroscopy

Table S10. Spin Hamiltonian Parameters for $Cp^*_2Gd(TIP)$, **1–Gd**.

Temperature (K)	D (cm^{-1})	$\|E\|$ (cm^{-1})	$\|E\|/D$	σ_D (cm^{-1})	σ_E (cm^{-1})	g_{iso}
5	-0.121	0.039	0.322	0.008	0.005	1.992
100	-0.122	0.037	0.304	0.008	0.005	1.992

Ab Initio Calculations

The magnetic properties of $Cp^*_2Dy(TIP)$ (**1–Dy**) and $Cp^*_2Dy(DMP)$ (**2–Dy**) were calculated via a Complete Active Space Self-Consistent Field (CASSCF)+N-Valence Electron Perturbation Theory (NEVPT2) approach with the RI-JK approximation as implemented in ORCA 5.0.4.[1,2]

Scalar relativistic effects were accounted for with the second order Douglas-Kroll approach,[2,3] where the DKH-def2-SVP basis set was used for H and Cp* methyl C atoms,[4] DKH-def2-TZVP[5] for N and I atoms and SARC2-DKH-QZVP/SARC2-DKH-QZVP/JK basis sets for the Dy atoms.[5] DKH-def2-TZVP was used for the C atoms of the first coordination sphere and pyrrole ligands. Auxiliary basis sets for C, N, I and H were generated via the autoaux feature.[6] The frozen core approximation was disabled for all calculations. Tight convergence criteria were employed throughout with an energy convergence tolerance of 1e−07. All calculations used a finer integration grid (defgrid 3). The calculations were carried out on the coordinates obtained from single-crystal XRD for **1–Dy** at 100 K, 200 K and 300 K, where all hydrogen position were initially optimized via PBE0 functional.[7–9] using an eleven-electrons-in-seven-4f-orbitals active space. 21 quintet, 128 triplet and 130 doublet roots were considered for the state averaged (SA) CASSCF calculation. The same active space was used **2–Dy**. Dynamic correlation effects were introduced via strongly contracted NEVPT2 (SC-NEVPT2).[6,10,11] The construction of the fourth order reduced density matrix was simplified via the efficient implementation (D4step efficient).[1,12] The orbital energies of the SA-CASSCF were chosen as diagonal elements of the state-specific Fock operators (canonstep 0). Spin-Orbit-Coupling (SOC) effects were included within the NEVPT2 step via Quasi-Degenerate Perturbation Theory (QDPT) using the mean-field/effective potential Hamiltonian RI-SOMF(1x).[13,14] The free-particle Foldy–Wouthuysen (fpFW) transformation was carried out in the first step of the DKH protocol by including the vector potential. Picture change corrections were included on the second order, as well as finite nucleus corrections.[15]

Lastly, the magnetic properties such as *g*-tensors, crystal field parameters and estimated single-ion anisotropy barrier were calculated via the SINGLE_ANISO standalone program.[15]

Table S11. Calculated Kramers doublet (KD) energies associated magnetic moments, *g*-tensors and wavefunction composition for Cp*$_2$Dy(TIP) (**1–Dy**) at 100 K. Only contributions > 10% are printed. The angle θ between the ground state anisotropy axis and excited KDs are given in degrees (°). The wavefunction decompositions correspond to the lowest atomic multiplet J = 15/2 in wave functions with definite projection of the total moment to the quantization axis.

KD	E (cm^{-1})	M (μ_B)	g_x	g_y	g_z	θ (°)	Wave function composition
1	0.0	9.73	0.0084	0.0161	19.4562	0.0	$\|\pm 15/2\rangle$ (93%)
2	202.2	7.88	0.3062	0.6631	15.7623	0.3	$\|\pm 13/2\rangle$ (81%); $\|\pm 9/2\rangle$ (14%)
3	296.8	1.49	2.9595	3.1846	14.9503	92.3	$\|\pm 11/2\rangle$ (12%); $\|\pm 7/2\rangle$ (20%); $\|\pm 5/2\rangle$ (11%); $\|\pm 3/2\rangle$ (26%); $\|\pm 1/2\rangle$ (23%)
4	376.3	2.67	3.5333	5.3309	7.9747	97.1	$\|\pm 11/2\rangle$ (47%); $\|\pm 5/2\rangle$ (16%); $\|\pm 1/2\rangle$ (10%)
5	488.5	0.69	1.3789	1.4444	11.7423	94.9	$\|\pm 11/2\rangle$ (23%); $\|\pm 9/2\rangle$ (38%); $\|\pm 3/2\rangle$ (15%)
6	628.6	0.06	0.0066	0.0270	14.7281	94.1	$\|\pm 11/2\rangle$ (10%); $\|\pm 9/2\rangle$ (30%); $\|\pm 7/2\rangle$ (36%); $\|\pm 5/2\rangle$ (12%);
7	819.6	0.04	0.0193	0.0200	17.2044	85.8	$\|\pm 7/2\rangle$ (25%); $\|\pm 5/2\rangle$ (37%); $\|\pm 3/2\rangle$ (25%)
8	1051.7	0.01	0.0034	0.0061	19.5906	94.9	$\|\pm 5/2\rangle$ (14%); $\|\pm 3/2\rangle$ (33%); $\|\pm 1/2\rangle$ (50%)

Table S12. Calculated Kramers doublet (KD) energies associated magnetic moments, *g*-tensors and wavefunction composition for Cp*$_2$Dy(TIP) (**1–Dy**) at 200 K. Only contributions > 10% are printed. The angle θ between the ground state anisotropy axis and excited KDs are given in degree (°). The wavefunction decompositions correspond to the lowest atomic multiplet J = 15/2 in wave functions with definite projection of the total moment to the quantization axis.

KD	E (cm^{-1})	M (μ_B)	g_x	g_y	g_z	θ (°)	Wave function composition
1	0.0	9.73	0.0084	0.0159	19.4527	0.0	$\|\pm 15/2\rangle$ (93%)
2	202.7	7.92	0.2654	0.5657	15.8498	0.3	$\|\pm 13/2\rangle$ (83%); $\|\pm 9/2\rangle$ (14%)
3	300.4	1.43	2.8650	3.0602	15.2788	93.1	$\|\pm 11/2\rangle$ (12%); $\|\pm 7/2\rangle$ (19%); $\|\pm 5/2\rangle$ (12%); $\|\pm 3/2\rangle$ (27%); $\|\pm 1/2\rangle$ (24%)
4	378.5	2.85	3.5676	5.6820	7.8494	99.0	$\|\pm 11/2\rangle$ (48%); $\|\pm 5/2\rangle$ (16%); $\|\pm 1/2\rangle$ (10%)
5	488.1	0.78	1.5503	1.6371	11.6915	95.5	$\|\pm 11/2\rangle$ (22%); $\|\pm 9/2\rangle$ (39%); $\|\pm 3/2\rangle$ (15%)
6	625.0	0.11	0.0045	0.0335	14.7198	94.4	$\|\pm 11/2\rangle$ (10%); $\|\pm 9/2\rangle$ (30%); $\|\pm 7/2\rangle$ (36%); $\|\pm 5/2\rangle$ 12%
7	814.7	0.05	0.0265	0.0268	17.2067	84.5	$\|\pm 7/2\rangle$ (25%); $\|\pm 5/2\rangle$ (37%); $\|\pm 3/2\rangle$ (25%)
8	1051.5	0.02	0.0040	0.0070	19.5906	95.9	$\|\pm 5/2\rangle$ (14%); $\|\pm 3/2\rangle$ (33%); $\|\pm 15/2\rangle$ (50%)

Table S13. Calculated Kramers doublet (KD) energies associated magnetic moments, *g*-tensors and wavefunction composition for Cp*$_2$Dy(TIP) (**1–Dy**) at 300 K. Only contributions > 10% are printed. The angle θ between the ground state anisotropy axis and excited KDs are given in degree (°). The wavefunction decompositions correspond to the lowest atomic multiplet *J* = 15/2 in wave functions with definite projection of the total moment to the quantization axis.

KD	E (cm^{-1})	*M* (μ_B)	g_x	g_y	g_z	*θ* (°)	Wave function composition
1	0.0	9.71	0.0071	0.0146	19.4144	0.0	$\|\pm 15/2\rangle$ (92%)
2	201.7	7.82	0.3808	0.8273	15.6386	0.4	$\|\pm 13/2\rangle$ (80%); $\|\pm 9/2\rangle$ (15%)
3	297.7	1.33	2.6485	3.2146	15.0056	92.8	$\|\pm 11/2\rangle$ (11%); $\|\pm 7/2\rangle$ (19%); $\|\pm 5/2\rangle$ (11%); $\|\pm 3/2\rangle$ (27%); $\|\pm 1/2\rangle$ (24%)
4	384.4	2.78	3.7543	5.5580	7.9333	98.5	$\|\pm 11/2\rangle$ (47%); $\|\pm 7/2\rangle$ (10%); $\|\pm 5/2\rangle$ (16%); $\|\pm 1/2\rangle$ (10%)
5	500.2	0.67	1.3441	1.4908	11.7458	95.0	$\|\pm 11/2\rangle$ (23%); $\|\pm 9/2\rangle$ (37%); $\|\pm 3/2\rangle$ (15%)
6	642.2	0.13	0.0087	0.0508	14.7230	93.7	$\|\pm 11/2\rangle$ (11%); $\|\pm 9/2\rangle$ (31%); $\|\pm 7/2\rangle$ (35%); $\|\pm 5/2\rangle$ (12%); $\|\pm 1/2\rangle$ (10%)
7	835.5	0.08	0.0332	0.0343	17.2023	86.0	$\|\pm 7/2\rangle$ (25%); $\|\pm 5/2\rangle$ (36%); $\|\pm 3/2\rangle$ (25%)
8	1081.5	0.01	0.0044	0.0072	19.6099	95.1	$\|\pm 5/2\rangle$ (14%); $\|\pm 3/2\rangle$ (33%); $\|\pm 1/2\rangle$ (49%)

Table S14. Calculated Kramers doublet (KD) energies associated magnetic moments, *g*-tensors and wavefunction composition for Cp*$_2$Dy(DMP) (**2–Dy**). Only contributions > 10% are printed. The angle θ between the ground state anisotropy axis and excited KDs are given in degree (°). The wavefunction decompositions correspond to the lowest atomic multiplet *J* = 15/2 in wave functions with definite projection of the total moment to the quantization axis.

KD	E (cm^{-1})	*M* (μ_B)	g_x	g_y	g_z	*θ* (°)	Wave function composition
1	0.0	9.30	0.1872	0.5077	18.5949	0.0	$\|\pm 15/2\rangle$ (83%); $\|\pm 11/2\rangle$ (13%)
2	125.6	2.34	2.3943	4.6816	13.9284	92.2	$\|\pm 13/2\rangle$ (17%); $\|\pm 9/2\rangle$ (15%); $\|\pm 5/2\rangle$ (20%); $\|\pm 3/2\rangle$ (16%); $\|\pm 1/2\rangle$ (23%)
3	210.7	3.82	7.6554	5.3214	0.8503	94.8	$\|\pm 13/2\rangle$ (51%); $\|\pm 9/2\rangle$ (10%); $\|\pm 7/2\rangle$ (11%); $\|\pm 3/2\rangle$ (15%)
4	369.6	1.93	3.8507	5.1872	8.3902	85.1	$\|\pm 13/2\rangle$ (14%); $\|\pm 11/2\rangle$ (30%); $\|\pm 7/2\rangle$ (20%); $\|\pm 5/2\rangle$ (16%)
5	524.2	0.38	0.2827	0.7335	11.9383	86.8	$\|\pm 13/2\rangle$ (12%); $\|\pm 11/2\rangle$ (35%); $\|\pm 9/2\rangle$ (26%); $\|\pm 3/2\rangle$ (13%)
6	687.9	0.24	0.1973	0.3052	14.7529	89.3	$\|\pm 11/2\rangle$ (16%); $\|\pm 9/2\rangle$ (34%); $\|\pm 7/2\rangle$ (28%)
7	903.6	0.21	0.0432	0.0510	17.2401	89.4	$\|\pm 9/2\rangle$ (12%); $\|\pm 7/2\rangle$ (27%); $\|\pm 5/2\rangle$ (34%); $\|\pm 3/2\rangle$ (21%)
8	1192.1	0.02	0.0040	0.0045	19.6655	87.8	$\|\pm 5/2\rangle$ (15%); $\|\pm 3/2\rangle$ (33%); $\|\pm 1/2\rangle$ (47%);

Table S15. Crystal field parameters calculated for Cp*$_2$Dy(TIP) (**1–Dy**) at 100 K via the SINGLE_ANISO program. The Hamiltonian employed to calculate the crystal field parameters is given by:

$$\hat{H}_{CF} = \sum_{k=2,4,6} \sum_{k=-q}^{+q} \left[B_k^q \hat{O}_k^q(S) \right]$$

where $\hat{O}_k^q$ is the extended Stevens operator as implemented in the "EasySpin" package for MATLAB, B_k^q the crystal field parameter, *k* is the rank of the irreducible tensor operator (ITO) (2,4,6), *q* is the component of the ITO (*q* = −*k*, −*k*+1,…0,1,…*k*).

k	*q*	Weight (%)	B_q^k	*k*	*q*	Weight (%)	B_q^k
2	−2	2.8	-4.90E-01	6	−6	2.1	1.31E-04
	−1	<1	-1.07E-03		−5	<1	-2.93E-05
	0	28.7	-4.07E+00		−4	<1	1.42E-05
	1	<1	-5.30E-02		−3	<1	1.18E-07
	2	37.4	6.50E+00		−2	3.1	1.35E-04
4	−4	2.7	8.89E-03		−1	<1	-9.25E-06
	−3	<1	7.06E-04		0	1.2	-9.95E-06
	−2	<1	1.36E-03		1	<1	1.42E-05
	−1	<1	4.98E-04		2	6.3	2.71E-04
	0	1.7	-1.30E-03		3	<1	1.45E-05
	1	<1	-2.97E-04		4	<1	-1.99E-05
	2	2.8	-6.85E-03		5	<1	3.48E-05
	3	<1	-8.34E-04		6	2.7	-1.74E-04
	4	3.6	-1.18E-02				

Table S16. Crystal field parameters calculated for Cp*$_2$Dy(TIP) (**1–Dy**) at 200 K via the SINGLE_ANISO program.

k	*q*	Weight (%)	B_q^k	*k*	*q*	Weight (%)	B_q^k
2	−2	3.0	-5.22E-01	6	−6	2.2	1.39E-04
	−1	<1	9.52E-03		−5	<1	-5.30E-05
	0	28.7	-4.07E+00		−4	<1	1.25E-05
	1	<1	-6.56E-02		−3	<1	7.43E-06
	2	37.1	6.44E+00		−2	2.9	1.25E-04
4	−4	2.8	9.27E-03		−1	<1	-7.21E-06
	−3	<1	-3.33E-04		0	1.2	-9.76E-06
	−2	<1	1.51E-03		1	<1	1.28E-05
	−1	<1	3.46E-04		2	6.7	2.85E-04
	0	1.6	-1.27E-03		3	<1	-1.34E-06
	1	<1	-4.08E-04		4	<1	-2.37E-05
	2	2.9	-7.07E-03		5	<1	2.81E-05
	3	<1	-5.53E-04		6	2.6	-1.65E-04
	4	3.4	-1.11E-02				

Table S17. Crystal field parameters calculated for Cp*$_2$Dy(TIP) (**1–Dy**) at 300 K via the SINGLE_ANISO program.

k	*q*	Weight (%)	B_q^k	*k*	*q*	Weight (%)	B_q^k
2	−2	3.3	-5.84E-01	6	−6	2.0	1.29E-04
	−1	<1	-6.72E-03		−5	<1	-2.41E-05
	0	28.3	-4.14E+00		−4	<1	1.45E-05
	1	<1	-1.27E-01		−3	<1	-4.71E-06
	2	37.9	6.79E+00		−2	2.8	1.21E-04
4	−4	2.6	8.82E-03		−1	<1	-8.46E-06
	−3	<1	3.51E-04		0	1.1	-9.16E-06
	−2	<1	1.30E-03		1	<1	1.95E-05
	−1	<1	3.77E-04		2	6.6	2.92E-04
	0	1.7	-1.33E-03		3	<1	6.23E-06
	1	<1	-4.01E-04		4	<1	-3.21E-05
	2	2.6	-6.51E-03		5	<1	3.61E-05
	3	<1	-1.02E-03		6	2.5	-1.61E-04
	4	3.3	-1.11E-02				

Table S18. Crystal field parameters calculated for Cp*$_2$Dy(DMP) (**2–Dy**) via the SINGLE_ANISO program.

k	*q*	Weight (%)	B_q^k	*k*	*q*	Weight (%)	B_q^k
2	−2	<1	3.13E-02	6	−6	<1	3.12E-05
	−1	<1	2.75E-02		−5	<1	1.01E-04
	0	23	-3.84E+00		−4	<1	-5.30E-06
	1	<1	-3.42E-01		−3	<1	-1.86E-05
	2	46	9.38E+00		−2	2	1.22E-04
4	−4	<1	3.82E-03		−1	<1	-1.32E-05
	−3	<1	4.65E-03		0	1	-1.07E-05
	−2	<1	1.09E-03		1	<1	1.73E-05
	−1	<1	2.75E-05		2	7	3.51E-04
	0	2	-1.85E-03		3	<1	5.32E-06
	1	<1	1.35E-03		4	1	-6.32E-05
	2	2	-5.54E-03		5	<1	1.10E-04
	3	<1	4.33E-03		6	3	-1.83E-04
	4	5	-1.77E-02				

Table S19. Calculated average transition dipole moments for the eight lowest lying Kramers doublets with opposing magnetization (+*I* → *I*−1), and for excited states (*I* → *I*+1), (*I* → *I*+2), (*I* → *I*+3), (*I* → *I*+4) and (*I* → *I*+5) of $Cp^*_2Dy(TIP)$ (**1–Dy**) at 100 K.

Through Barrier (+*I* → −*I*)			**Through Excited States (+*I* → *I*+1)**			**Through Excited States (+*I* → *I*+2)**		
KD1	**KD2**	**Magnitude**	**KD**	**KD+1**	**Magnitude**	**KD**	**KD+2**	**Magnitude**
+1	−1	4.080E-03	+1	+2	1.821E+00	+1	+3	1.580E-01
+2	−2	1.618E-01	+1	−2	1.410E-03	+1	−3	1.835E-01
+3	−3	3.033E+00	+2	+3	1.833E+00	+2	+4	1.586E+00
+4	−4	1.917E+00	+2	−3	4.508E-01	+2	−4	2.954E-01
+5	−5	2.227E+00	+3	+4	1.364E+00	+3	+5	1.446E-01
+6	−6	1.744E-01	+3	−4	1.805E+00	+3	−5	2.737E-01
+7	−7	8.650E-01	+4	+5	1.961E+00	+4	+6	2.040E-01
+8	−8	5.239E-01	+4	−5	1.387E+00	+4	−6	1.919E-01
			+5	+6	1.958E+00	+5	+7	1.764E-01
			+5	−6	2.021E+00	+5	−7	1.416E-01
			+6	+7	2.331E+00	+6	+8	4.458E-02
			+6	−7	3.190E-01	+6	−8	4.965E-01
			+7	+8	2.590E-01			
			+7	−8	1.658E+00			

Through Excited States (+*I* → *I*+3)			**Through Excited States (+*I* → *I*+4)**			**Through Excited States (+*I* → *I*+5)**		
KD	**KD+3**	**Magnitude**	**KD**	**KD+4**	**Magnitude**	**KD**	**KD+5**	**Magnitude**
+1	+4	2.061E-01	+1	+5	1.203E-01	+1	+6	8.151E-02
+1	−4	1.222E-01	+1	−5	6.700E-02	+1	−6	8.742E-02
+2	+5	1.879E-01	+2	+6	1.483E-01	+2	+7	9.363E-02
+2	−5	4.932E-01	+2	−6	1.472E-01	+2	−7	7.670E-02
+3	+6	1.705E-01	+3	+7	1.168E-01	+3	+8	3.181E-02
+3	−6	1.712E-01	+3	−7	1.341E-01	+3	−8	3.063E-02
+4	+7	1.690E-01	+4	+8	5.655E-02			
+4	−7	1.718E-01	+4	−8	5.288E-02			
+5	+8	2.299E-01						
+5	−8	2.167E-01						

Table S20. Calculated average transition dipole moments for the eight lowest lying Kramers doublets with opposing magnetization (+*I* → *I*−1), and for excited states (*I* → *I*+1), (*I* → *I*+2), (*I* → *I*+3), (*I* → *I*+4) and (*I* → *I*+5) of for $Cp^*_2Dy(TIP)$ (**1–Dy**) at 200 K.

Through Barrier (+*I* → −*I*)			**Through Excited States (+*I* → *I*+1)**			**Through Excited States (+*I* → *I*+2)**		
KD1	**KD2**	**Magnitude**	**KD**	**KD+1**	**Magnitude**	**KD**	**KD+2**	**Magnitude**
+1	−1	4.040E-03	+1	+2	1.825E+00	+1	+3	1.555E-01
+2	−2	1.388E-01	+1	−2	2.350E-03	+1	−3	1.658E-01
+3	−3	3.078E+00	+2	+3	1.780E+00	+2	+4	1.624E+00
+4	−4	1.901E+00	+2	−3	4.126E-01	+2	−4	2.879E-01
+5	−5	2.249E+00	+3	+4	1.306E+00	+3	+5	1.466E-01
+6	−6	1.575E-01	+3	−4	1.765E+00	+3	−5	2.882E-01
+7	−7	8.808E-01	+4	+5	1.994E+00	+4	+6	2.238E-01
+8	−8	3.308E-01	+4	−5	1.371E+00	+4	−6	2.053E-01
			+5	+6	1.971E+00	+5	+7	1.900E-01
			+5	−6	2.016E+00	+5	−7	1.424E-01
			+6	+7	2.337E+00	+6	+8	2.736E-02
			+6	−7	3.215E-01	+6	−8	5.074E-01
			+7	+8	2.490E-01			
			+7	−8	1.664E+00			

Through Excited States (+*I* → *I*+3)			**Through Excited States (+*I* → *I*+4)**			**Through Excited States (+*I* → *I*+5)**		
KD	**KD+3**	**Magnitude**	**KD**	**KD+4**	**Magnitude**	**KD**	**KD+5**	**Magnitude**
+1	+4	2.079E-01	+1	+5	1.207E-01	+1	+6	8.639E-02
+1	−4	1.095E-01	+1	−5	6.339E-02	+1	−6	8.609E-02
+2	+5	1.947E-01	+2	+6	1.467E-01	+2	+7	9.547E-02
+2	−5	4.962E-01	+2	−6	1.456E-01	+2	−7	7.596E-02
+3	+6	1.809E-01	+3	+7	1.193E-01	+3	+8	3.244E-02
+3	−6	1.811E-01	+3	−7	1.379E-01	+3	−8	3.107E-02
+4	+7	1.710E-01	+4	+8	5.661E-02			
+4	−7	1.717E-01	+4	−8	5.406E-02			
+5	+8	2.248E-01						
+5	−8	2.151E-01						

Table S21. Calculated average transition dipole moments for the eight lowest lying Kramers doublets with opposing magnetization (+*I* → *I*−1), and for excited states (*I* → *I*+1), (*I* → *I*+2), (*I* → *I*+3), (*I* → *I*+4) and (*I* → *I*+5) of for $Cp^*_2Dy(TIP)$ (**1–Dy**) at 300 K.

Through Barrier (+*I* → −*I*)			**Through Excited States (+*I* → *I*+1)**			**Through Excited States (+*I* → *I*+2)**		
KD1	**KD2**	**Magnitude**	**KD**	**KD+1**	**Magnitude**	**KD**	**KD+2**	**Magnitude**
+1	−1	3.610E-03	+1	+2	1.832E+00	+1	+3	1.694E-01
+2	−2	2.018E-01	+1	−2	3.280E-03	+1	−3	1.960E-01
+3	−3	3.047E+00	+2	+3	1.840E+00	+2	+4	1.582E+00
+4	−4	1.945E+00	+2	−3	5.098E-01	+2	−4	2.907E-01
+5	−5	2.236E+00	+3	+4	1.345E+00	+3	+5	1.509E-01
+6	−6	5.228E-01	+3	−4	1.807E+00	+3	−5	2.930E-01
+7	−7	6.979E-01	+4	+5	1.958E+00	+4	+6	2.167E-01
+8	−8	5.220E-01	+4	−5	1.384E+00	+4	−6	1.712E-01
			+5	+6	1.944E+00	+5	+7	1.751E-01
			+5	−6	2.022E+00	+5	−7	1.386E-01
			+6	+7	2.337E+00	+6	+8	2.898E-02
			+6	−7	2.407E-01	+6	−8	4.639E-01
			+7	+8	2.173E-01			
			+7	−8	1.673E+00			

Through Excited States (+*I* → *I*+3)			**Through Excited States (+*I* → *I*+4)**			**Through Excited States (+*I* → *I*+5)**		
KD	**KD+3**	**Magnitude**	**KD**	**KD+4**	**Magnitude**	**KD**	**KD+5**	**Magnitude**
+1	+4	2.189E-01	+1	+5	1.149E-01	+1	+6	9.137E-02
+1	−4	1.116E-01	+1	−5	7.174E-02	+1	−6	7.868E-02
+2	+5	1.971E-01	+2	+6	1.372E-01	+2	+7	8.742E-02
+2	−5	4.934E-01	+2	−6	1.498E-01	+2	−7	7.340E-02
+3	+6	1.740E-01	+3	+7	1.186E-01	+3	+8	3.152E-02
+3	−6	1.639E-01	+3	−7	1.301E-01	+3	−8	3.031E-02
+4	+7	1.662E-01	+4	+8	5.678E-02			
+4	−7	1.706E-01	+4	−8	4.955E-02			
+5	+8	2.158E-01						
+5	−8	2.021E-01						

Table S22. Calculated average transition dipole moments for the eight lowest lying Kramers doublets with opposing magnetization (+*I* → *I*−1), and for excited states (*I* → *I*+1), (*I* → *I*+2), (*I* → *I*+3), (*I* → *I*+4) and (*I* → *I*+5) of $Cp^*_2Dy(DMP)$ (**2–Dy**).

Through Barrier (+*I* → −*I*)			**Through Excited States (+*I* → *I*+1)**			**Through Excited States (+*I* → *I*+2)**		
KD1	**KD2**	**Magnitude**	**KD**	**KD+1**	**Magnitude**	**KD**	**KD+2**	**Magnitude**
+1	−1	1.158E-01	+1	+2	1.569E+00	+1	+3	1.236E+00
+2	−2	2.722E+00	+1	−2	3.971E-01	+1	−3	2.646E-01
+3	−3	1.029E+00	+2	+3	1.402E+00	+2	+4	4.072E-01
+4	−4	2.258E+00	+2	−3	1.770E+00	+2	−4	3.707E-01
+5	−5	1.976E+00	+3	+4	2.263E+00	+3	+5	3.447E-01
+6	−6	1.635E+00	+3	−4	1.354E+00	+3	−5	3.133E-01
+7	−7	3.623E-01	+4	+5	1.781E+00	+4	+6	6.392E-02
+8	−8	3.369E-01	+4	−5	1.705E+00	+4	−6	1.057E-01
			+5	+6	1.570E+00	+5	+7	5.401E-02
			+5	−6	2.093E+00	+5	−7	1.017E-01
			+6	+7	2.139E+00	+6	+8	2.779E-01
			+6	−7	7.968E-01	+6	−8	1.118E-01
			+7	+8	1.687E+00			
			+7	−8	8.369E-02			

Through Excited States (+*I* → *I*+3)			**Through Excited States (+*I* → *I*+4)**			**Through Excited States (+*I* → *I*+5)**		
KD	**KD+3**	**Magnitude**	**KD**	**KD+4**	**Magnitude**	**KD**	**KD+5**	**Magnitude**
+1	+4	2.527E-01	+1	+5	1.189E-01	+1	+6	1.160E-01
+1	−4	2.053E-01	+1	−5	9.017E-02	+1	−6	7.023E-02
+2	+5	3.512E-01	+2	+6	1.344E-01	+2	+7	7.323E-02
+2	−5	9.233E-02	+2	−6	1.678E-01	+2	−7	7.240E-02
+3	+6	7.176E-02	+3	+7	9.934E-02	+3	+8	3.137E-02
+3	−6	6.191E-02	+3	−7	8.091E-02	+3	−8	3.535E-02
+4	+7	2.161E-01	+4	+8	4.797E-02			
+4	−7	2.084E-01	+4	−8	5.024E-02			
+5	+8	1.773E-01						
+5	−8	2.308E-01						

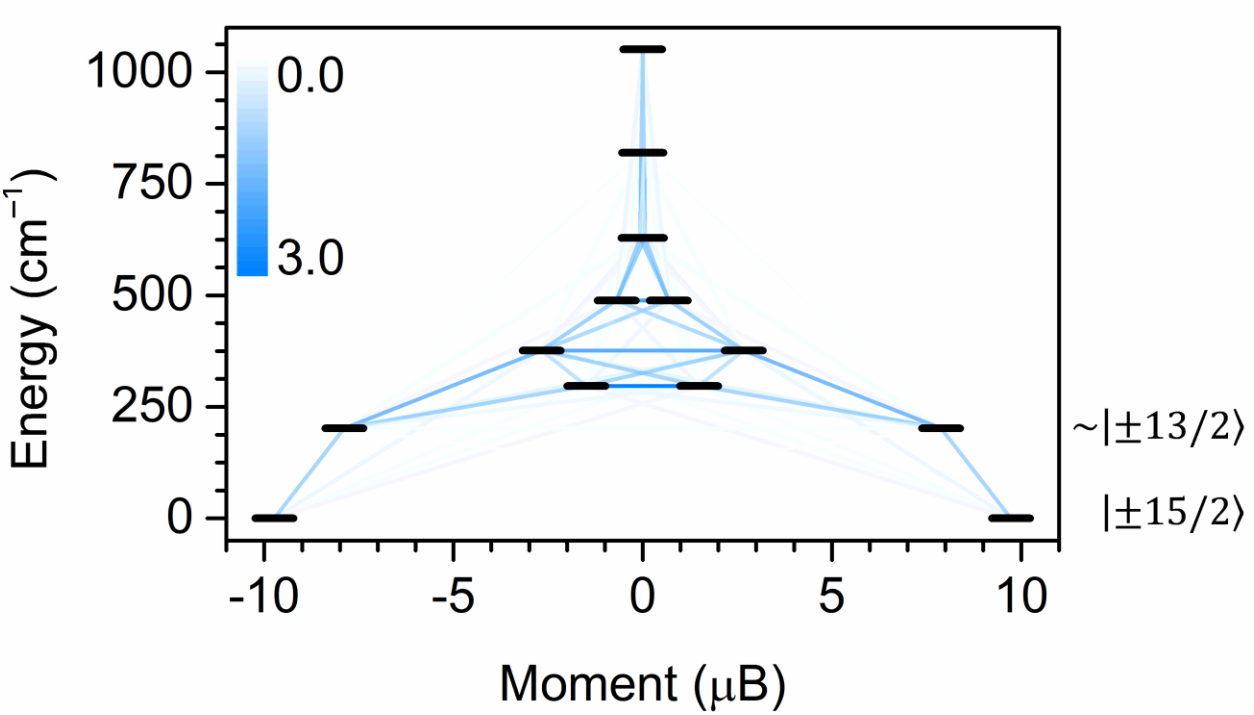

Figure S62. Calculated full relaxation barrier for Cp*$_2$Dy(TIP) (**1–Dy**) at 100 K. Solid lines represent possible relaxation processes as indicated by calculated transition magnetic dipole moments, where dark blue coloration represents most probable transitions and faded blue indicates vanishing probabilities. The numbers on the right are given for the primary M_J state comprising the wave function for each state. States above KD2 are heavily mixed and therefore no M_J states are assigned.

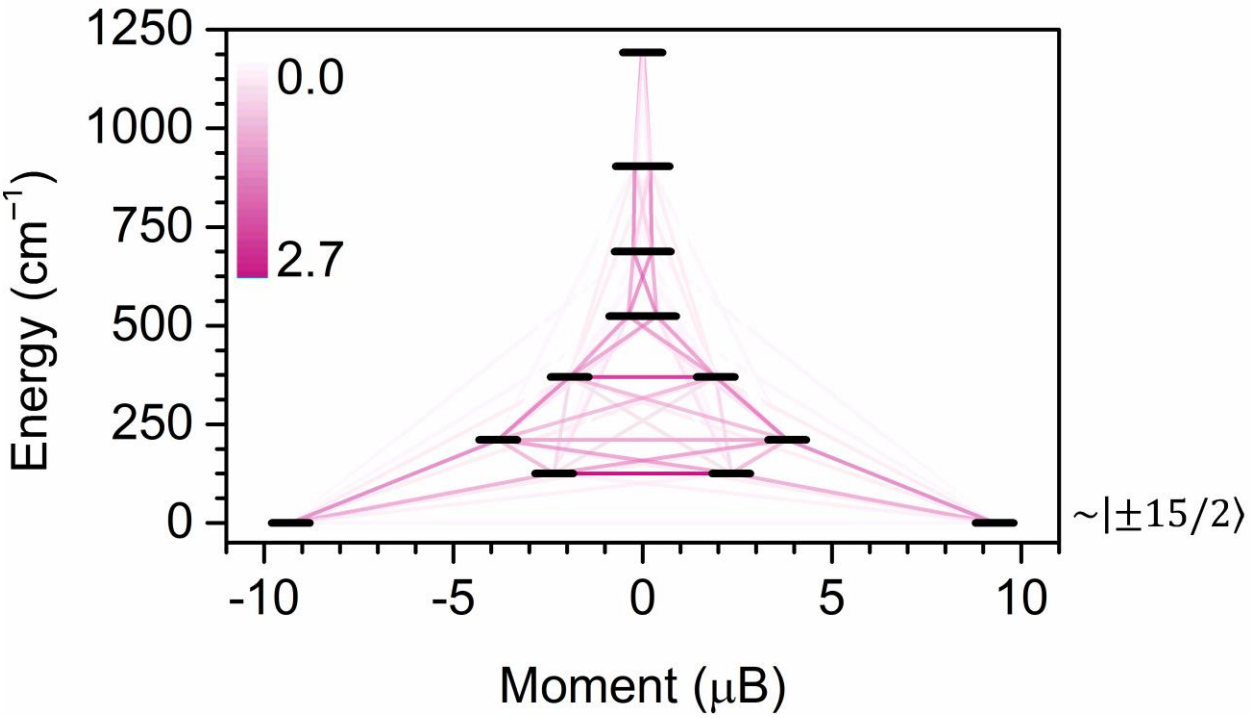

Figure S63. Calculated full relaxation barrier for Cp*$_2$Dy(DMP) (**2–Dy**). Solid lines represent possible relaxation processes as indicated by calculated transition magnetic dipole moments, where dark purple coloration represents most probable transitions and faded blue indicates vanishing probabilities. The numbers on the right are given for the primary M_J state comprising the wave function for each state. States above KD1 are heavily mixed and therefore no M_J states are assigned.

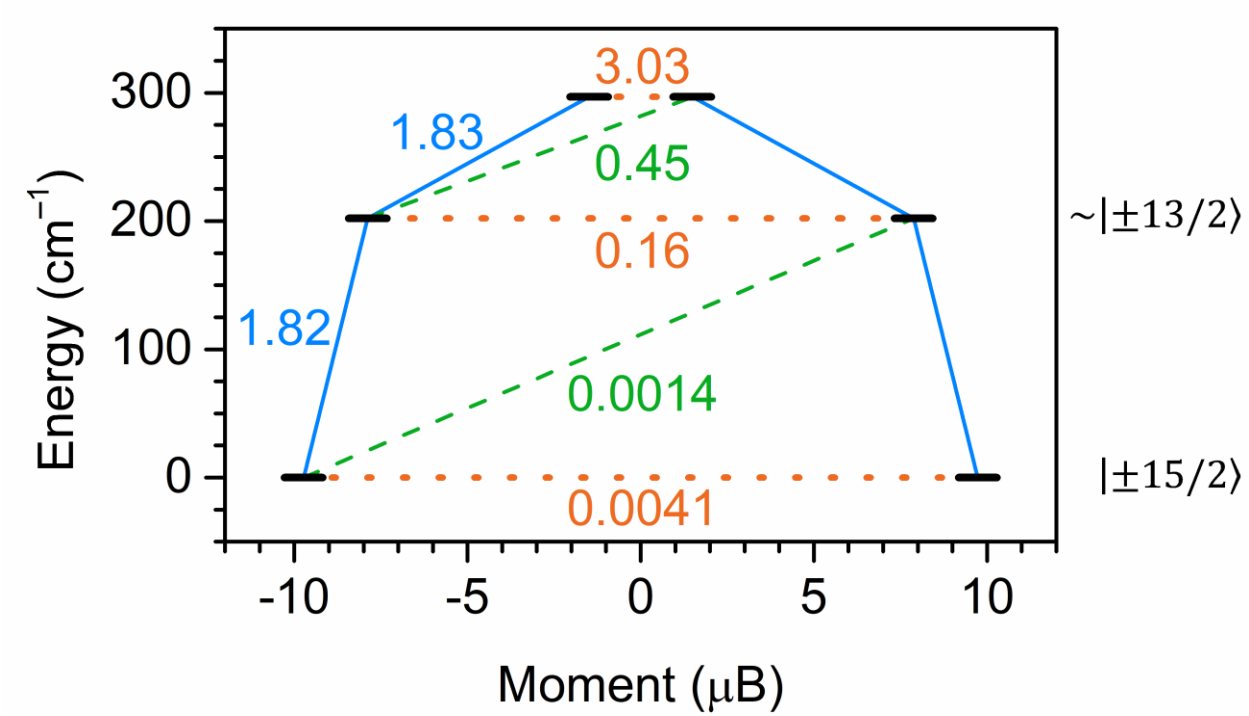

Figure S64. Estimated relaxation barrier comprising the four lowest-lying Kramers doublets with relaxation pathways shown for Cp*$_2$Dy(TIP) (**1–Dy**) at 100 K. Solid blue and dashed green lines indicate Orbach processes, orange dotted line indicates quantum tunneling (QTM)/thermally activated QTM pathways. Values next to the arrows correspond to the respective transition magnetic moment matrix elements. The numbers on the right are given for the primary M_J state comprising the wave function for each state.

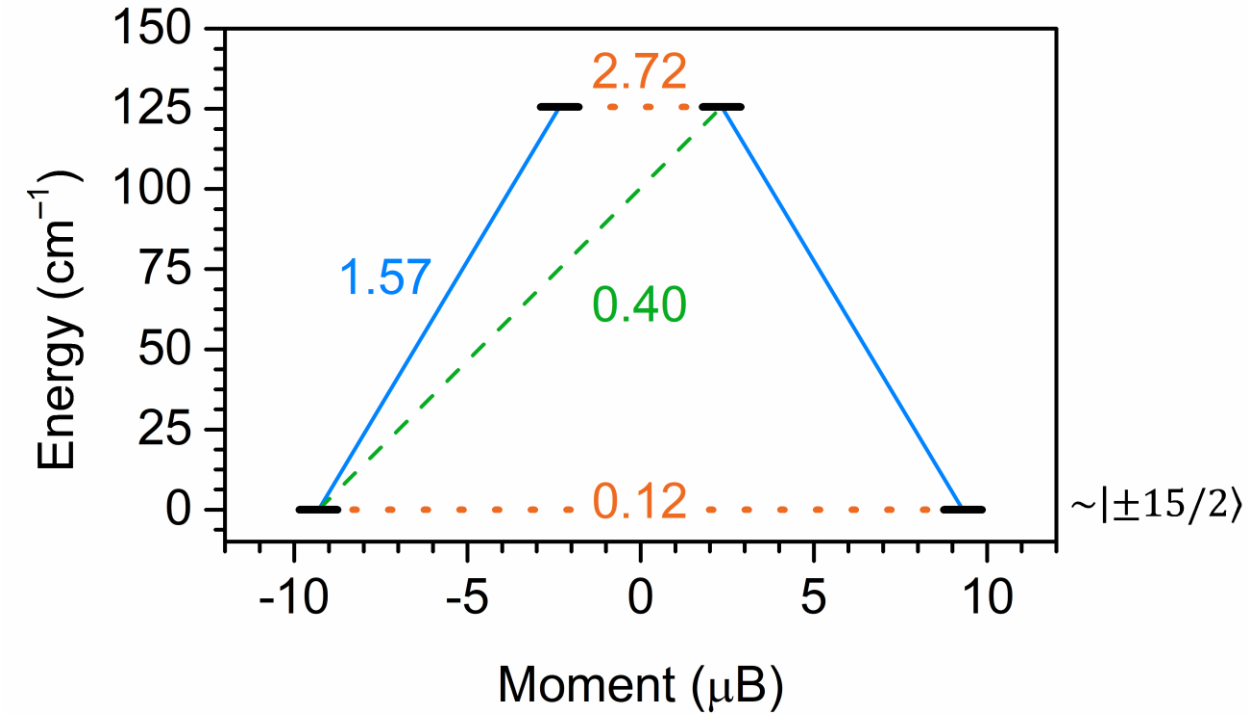

Figure S65. Estimated relaxation barrier comprising the two lowest-lying Kramers doublets with relaxation pathways shown for Cp*$_2$Dy(DMP) (**2–Dy**). Solid blue and dashed green lines indicate Orbach processes, orange dotted line indicates quantum tunneling (QTM)/thermally activated QTM pathways. Values next to the arrows correspond to the respective transition magnetic moment matrix elements. The numbers on the right are given for the primary M_J state comprising the wave function for each state.

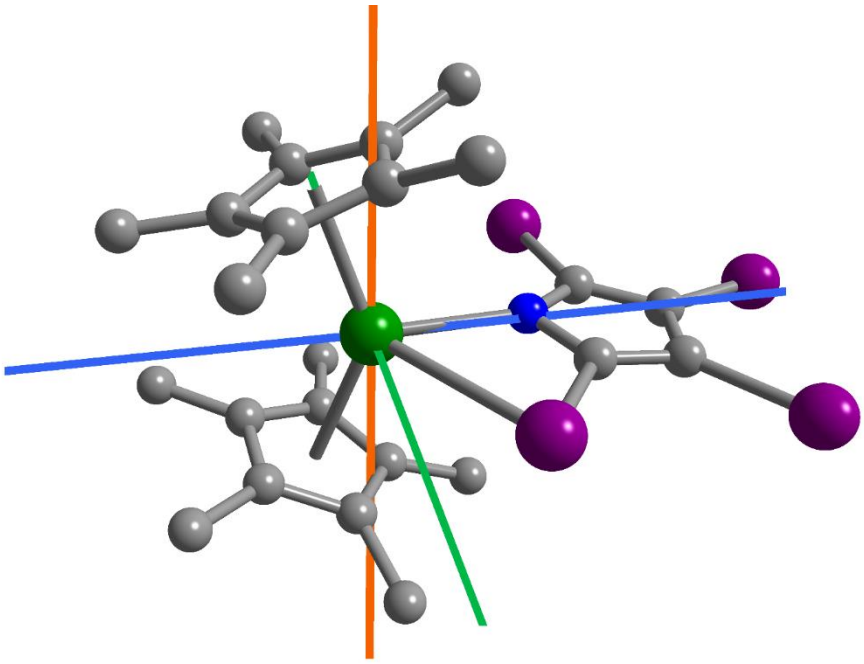

Figure S66. Plot of the *g*-tensor components calculated for the $|\pm 15/2\rangle$ ground state Kramers doublet of Cp*$_2$Dy(TIP) (**1–Dy**) at 100 K. Color code: g_x(green), g_y (blue) and g_z (orange) with respective compositions 0.0084 (g_x), 0.0161 (g_y) and 19.4562 (g_z).

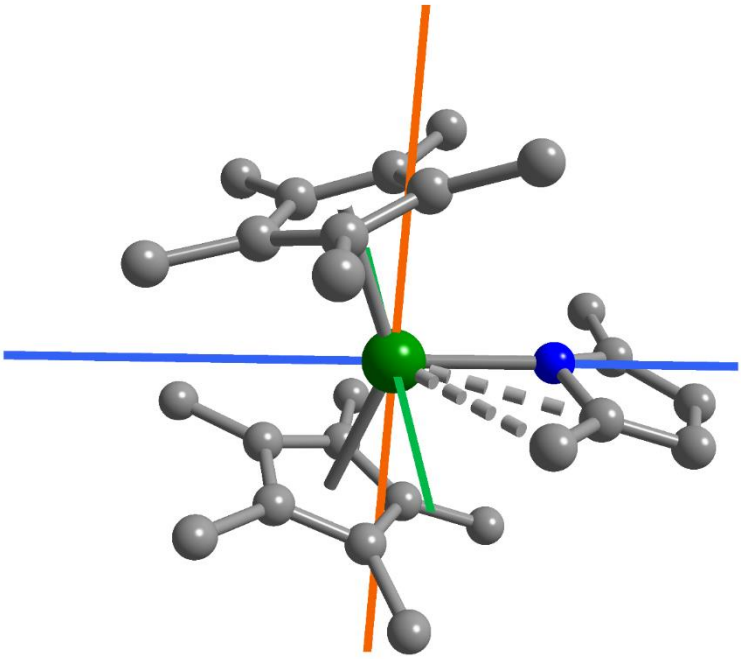

Figure S67. Plot of the *g*-tensor components calculated for the $|\pm 15/2\rangle$ ground state Kramers doublet of Cp*$_2$Dy(DMP) (**2–Dy**). Color code: g_x (green), g_y (blue) and g_z (orange) with respective compositions 0.1872 (g_x), 0.5077 (g_y) and 18.5949 (g_z).

Table S23. Spin-orbit coupling constants (ζ) and Slater Condon parameters (F^2, F^4 and F^6, interelectronic repulsion) derived via *ab initio* ligand field (AILFT) analysis from CASSCF/NEVPT2 calculations of $Cp^*_2Dy(TIP)$ (**1–Dy**) at 100 K and $Cp^*_2Dy(DMP)$ (**2–Dy**). For comparison, the free Dy^{III} ion was calculated, using the same methodology as described for **1–Dy** and **2–Dy** in the method description.

	Slater Condon Parameters (cm^{-1})			
Complex	**F^2**	**F^4**	**F^6**	**ζ (cm^{-1})**
1–Dy (100 K)	122933.4	77132.5	55520.5	1929.2
1–Dy (200 K)	122936.8	77135.3	55522.3	1929.2
1–Dy (300 K)	122950.3	77143.6	55528.4	1929.4
2–Dy	122911.3	77088.2	55501.1	1928.9
Free Dy^{III} ion	124143.1	77935.5	56082.0	1941.5
Nephelauxetic contraction (%)				
1–Dy (100 K)	0.97	1.0	1.0	0.6
1–Dy (200 K)	0.97	1.0	1.0	0.6
1–Dy (300 K)	0.96	1.0	1.0	0.6
2–Dy	0.99	1.1	1.0	0.6

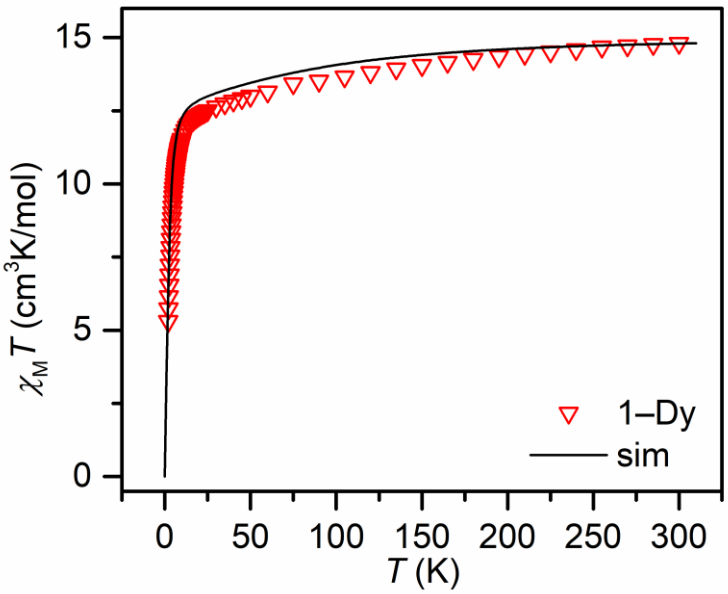

Figure S68. Variable-temperature dc magnetic susceptibility data ($\chi_M T$ *vs*. *T*) for Cp*$_2$Dy(TIP) (**1–Dy**) under a 1.0 T applied dc field (red triangles). Solid black line represents the calculated values for **1–Dy**. Calculated $\chi_M T$ values were scaled to match the experimental $\chi_M T$ value at room temperature.

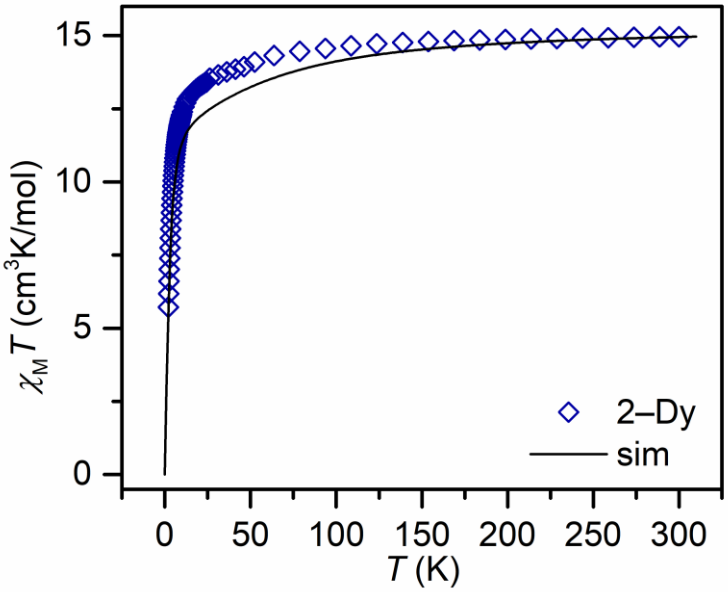

Figure S69. Variable-temperature dc magnetic susceptibility data ($\chi_M T$ *vs*. *T*) for Cp*$_2$Dy(DMP) (**2–Dy**) under a 1.0 T applied dc field (dark blue diamonds). Solid black line represents the calculated values for **2–Dy**. Calculated $\chi_M T$ values were scaled to match the experimental $\chi_M T$ value at room temperature.

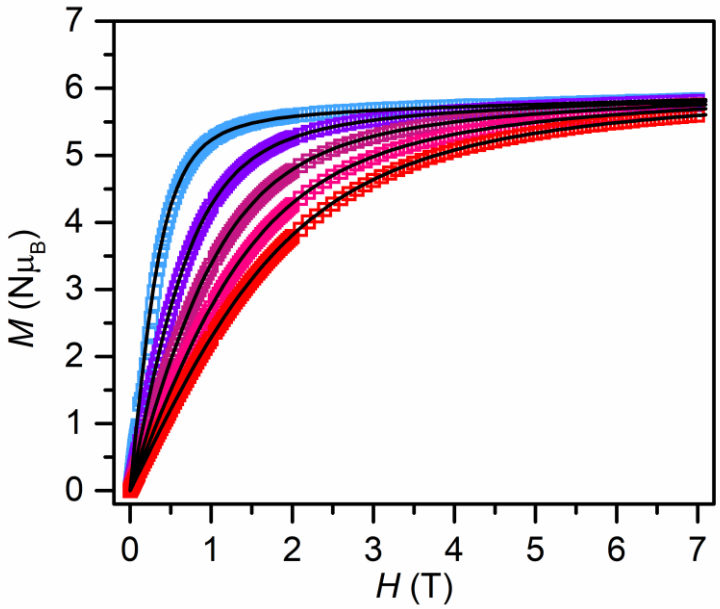

Figure S70. Field-dependent magnetization data for Cp*$_2$Dy(TIP) (**1–Dy**) at 2 K, 4 K, 6 K, 8 K, and 10 K. Solid black lines represent *ab initio* calculated *M* values (obtained from optimized crystal coordinates of the structure collected at 100 K). Calculated *M* values were scaled to match the experimental maximum *M* value.

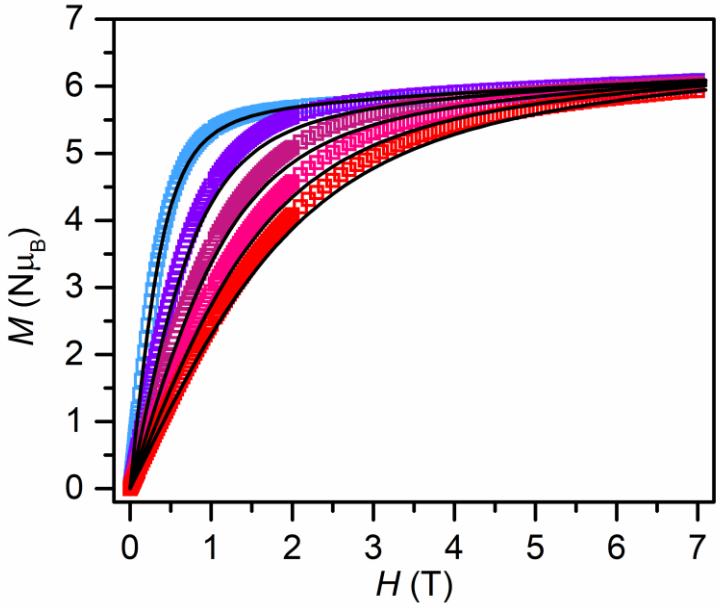

Figure S71. Field-dependent magnetization data for Cp*$_2$Dy(DMP) (**2–Dy**) at 2 K, 4 K, 6 K, 8 K, and 10 K. Solid black lines represent *ab initio* calculated *M* values (obtained from optimized crystal coordinates of the structure collected at 100 K). Calculated *M* values were scaled to match the experimental maximum *M* value.

DFT Calculations

Method for Estimating pK_a values of Heterocycles

The pK_a values for TIPH, H-pyrrole, and DMPH heterocycles were calculated via the Gibbs free energy for the acid, its conjugate base in both the gas phase and including solvation effects. This procedure has been outlined elsewhere,[16–18] and follows the thermodynamic cycle presented below:

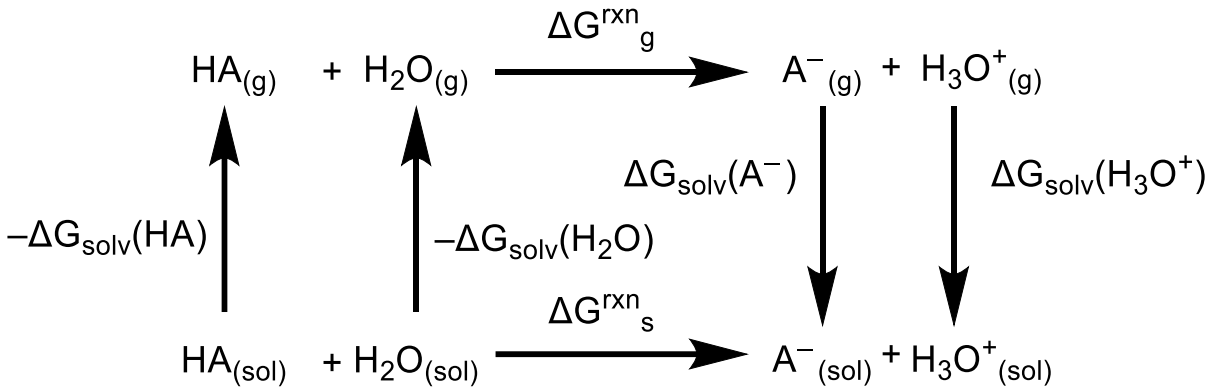

The value of ΔG^{rxn}_s can subsequently be determined using:

$$\Delta G_s^{rxn} = \Delta G_g^{rxn} + \Delta G_{solv}(A^-) + \Delta G_{solv}(H_3O^+) - \Delta G_{solv}(HA) - \Delta G_{solv}(H_2O)$$

The resulting ΔG^{rxn}_s can then be used to solve for pK_a using the following relationship:

$$pK_a = \frac{\Delta G_s^{rxn}}{1.364} - \log[H_2O]$$

Where the concentration of water is 55.49 M. To account for issues regarding the solvation free energy of the hydronium ion, the determined pK_a must be corrected:

$$pK_a^{corr} = pK_a^{uncorr} - 4.54$$

Table S24. Computed Gibbs free energies (kcal mol^{-1}) and pK_a values for the deprotonation of TIPH, H–pyrrole, and DMPH under both gaseous and solvated conditions. All calculations were completed using the CAMB3LYP functional at the def2–TZVP level. A H_2O CPCM solvent model was included for the solvated reaction energies.

	ΔG^{rxn}_g	ΔG^{rxn}_s	Uncorrected pK_a	Corrected pK_a
H-TIP + H_2O → TIP^- + H_3O^+	159.02	17.02	10.73	6.19
H-Pyrrole + H_2O → $Pyrrole^-$ + H_3O^+	196.85	40.55	27.99	23.45
H-DMP + H_2O → DMP^- + H_3O^+	196.08	37.35	25.64	21.10

Table S25. Computed energies of solvation (kcal mol^{-1}) of TIPH, H–pyrrole, DMPH, H_3O^+, and their conjugate bases. All calculations were completed using the CAMB3LYP functional at the def2–TZVP level. A H_2O CPCM solvent model was included for the solvated reaction energies.

	ΔG_s
H-TIP	–4.28
TIP^-	–42.30
H-DMP	–3.90
DMP^-	–56.43
H-Pyrrole	–4.04
$Pyrrole^-$	–59.55
H_2O	–110.3
H_3O^+	–6.32

Table S26. Computed and average experimental bond metrics of $Cp^*_2Y(TIP)$, **1–Y** with six different functionals using the def2–SVP basis set and a 28 electron ECP on Y and I.

		Calculated					
	Experimental (Å)	**B3LYP**	**CAM**	**M06**	**PBE0**	**TPSS**	**TPSSh**
		Distances (Å)					
$Y–C^*_{avg}$	2.643	2.660	2.645	2.642	2.635	2.646	2.640
$Y–C^‡_{avg}$	2.642	2.662	2.645	2.637	2.637	2.648	2.642
$Y–N_{py}$	2.376	2.385	2.375	2.371	2.375	2.378	2.375
$N_{N1}–C_{C21}$	1.364	1.361	1.355	1.357	1.355	1.369	1.363
$N_{N1}–C_{C24}$	1.370	1.361	1.355	1.355	1.355	1.369	1.363
$C_{C21}–C_{C22}$	1.385	1.383	1.376	1.379	1.380	1.389	1.384
$C_{C22}–C_{C23}$	1.417	1.425	1.418	1.416	1.417	1.427	1.423
$C_{C23}–C_{C24}$	1.390	1.389	1.382	1.385	1.386	1.396	1.391
$C_{C21}–I_{I1}$	2.086	2.104	2.085	2.089	2.079	2.103	2.093
$C_{C22}–I_{I2}$	2.060	2.084	2.066	2.064	2.057	2.077	2.070
$C_{C23}–I_{I3}$	2.063	2.086	2.069	2.066	2.059	2.081	2.072
$C_{C24}–I_{I4}$	2.077	2.094	2.076	2.078	2.069	2.090	2.082
	MD	0.0125	0.0051	0.0048	0.0057	0.0085	**0.0043**
	MSE	2.2E-4	4.5E-5	3.6E-5	4.8E-5	1.1E-4	**3.0E-5**
	RMSE	1.5E-2	6.7E-3	6.0E-3	6.9E-3	1.0E-2	**5.4E-3**
	MAPE	0.61%	0.33%	0.29%	0.33%	0.45%	**0.24%**

C^*_{avg} = Average Y–C (Cp^*_1) distances.
$C^‡_{avg}$ = Average Y–C (Cp^*_2) distances.

Table S27. Computed and average experimental bond metrics of $Cp^*_2Y(TIP)$, **1–Y** with six different functionals using the def2–SVP basis set and a 28 electron ECP on Y and I. Relevant atoms selected to better gauge the metal pyrrole interaction.

		Calculated					
	Experimental (Å)	**B3LYP**	**CAM**	**M06**	**PBE0**	**TPSS**	**TPSSh**
		Distances (Å)					
$Y–N_{py}$	2.376	2.385	2.375	2.371	2.375	2.378	2.375
$N_{N1}–C_{C21}$	1.364	1.361	1.355	1.357	1.355	1.369	1.363
$N_{N1}–C_{C24}$	1.370	1.361	1.355	1.355	1.355	1.369	1.363
$C_{C21}–C_{C22}$	1.385	1.383	1.376	1.379	1.380	1.389	1.384
$C_{C22}–C_{C23}$	1.417	1.425	1.418	1.416	1.417	1.427	1.423
$C_{C23}–C_{C24}$	1.390	1.389	1.382	1.385	1.386	1.396	1.391
$C_{C21}–I_{I1}$	2.086	2.104	2.085	2.089	2.079	2.103	2.093
$C_{C22}–I_{I2}$	2.060	2.084	2.066	2.064	2.057	2.077	2.070
$C_{C23}–I_{I3}$	2.063	2.086	2.069	2.066	2.059	2.081	2.072
$C_{C24}–I_{I4}$	2.077	2.094	2.076	2.078	2.069	2.090	2.082
	MD	0.0114	0.0057	0.0050	0.0056	0.0093	**0.0048**
	MSE	2.E-04	5.3E-5	4.0E-5	4.9E-5	1.3E-4	**3.4E-5**
	RMSE	1.3E-2	6.6E-3	5.7E-3	6.4E-3	1.0E-2	**5.4E-3**
	MAPE	0.60%	0.38%	0.32%	0.35%	0.51%	**0.27%**

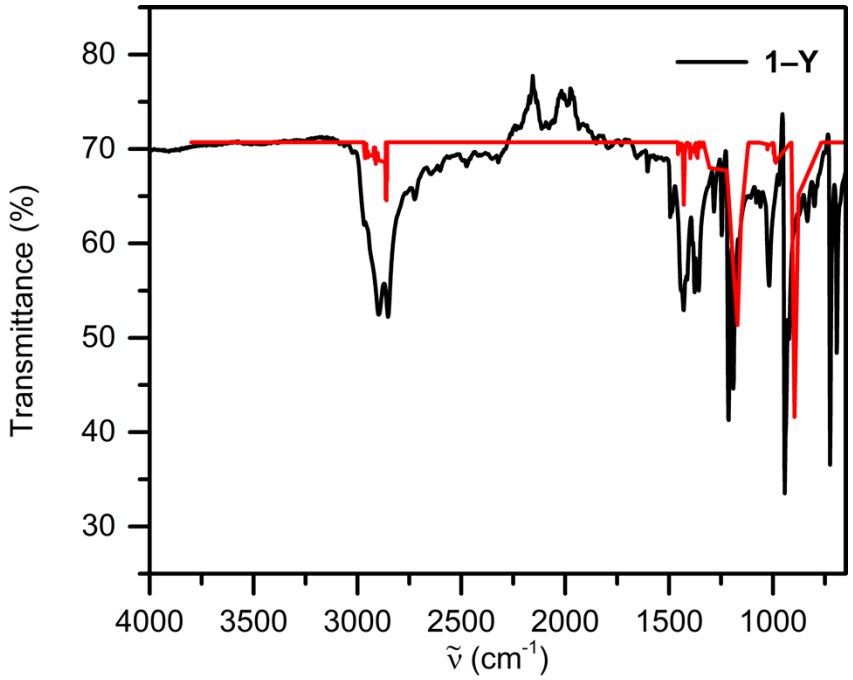

Figure S72. Comparison of experimental FTIR spectrum (black) and calculated stretching frequencies (red) of $Cp^*_2Y(TIP)$, **1–Y**.

Table S28. Major contributions of the TDDFT–calculated transitions for $Cp^*_2Y(TIP)$, **1–Y**, on the def2-TZVP/ECP28MDF(Y,I) level using the TPSSh functional with GD3 dispersion correction and dichloromethane implicit solvent model. The calculated excitation energies were empirically shifted by 0.1 eV. Isovalue for all depictions is 0.04. Oscillator strength cutoff value: 0.01.

λ (nm)	ν (cm^{-1})	Oscillator Strength	Occupied	Virtual	Weight (%)
355	28150.4	0.0328	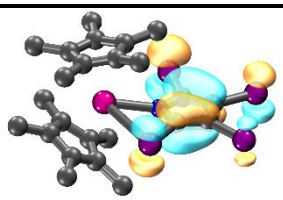 146	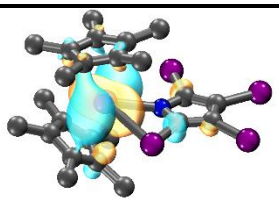 148	67.6
332	30140.7	0.0105	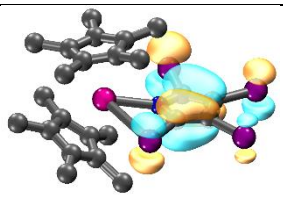 146	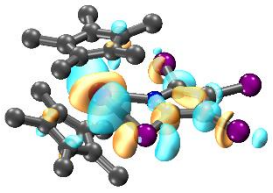 149	50.8
327	30580.8	0.0249	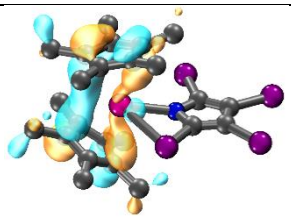 143	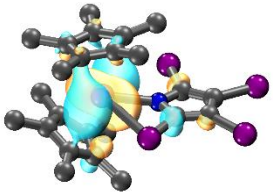 148	49.8
321	31132.8	0.0166	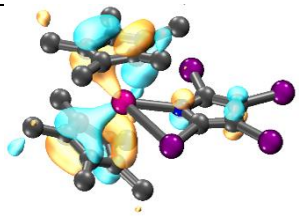 145	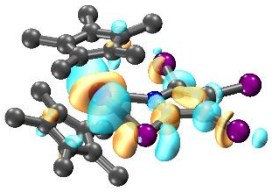 149	58.0
314	31883.9	0.0211	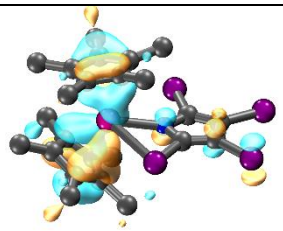 142	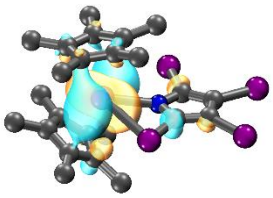 148	59.7
285	35030.6	0.0102	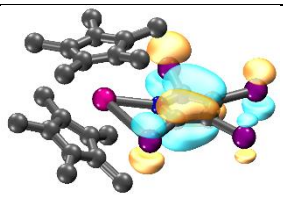 146	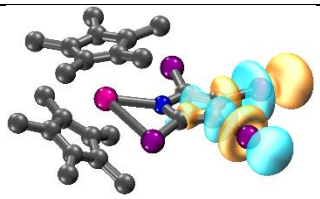 152	67.0

272	36769.1	0.0200	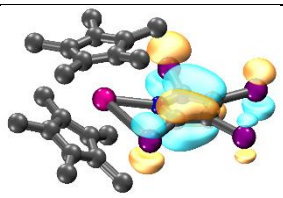 146	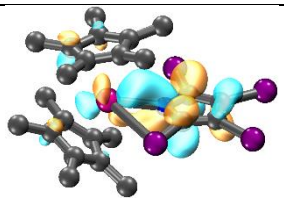 153	63.7
270	37070.8	0.0275	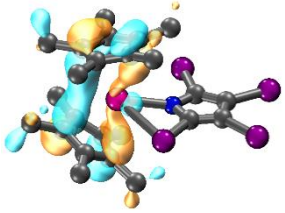 143	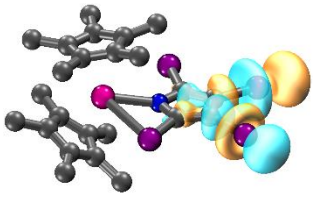 152	56.5
264	37778.2	0.1413	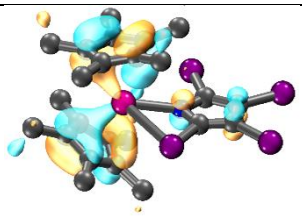 145	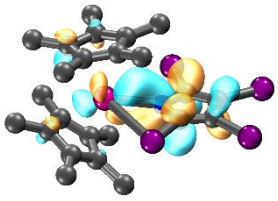 153	66.8
261	38355.3	0.0183	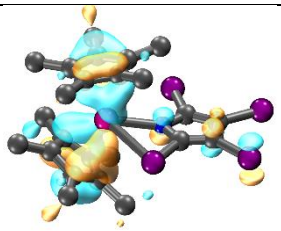 142	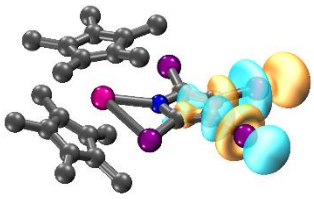 152	48.3
260	38469.2	0.0179	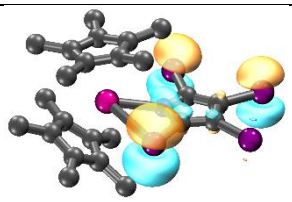 136	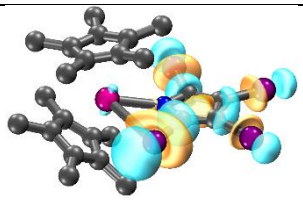 147	68.7
255	39159.9	0.0842	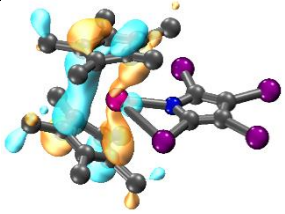 143	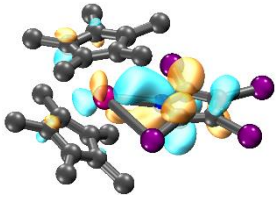 153	43.4
250	39949.9	0.0881	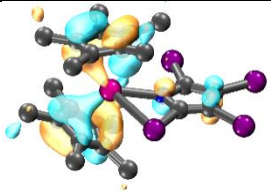 145	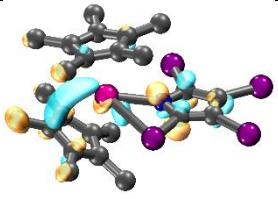 154	39.9

250	40078.2	0.0472	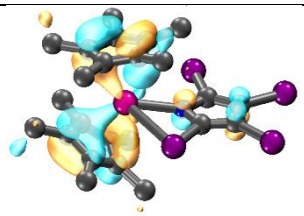 145	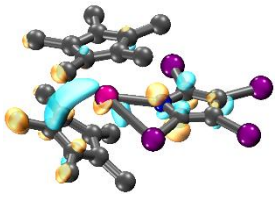 154	51.9
247	40410.2	0.0194	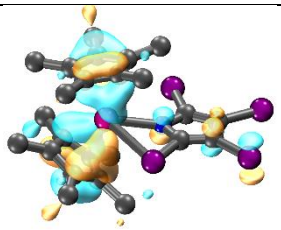 142	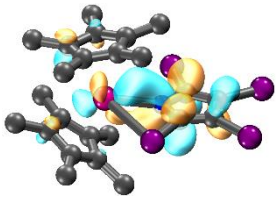 153	43.5
247	40529.4	0.0295	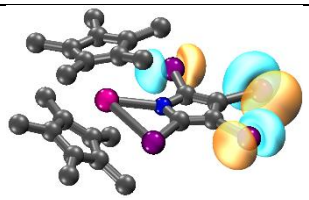 140	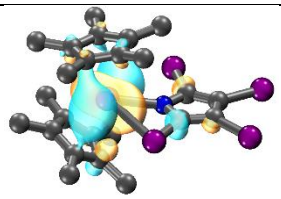 148	46.8
243	41076.5	0.0353	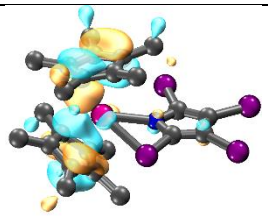 144	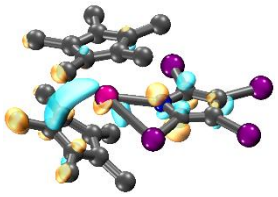 154	57.4
242	41348.4	0.0226	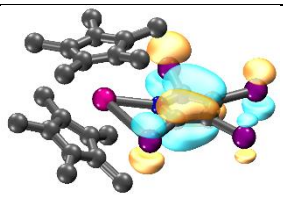 146	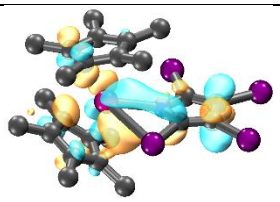 155	67.0

Table S29. Results of the second order perturbation analysis of **1–Y** from NLMO calculations on the optimized structure of **1–Y**. Only interactions between the tetraiodopyrrole unit and metal ions are shown (> 1 kcal mol^{-1}).

Donor NLMO	Acceptor NLMO	E (kcal mol^{-1})
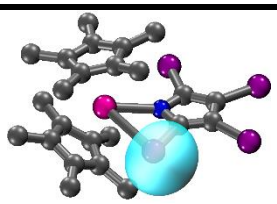 LP1 I1	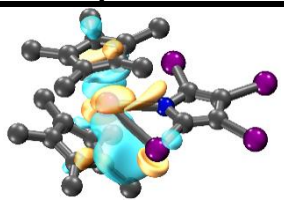 LV1 Y2	1.60
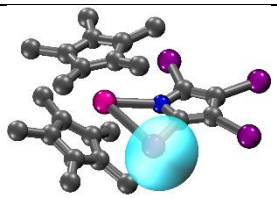 LP1 I1	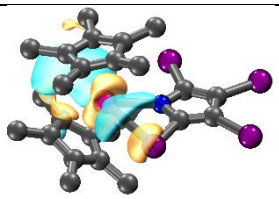 LV2 Y2	12.38
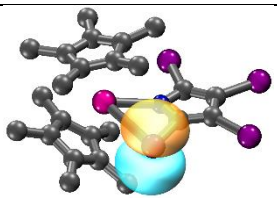 LP2 I1	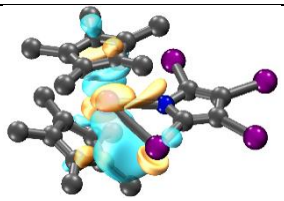 LV1 Y2	9.92
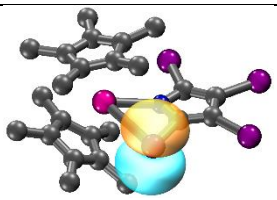 LP2 I1	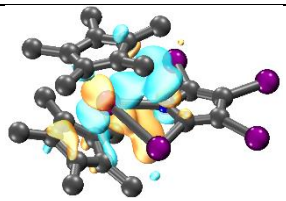 LV4 Y2	1.11
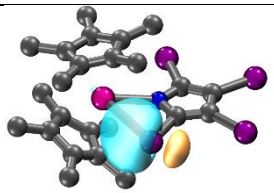 LP3 I1	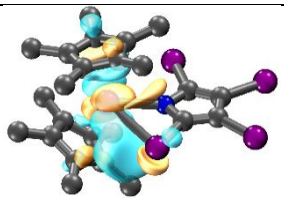 LV1 Y2	9.90
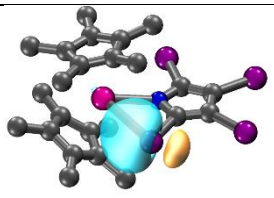 LP3 I1	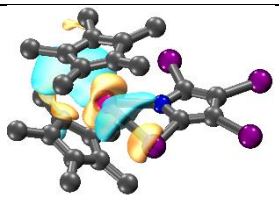 LV2 Y2	56.61

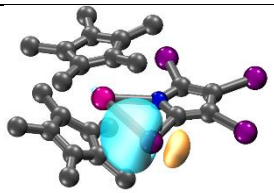 LP3 I1	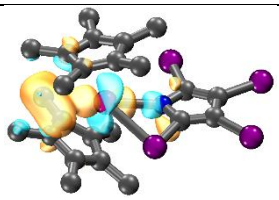 LV3 Y2	1.64
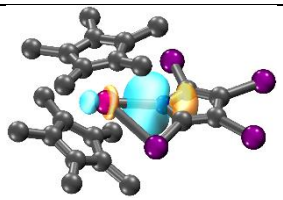 LP1 N3	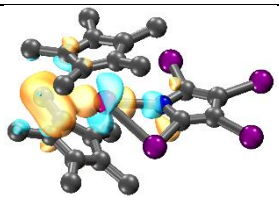 LV3 Y2	18.38
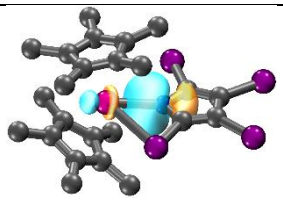 LP1 N3	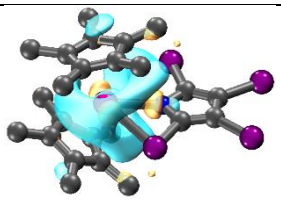 LV5 Y2	13.04
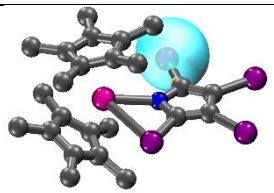 LP1 I16	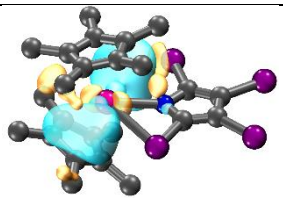 LV6 Y2	2.41
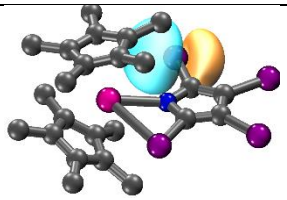 LP3 I16	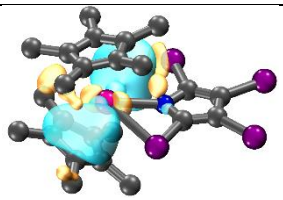 LV6 Y2	11.93
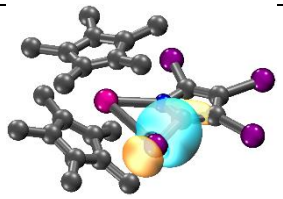 BD1 I1–C4	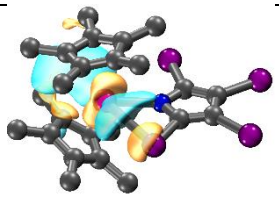 LV2 Y2	8.89
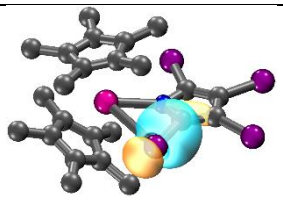 BD1 I1–C4	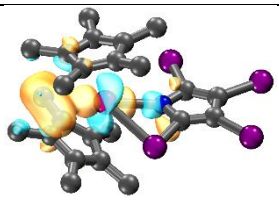 LV3 Y2	2.79

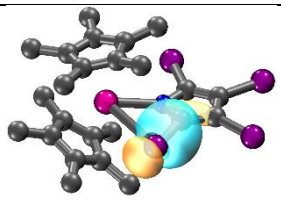 BD1 I1–C4	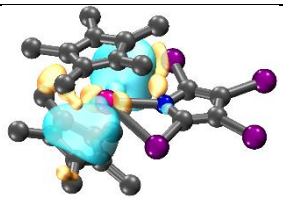 LV6 Y2	5.48
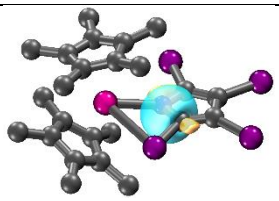 BD1 N3–C4	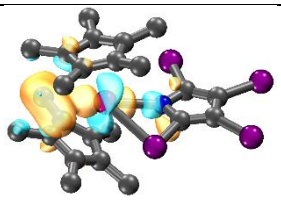 LV3 Y2	7.54
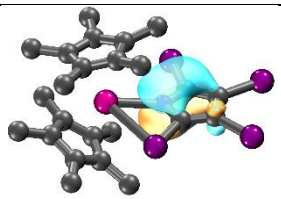 BD1 N3–C5	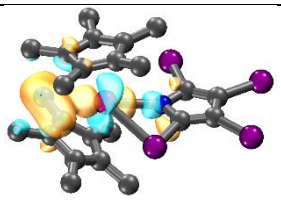 LV3 Y2	5.18
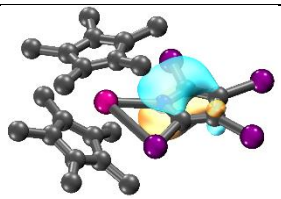 BD2 N3–C5	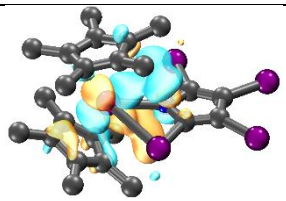 LV4 Y2	1.84
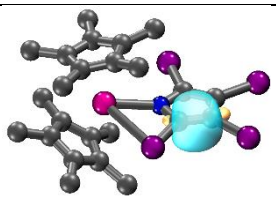 BD1 C4–C17	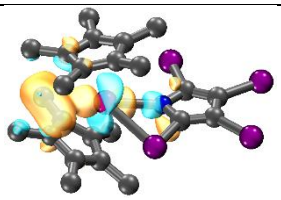 LV3 Y2	1.31
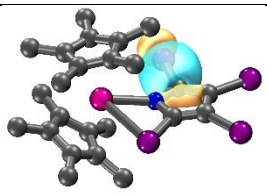 BD1 C5–I16	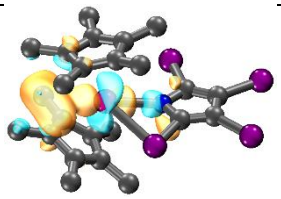 LV3 Y2	1.88
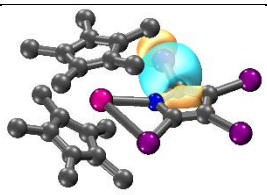 BD1 C5–I16	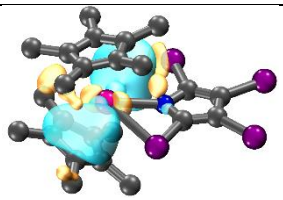 LV6 Y2	1.13

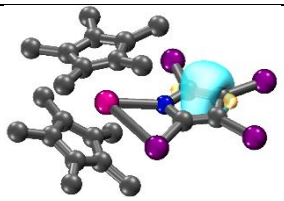 BD1 C5–C18	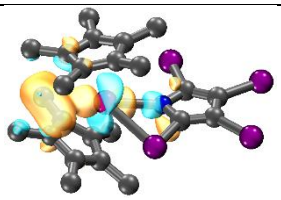 LV3 Y2	1.26

Table S30. Computed and average experimental bond metrics of $Cp^*_2Y(DMP)$, **2–Y** with six different functionals using the def2–SVP basis and a 28 electron ECP on Y.

		Calculated					
Experimental (Å)		**B3LYP**	**CAM**	**M06**	**PBE0**	**TPSS**	**TPSSh**
Distances (Å)							
Y_{Y1}-C^*_{avg}	2.636	2.653	2.638	2.635	2.634	2.644	2.639
Y_{Y1}-$C^{‡}_{avg}$	2.632	2.655	2.639	2.632	2.635	2.644	2.639
Y_{Y1}-N_{N1}	2.289	2.289	2.282	2.284	2.283	2.289	2.286
Y_{Y1}-C_{C4}	2.983	2.992	2.976	2.946	2.937	2.912	2.918
Y_{Y1}-C_{C10}	2.993	3.045	3.020	2.968	2.966	2.936	2.941
N_{N1}-C_{C13}	1.375	1.374	1.368	1.367	1.367	1.379	1.374
N_{N1}-C_{C4}	1.384	1.386	1.380	1.382	1.379	1.394	1.388
C_{C13}-C_{C25}	1.379	1.392	1.384	1.388	1.389	1.399	1.394
C_{C17}-C_{C25}	1.413	1.423	1.420	1.417	1.417	1.424	1.421
C_{C4}-C_{C17}	1.378	1.391	1.383	1.387	1.388	1.398	1.393
C_{C4}-C_{C10}	1.503	1.502	1.501	1.495	1.497	1.506	1.503
C_{C13}-C_{C26}	1.496	1.499	1.496	1.491	1.493	1.503	1.500
	MD	0.0121	0.0068	0.0094	0.0108	0.0186	0.0148
	MSE	3.4E-4	8.8E-5	2.0E-4	2.7E-4	8.0E-4	6.3E-4
	RMSE	1.8E-2	9.4E-3	1.4E-2	1.6E-2	2.8E-2	2.5E-2
	MAPE	0.56%	0.33%	0.46%	0.51%	0.87%	0.65%

Table S31. Computed and average experimental bond metrics of $Cp^*_2Y(DMP)$, **2–Y** with six different functionals using the def2–SVP basis set and a 28 electron ECP on Y. Relevant atoms selected to better gauge the metal pyrrole interaction.

		Calculated					
	Experimental (Å)	**B3LYP**	**CAM**	**M06**	**PBE0**	**TPSS**	**TPSSh**
		Distances (Å)					
Y_{Y1}-N_{N1}	2.289	2.289	2.282	2.284	2.283	2.289	2.286
Y_{Y1}-C_{C4}	2.983	2.992	2.976	2.946	2.937	2.912	2.918
Y_{Y1}-C_{C10}	2.993	3.045	3.020	2.968	2.966	2.936	2.941
N_{N1}-C_{C13}	1.375	1.374	1.368	1.367	1.367	1.379	1.374
N_{N1}-C_{C4}	1.384	1.386	1.380	1.382	1.379	1.394	1.388
C_{C13}-C_{C25}	1.379	1.392	1.384	1.388	1.389	1.399	1.394
C_{C17}-C_{C25}	1.413	1.423	1.420	1.417	1.417	1.424	1.421
C_{C4}-C_{C17}	1.378	1.391	1.383	1.387	1.388	1.398	1.393
C_{C4}-C_{C10}	1.503	1.502	1.501	1.495	1.497	1.506	1.503
C_{C13}-C_{C26}	1.496	1.499	1.496	1.491	1.493	1.503	1.500
	MD	0.0104	0.0071	0.0112	0.0125	0.0203	0.0167
	MSE	3.2E-4	1.0E-4	2.4E-4	3.2E-4	9.4E-4	7.5E-4
	RMSE	1.8E-2	1.0E-2	1.5E-2	1.8E-2	3.1E-2	2.7E-2
	MAPE	0.51%	0.36%	0.55%	0.60%	0.96%	0.74%

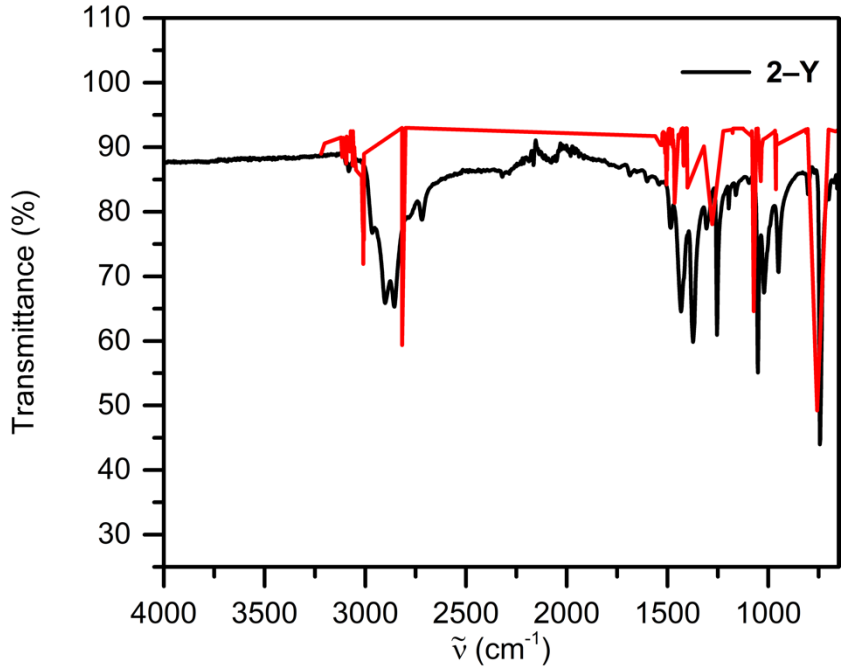

Figure S73. Comparison of experimental FTIR spectrum (black) and calculated stretching frequencies (red) of Cp*$_2$Y(DMP), **2–Y**.

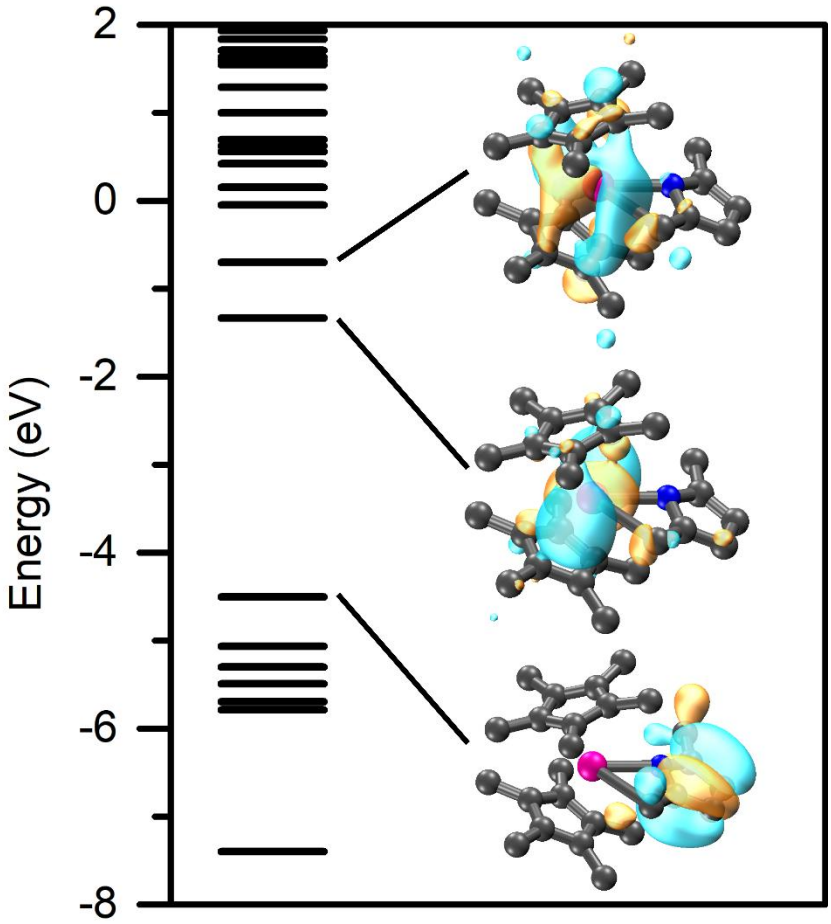

Figure S74. Calculated frontier orbitals of $Cp^*_2Y(DMP)$, **2–Y**, with the TPSSh functional and def2–TZVP basis set. All isovalues were set to 0.4.

Table S32. Results of the second order perturbation analysis of **2–Y** from NLMO calculations on the optimized structure of **2–Y**. Only strongest interactions between the dimethylpyrrole and metal ions are shown (> 1 kcal/mol).

Donor NLMO	Acceptor NLMO	E (kcal mol^{-1})
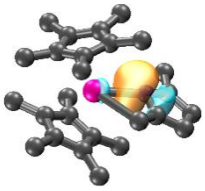 LP1 N2	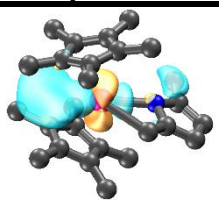 LV2 Y1	29.36
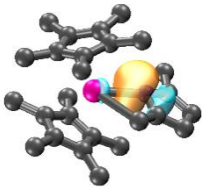 LP1 N2	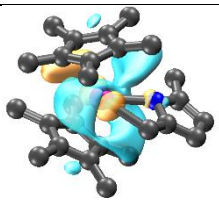 LV4 Y1	11.76
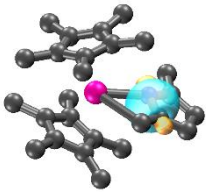 BD1 N2–C6	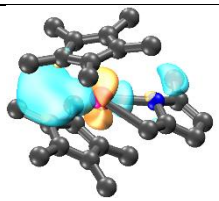 LV2 Y1	7.93
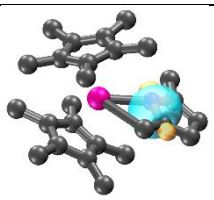 BD1 N2–C6	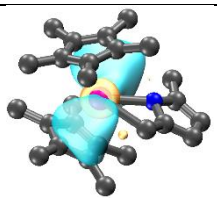 LV6 Y1	1.39
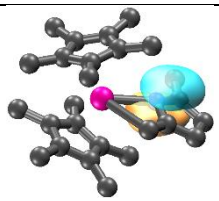 BD1 N2–C15	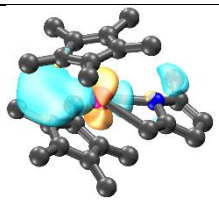 LV2 Y1	4.40
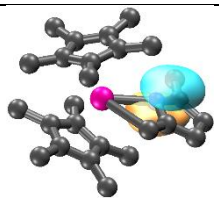 BD1 N2–C15	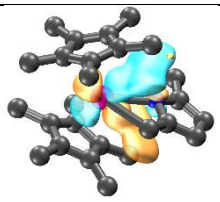 LV3 Y1	3.11

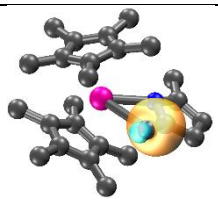 BD1 C6–C12	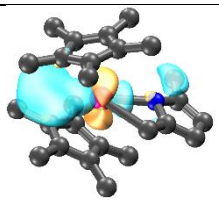 LV2 Y1	3.60
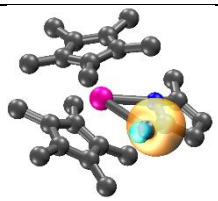 BD1 C6–C12	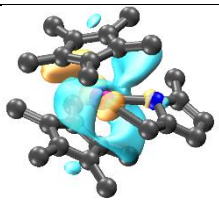 LV4 Y1	1.55
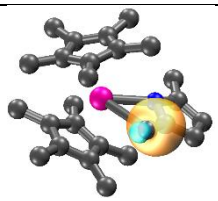 BD1 C6–C12	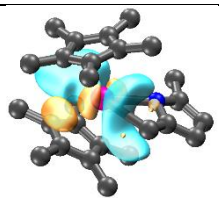 LV5 Y1	4.29
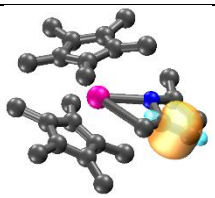 BD1 C6–C19	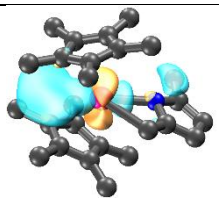 LV2 Y1	1.86
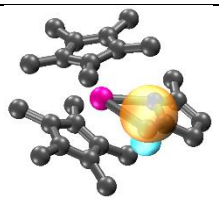 BD1 C12–H32	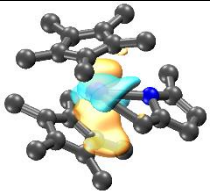 LV1 Y1	1.48
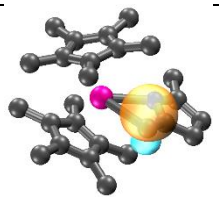 BD1 C12–H32	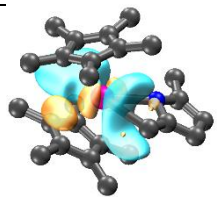 LV5 Y1	4.76
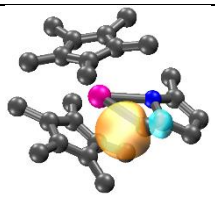 BD1 C12–H34	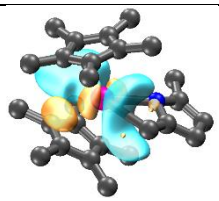 LV5 Y1	11.32

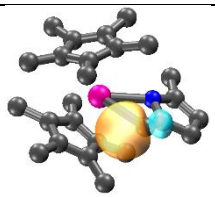 BD1 C12–H34	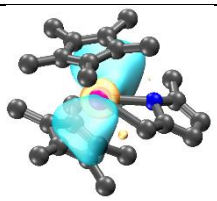 LV6 Y1	6.01
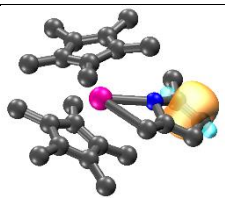 BD1 C15–C27	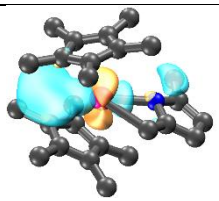 LV2 Y1	1.75
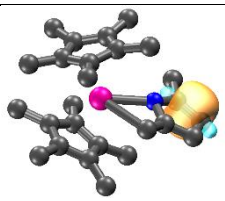 BD1 C15–C27	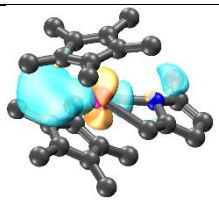 LV2 Y1	1.32
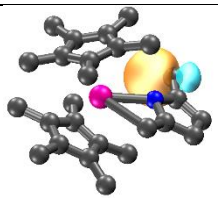 BD1 C23–H49	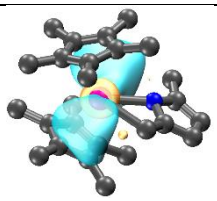 LV6 Y1	2.50

Table S33. Coordinates of the geometry optimized structure of $Cp^*_2Y(TIP)$, **1–Y**, on the def2-TZVP/ECP28MDF(Y,I) level using the TPSSh functional with GD3 dispersion correction.

I	0.24690	-2.71630	0.21770
Y	2.04110	-0.02070	-0.04480
N	-0.30460	0.22020	0.23690
C	-0.93200	-0.98760	0.15950
C	-1.30690	1.14320	0.19180
C	3.20560	-0.77220	-2.28700
C	2.13560	-0.41750	2.57370
C	3.66220	0.55310	-2.04250
C	1.41250	0.65370	-2.53430
C	3.25480	-1.10980	2.03060
C	2.34860	0.97220	2.38020
C	4.16670	-0.14440	1.51960
C	1.81860	-0.70480	-2.60500
C	3.60000	1.14760	1.72500
C	2.54630	1.43270	-2.17100
I	-0.88030	3.18040	0.22490
C	-2.30810	-0.86710	0.06630
C	-2.55360	0.53470	0.08900
C	4.04890	-2.01470	-2.34190
C	0.98210	-0.99750	3.33910
C	5.09390	0.99240	-1.95920
C	0.05970	1.15920	-2.93890
C	3.52910	-2.58500	2.10360
C	1.47780	2.05680	2.94070
C	5.57100	-0.45580	1.09190
C	0.97660	-1.81850	-3.15530
C	4.26890	2.47240	1.49310
C	2.60900	2.93270	-2.10760
I	-3.68060	-2.41090	-0.06040
I	-4.39890	1.47240	-0.01540
H	4.97670	-1.89740	-1.77890
H	4.32280	-2.26320	-3.37340
H	3.52010	-2.88140	-1.93400
H	0.01990	-0.65370	2.94930
H	1.03470	-0.69620	4.39090
H	0.98330	-2.08710	3.30650
H	5.23460	1.83090	-1.27510
H	5.43640	1.32430	-2.94620
H	5.75210	0.18370	-1.64370
H	1.60590	3.00050	2.40930
H	1.72570	2.23510	3.99400
H	0.42010	1.79120	2.89330

H	1.65600	3.36240	-1.79270
H	2.85220	3.35460	-3.08960
H	3.37670	3.27490	-1.40990
H	-0.74520	0.54260	-2.53280
H	-0.03640	1.14880	-4.03060
H	-0.10690	2.18290	-2.60360
H	2.62400	-3.15020	2.33200
H	3.93880	-2.97380	1.16590
H	1.35020	-2.79980	-2.85940
H	0.97980	-1.78090	-4.25110
H	-0.06390	-1.74460	-2.83130
H	5.08710	2.39320	0.77660
H	4.68980	2.86210	2.42670
H	3.56920	3.22440	1.11890
H	5.61930	-1.29530	0.39330
H	6.17500	-0.73270	1.96370
H	6.05190	0.40100	0.62200
H	4.26230	-2.80680	2.88740

Table S34. Coordinates of the geometry optimized structure of $Cp^*_2Y(DMP)$, **2–Y**, on the def2-TZVP/ECP28MDF(Y) level using the TPSSh functional with GD3 dispersion correction.

Y	-0.16090	-0.00820	-0.08290
N	1.97330	-0.81290	0.06460
C	-1.77360	-1.81270	-1.14760
C	-0.81150	-2.55580	-0.40640
C	-0.88960	2.42620	-0.83950
C	2.44080	-0.67620	-1.23380
C	0.53550	2.41500	-0.88590
C	-1.28240	2.31670	0.52200
C	-0.09820	2.20940	1.31190
C	-1.00210	-2.26120	0.96790
C	1.02340	2.29030	0.44150
C	1.50600	-0.66160	-2.40560
C	-2.58190	-1.08920	-0.22460
C	-2.09880	-1.36040	1.08670
C	3.07630	-0.87950	0.87820
C	-2.01990	-1.87570	-2.62910
C	0.18810	-3.54380	-0.93510
C	-1.79420	2.66310	-2.01600
C	3.82460	-0.66180	-1.23690
C	1.39220	2.66750	-2.09340
C	-2.66220	2.53920	1.06700
C	-0.05330	2.16790	2.81380
C	-0.23880	-2.88100	2.10140
C	2.47050	2.34430	0.82930
C	-3.84730	-0.36930	-0.58870
C	-2.72990	-0.94890	2.38630
C	4.22900	-0.79970	0.11390
C	2.94490	-1.00420	2.36310
H	2.63160	1.96740	1.84010
H	2.83410	3.37820	0.80140
H	3.09080	1.74840	0.15610
H	1.03750	-1.63080	-2.59590
H	2.04510	-0.36600	-3.30640
H	0.68810	0.09340	-2.34900
H	-3.43440	2.30580	0.33400
H	-2.78950	3.59110	1.34890
H	-2.85430	1.94410	1.96130
H	-2.28860	-0.89730	-3.03900
H	-2.84720	-2.55620	-2.86130
H	-1.14360	-2.23240	-3.17340
H	-1.48530	2.08990	-2.89590
H	-1.79250	3.71930	-2.30790

H	-2.82600	2.39040	-1.78980
H	5.24260	-0.82920	0.48840
H	4.45960	-0.58730	-2.10870
H	0.10880	-3.65190	-2.01840
H	0.01410	-4.53230	-0.49860
H	1.21470	-3.25120	-0.69500
H	2.14040	-0.36870	2.74900
H	3.87150	-0.70140	2.85460
H	2.72290	-2.02980	2.67740
H	-4.22150	0.23360	0.23820
H	-4.63230	-1.08840	-0.85000
H	-3.71850	0.28810	-1.45240
H	-1.98830	-0.62850	3.12420
H	-3.27810	-1.78680	2.83130
H	-3.43840	-0.13170	2.25050
H	2.30720	2.07050	-2.06490
H	1.68870	3.72170	-2.13730
H	0.86390	2.44230	-3.02280
H	-0.92110	1.65090	3.23130
H	-0.04680	3.17900	3.23680
H	0.84440	1.66250	3.17760
H	0.76930	-3.15670	1.78900
H	-0.73850	-3.78850	2.46080
H	-0.15120	-2.20390	2.95510

Table S35. Coordinates of $Cp^*_2Dy(TIP)$, **1–Dy**, at 100 K, with optimized hydrogen positions.

Dy	6.87044882041268	10.15230231328233	7.07452302479285
I	4.22430280102981	8.71054934477510	5.90512126831061
N	5.95046331016978	11.00494350502335	5.06071145869707
C	4.80833888547841	10.33051666856639	4.72680802257397
C	8.77599032907106	9.22711190702915	5.46582988055701
C	7.96448381341903	8.10041649331064	5.78895890930684
C	9.05683406560790	8.79332759524651	7.70370996444711
C	5.45510002910332	12.16615490809824	8.05232829015044
C	6.79862566312540	12.39456466462319	8.45225852072130
C	9.43013476098532	9.66093424377439	6.64442483983303
C	4.98806448576127	11.02036688293468	8.75561777903726
C	6.04751011899796	10.52582042543248	9.57064347294735
C	7.16018571160297	11.38999835345509	9.40137335044199
C	8.13356883853426	7.84082610151463	7.17285958509276
I	7.58996294331310	13.38987607757546	4.20292483415212
C	6.03227738517249	12.02117670101825	4.14426872742210
C	4.15992456021457	10.89076341798967	3.63564599795484
C	8.98417618952766	9.74185189129471	4.06763679759795
C	7.27733501535021	7.23620336868289	4.77091546052058
C	9.72446620828291	8.67765276461745	9.04665782016405
C	4.62305431402863	13.05839689972338	7.17976559866276
C	7.66043748119707	13.58752448037250	8.11075580018650
C	10.47622077572001	10.73644194530238	6.71599739719964
C	3.55639651946455	10.54664468073302	8.82762837884014
C	5.95151308707335	9.40287319344890	10.55437585648375
C	8.37979177097281	11.43915534585026	10.27578870604038
C	7.53127849816069	6.68204435429076	7.92879238705668
C	4.96885939777631	11.98978908139309	3.25722456431806
I	2.44093899948921	10.19464351904115	2.74286585409705
H	8.04423716709351	9.80921301840396	3.50828247657827
H	9.65022002980606	9.06911328151486	3.50745174097003
H	9.44299928116371	10.73500868662061	4.05946731441358
H	6.57147109716937	6.53626199635902	5.22809890840387
H	8.02164167182340	6.63860617063523	4.22435352455743
H	6.72900273933656	7.82349400878124	4.02472611875358
H	10.23073399431726	9.60085084392836	9.33892671099242
H	10.48832777216739	7.88673135840780	9.01428744965203
H	9.02384259307757	8.40783917186937	9.84507008991500
H	5.24188129766537	13.67378656691240	6.51962006533303
H	4.01416251247282	13.74079665413321	7.79020585631967
H	3.93601183470487	12.49033955364488	6.54209293385320
H	8.68650751504856	13.30523756207196	7.84278111240479
H	7.73029174752342	14.26653424927025	8.97311665014365

H	7.24922567847433	14.15826132968635	7.27405446607515
H	10.27404255618419	11.55204683225462	6.01156947855637
H	11.47108235955108	10.33783270004801	6.46986846387637
H	10.54639681825004	11.17582682704763	7.71768248403106
H	2.99433198415869	10.77977445454790	7.91810584061368
H	3.04243930330559	11.04454367271187	9.66351499556010
H	3.48035736763346	9.46763365594572	9.00137691319372
H	5.31606371185644	8.58494902865116	10.19175625700419
H	5.51533948340023	9.74034036811042	11.50643495977570
H	6.93383895717492	8.97722675880396	10.78707515205629
H	8.55470890282830	10.49594190037046	10.79879428338522
H	8.25286411120795	12.21592973905473	11.04478224943578
H	9.29039144214281	11.69336998535828	9.72093820394140
H	7.31822342640458	6.93594740619459	8.97440588833339
H	8.21152361274300	5.81774015733870	7.94342849377596
H	6.59441600385608	6.34343001590135	7.47115584827923
I	4.61375824841552	13.29823091702060	1.68998252220936

Table S36. Coordinates of $Cp^*_2Dy(TIP)$, **1–Dy**, at 200 K, with optimized hydrogen positions.

Dy	6.84953950859797	10.25797456473941	7.08147419803093
I	4.20756017476614	8.83096353977631	5.86603239423677
N	5.96654944936772	11.10350344490065	5.03944106411165
C	4.81774342308472	10.45170544761234	4.70236273419940
C	8.76806801032263	9.30557956912269	5.51099421627338
C	7.96916584559699	8.18523723854363	5.85802125756453
C	9.02662986237387	8.90131138349127	7.75656828108749
C	5.37682836642864	12.24210367308627	8.04972994028863
C	6.71521697723490	12.50270375260304	8.42601922780599
C	9.40676777642135	9.75464994935058	6.68658637781398
C	4.94997711284253	11.09304003381569	8.76766988721158
C	6.02108124717197	10.64369284013025	9.57801202846218
C	7.10406215199972	11.52699298621255	9.38886508299542
C	8.11484728112117	7.95051341096037	7.24080765521354
I	7.62846109522279	13.48366954962316	4.18671280648556
C	6.05900463041193	12.13148549701086	4.13710841539235
C	4.18237801576619	11.02007985278288	3.62627585764868
C	9.00237275023967	9.79214106879377	4.11876846606394
C	7.28519517991890	7.30433246205622	4.84958699541071
C	9.69110211217630	8.81531403218130	9.09287768947522
C	4.52734705415678	13.09548826124230	7.16379500779101
C	7.54799025938949	13.71507417701219	8.08597828334025
C	10.44577654974178	10.84086981112529	6.73649216991763
C	3.52977331596952	10.58768771468838	8.85568873160658
C	5.94405904929361	9.52465016188862	10.57950153119019
C	8.32740382390675	11.61283013913820	10.26391784063751
C	7.52307691356876	6.80647131903652	8.01536456776505
C	5.00054983598928	12.11074240755668	3.24789556893000
I	2.46106636616715	10.35315871423977	2.71612033223583
H	8.08015183993165	9.82116168363416	3.52741827821689
H	9.70435417983328	9.12885588441170	3.59185264345663
H	9.43254179181992	10.79790540780528	4.10021539079645
H	6.56999043963829	6.61789614029334	5.31283871656791
H	8.03023791993727	6.69030232264388	4.32258631747113
H	6.74834766656243	7.87868241571561	4.08557666596940
H	10.19464525437273	9.74539645208680	9.36786410293796
H	10.45886780749800	8.02743042317900	9.07779006706391
H	8.99550916838912	8.55892508036453	9.90016147819751
H	5.13258910670252	13.71723645697112	6.49708300088597
H	3.89774812036746	13.77210514015526	7.75955392859994
H	3.85653247979568	12.50375765862388	6.53033339702164
H	8.58521945194889	13.45822026508481	7.83695577180528
H	7.58579690229315	14.40289562692853	8.94319285347322

H	7.13704813595954	14.26873840792997	7.23767161205759
H	10.21417286679945	11.66141974449037	6.04698464249352
H	11.43615159352323	10.45521203834750	6.45460235201627
H	10.54433295767222	11.27190606542937	7.73921950580760
H	2.94612634159444	10.83810190520515	7.96481429596520
H	3.02377731027403	11.04871668457169	9.71690906355961
H	3.47506324561155	9.50239561228345	8.99633144647801
H	5.33124444238665	8.68910758630354	10.21944056625057
H	5.49079550599119	9.86466760352369	11.52217190154162
H	6.93382579744289	9.12577473804079	10.82592158162361
H	8.51344721116254	10.68249251649518	10.80537044343027
H	8.18939865417164	12.40366857637014	11.01610049439026
H	9.23501917925178	11.86695704596971	9.70435917542239
H	7.33053501464728	7.07259972747787	9.06142156719935
H	8.19908129627657	5.93881513303592	8.02731400096108
H	6.57620844369676	6.46414874589415	7.58121236498656
I	4.65651573519826	13.44689990801190	1.70721376416623

Table S37. Coordinates of $Cp^*_2Dy(TIP)$, **1–Dy**, at 300 K, with optimized hydrogen positions.

Dy	6.81619973618705	10.33596810347693	7.13271299605419
I	4.16390617741545	8.92398764562069	5.87614535355595
N	5.95114411695721	11.18350974927183	5.07819623475085
C	4.80679769688728	10.53368192733775	4.72152896375780
C	8.75398398309884	9.36765752294352	5.59694552114024
C	7.94519364326909	8.25244092072064	5.93714755248902
C	8.98391653737404	8.96844317358133	7.84078787813750
C	5.30159962821177	12.27675342181828	8.10557149122426
C	6.63296463831642	12.57953798080780	8.49198294101707
C	9.37539400627710	9.79650179791494	6.77180804805238
C	4.90662255890697	11.12619560397728	8.84076947739763
C	5.98667356325581	10.71900134298294	9.62559905080948
C	7.04366430455211	11.61718925715262	9.43611828286896
C	8.07109627579842	8.01851354692957	7.31052026015686
H	2.89402567482575	10.84539132901535	8.06524499378562
I	7.64034068510867	13.55238389784977	4.23454078759556
C	6.05587266349013	12.20610433225215	4.17908362907234
C	4.18775212108028	11.12409292177884	3.64499757587053
C	9.00896672251942	9.82402685947521	4.20365587356927
C	7.24817329142216	7.34893476880664	4.92781499527365
C	9.62532956015110	8.88906987048777	9.18857066206655
C	4.42388824245555	13.11706243753602	7.23093698016044
C	7.41428653880042	13.83833535916488	8.12392274661813
C	10.40529634377748	10.90029875039912	6.83635354509952
C	3.49264804071495	10.59557044697153	8.94585414500186
C	5.94216179252536	9.60638612167153	10.66103306891467
C	8.27446123572347	11.72646227903120	10.31799664252912
C	7.46485743006011	6.87953818613181	8.08252434113455
C	5.01252844211819	12.19882625871512	3.29838027777860
I	2.46419398248255	10.47309561468449	2.72277267164397
H	8.09485902381789	9.84134949849810	3.59954489803826
H	9.71707952906742	9.14924010019064	3.70010041148332
H	9.44047437892300	10.82913007814296	4.16637522227115
H	6.52439842885870	6.68255896714461	5.40546900525445
H	7.99192744024966	6.71838471408534	4.41986037017416
H	6.72284135320692	7.91674386422652	4.15158033206731
H	10.12509219480702	9.82045372871309	9.46646206101152
H	10.39295017842399	8.10091241772284	9.19221925031873
H	8.91534499126526	8.63805266047892	9.98447663396112
H	5.00714432115588	13.72498943651476	6.53249240269173
H	3.81360903598513	13.80537576360701	7.83329333671328
H	3.73368756384369	12.51374378699535	6.63013152883509
H	8.46654433261484	13.62755329756490	7.89722873683266

H	7.39966597559610	14.54787038029788	8.96336703497222
H	6.98334143203622	14.34127484455224	7.25495609444874
H	10.18094603160965	11.70905121276678	6.13098249653396
H	11.40660767056954	10.52283621560843	6.58422029631653
H	10.47291353368963	11.34308486505678	7.83633492765386
H	2.99425807065588	11.04200982052822	9.81865931253675
H	3.45704853532419	9.50817156359526	9.07726613545306
H	5.30931521226007	8.77176411958565	10.33725083115480
H	5.52860865604863	9.97176118972460	11.61183874931282
H	6.93796270428314	9.20517216817501	10.87471204024293
H	8.47491532345628	10.79995765770618	10.86001781504469
H	8.12015347696926	12.51622960211123	11.06740314375194
H	9.17609414113093	11.99512340674098	9.75575485355117
H	7.29267471993841	7.14144214092910	9.13294027909462
H	8.12284148273914	5.99811704665105	8.07777597433597
H	6.50494937098769	6.55965152258257	7.65988628803887
I	4.69318125672229	13.55035250099497	1.75260255037731

Table S38. Coordinates of $Cp^*_2Dy(DMP)$, **2–Dy**, at 100 K, with optimized hydrogen positions.

Dy	1.72076627644233	6.27482335048025	3.99713690248379
N	-0.15745262591005	5.82171264459260	5.24277301077361
C	1.58312613870246	5.01598184302940	1.68341954483033
C	0.25991293435822	5.45054704604919	1.96079635171844
C	4.22828742393703	6.39900029863462	4.81357439862223
C	2.85894239621189	8.13854996202920	5.43963426951118
C	-0.02223818835706	4.51108699671905	5.66307490163642
C	0.25385873428220	6.87126400051639	1.91094141997567
C	2.38833182763258	6.16482145556559	1.42156895235857
C	2.64260384957302	7.06338363642457	6.33912670058489
C	3.48302272794396	5.99154415537630	5.95212147002002
C	3.85496810570914	7.72943811883714	4.50592969475718
C	1.55113426929993	7.31040639283318	1.57627037636620
C	-1.12572528779368	6.38627703571888	6.03814103651847
C	2.07352914707616	3.59277338301952	1.55745017950452
C	-0.94450804105088	4.56385524925782	2.17601154905526
C	5.28749420479477	5.57084790181359	4.13236929491092
C	2.23144278685569	9.50900999250608	5.51076116350766
C	-0.89224629761503	4.24442182336562	6.70043282676648
C	0.93294686205352	3.56401337224056	4.99795152669102
C	-0.93779738454850	7.77086200802621	2.10036810450672
C	3.77901581783609	6.12492196946642	0.85764494396614
C	1.76492156494883	7.08307787305688	7.56569591500242
C	3.68958510268392	4.72134031409211	6.73120187747519
C	4.55365305050013	8.66057344414328	3.54418767259677
C	1.90701539527006	8.74476421019451	1.24427790024915
C	-1.60699744934042	5.44274425159704	6.93388204034057
C	-1.52976853078333	7.81893399242078	5.89095418267708
H	1.33059881908459	2.87032258386325	1.90819412652905
H	2.99843415290252	3.41352434778013	2.12227282040029
H	2.29438714304326	3.34487849377941	0.50948097049189
H	-1.39448211062943	4.70336214209431	3.16739589282496
H	-0.68469434440396	3.50610012774452	2.06920181870300
H	-1.71750814193568	4.77966810700616	1.42665340780682
H	5.60891664304563	6.02426739408099	3.19022120387318
H	4.94803930828063	4.54987411777537	3.91072175465054
H	6.18107934363736	5.47132808998519	4.76528885083873
H	1.32026377119162	9.50499427466755	6.11683114197169
H	1.97030428059706	9.90290453060759	4.51989835361797
H	2.91761878768237	10.23714132204436	5.96685583186229
H	-1.00822263202094	3.29760055005229	7.20971393015896
H	1.96872199006799	3.94395245589875	4.89533898566642
H	0.59920600720587	3.23766970160052	4.00966226314050

H	1.05405173746769	2.67093571303537	5.61300623505021
H	-0.68579804141029	8.68741389018824	2.64834610150527
H	-1.73678068098597	7.26270447738304	2.64990750315381
H	-1.35285761768062	8.08700295877705	1.13180544186365
H	4.38274075746306	5.32231062537987	1.29588666934770
H	4.31598406299356	7.06665413956238	1.00545030073597
H	3.74834294285124	5.94128272139814	-0.22683878584947
H	1.14023492918319	6.18526444874859	7.64235873390988
H	1.09265407605509	7.94542923265247	7.56891710139220
H	2.38010101241505	7.14569373601935	8.47479905901418
H	4.07267985377513	3.90700100023586	6.10514478864214
H	2.76402735772237	4.37898756466839	7.20855359509266
H	4.42611858438760	4.87933773109657	7.53272535873031
H	3.88457911741084	9.43791133518855	3.16289052267484
H	4.98360602860838	8.13432750236984	2.68669826209815
H	5.38244181404369	9.17421811943355	4.05331277056310
H	2.98229161049396	8.87019010402746	1.09189531648878
H	1.59395158255416	9.45170046048661	2.02377210742200
H	1.40652115605558	9.05797338853586	0.31709822659604
H	-2.38010277329381	5.60824538729714	7.67157635367818
H	-2.02441351465732	8.01600452623303	4.93464028915418
H	-0.67332112751728	8.49788672994567	5.95809054205188
H	-2.22695069639731	8.09463924634929	6.68386394674084

References

1. Y. Guo, K. Sivalingam, C. Kollmar and F. Neese, *J. Chem. Phys.*, 2021, **154**, 214113.
2. F. Neese, *WIREs Comput. Mol. Sci.*, 2022, **12**, e1606.
3. M. Douglas and N. M. Kroll, *Ann. Phys.*, 1974, **82**, 89–155.
4. F. Weigend and R. Ahlrichs, *Phys. Chem. Chem. Phys.*, 2005, **7**, 3297–3305.
5. J. D. Rolfes, F. Neese and D. A. Pantazis, *J. Comput. Chem.*, 2020, **41**, 1842–1849.
6. G. L. Stoychev, A. A. Auer and F. Neese, *J. Chem. Theory Comput.*, 2017, **13**, 554–562.
7. C. Adamo and V. Barone, *J. Chem. Phys.*, 1999, **110**, 6158–6170.
8. J. P. Perdew, K. Burke and M. Ernzerhof, *Phys. Rev. Lett.*, 1996, **77**, 3865–3868.
9. J. P. Perdew, K. Burke and M. Ernzerhof, *Phys. Rev. Lett.*, 1997, **78**, 1396–1396.
10. C. Angeli, R. Cimiraglia, S. Evangelisti, T. Leininger and J.-P. Malrieu, *J. Chem. Phys.*, 2001, **114**, 10252–10264.
11. C. Angeli, R. Cimiraglia and J.-P. Malrieu, *J. Chem. Phys.*, 2002, **117**, 9138–9153.
12. C. Kollmar, K. Sivalingam, Y. Guo and F. Neese, *J. Chem. Phys.*, 2021, **155**, 234104.
13. F. Neese, *J. Chem. Phys.*, 2005, **122**, 034107.
14. M. Atanasov, D. Aravena, E. Suturina, E. Bill, D. Maganas and F. Neese, *Coord. Chem. Rev.*, 2015, **289–290**, 177–214.
15. L. Visscher and K. G. Dyall, *At. Data Nucl. Data Tables*, 1997, **67**, 207–224.
16. J. R. Pliego, *Chem. Phys. Lett.*, 2003, **367**, 145–149.
17. M. Rupp, R. Korner and I. V. Tetko, *Comb. Chem. High Throughput Screen.*, 2011, **14**, 307–327.
18. Determining the pK_a of Simple Molecules Using Gaussian 2009, S. A. McKee and T. V. Pogorelov, 2019.